

*Phenomenological studies of strongly  
interacting matter under extreme  
conditions*

A THESIS

*submitted for the Award of Ph.D. degree from*  
MOHANLAL SUKHADIA UNIVERSITY

*in the*

*Faculty of Science*

*by*

Guruprasad Prakash Kadam



*Under the Supervision of*

Prof. Hiranmaya Mishra

Professor

Theoretical Physics Division

Physical Research Laboratory

Ahmedabad, India.

DEPARTMENT OF PHYSICS  
MOHANLAL SUKHADIA UNIVERSITY  
UDAIPUR

Year of submission: 2016



*To*  
*My Family*



## ***DECLARATION***

*I, Mr. Guruprasad Prakash Kadam, Theoretical Physics Division, Physical Research Laboratory, Navarangpura, Ahmedabad-380009, hereby declare that the research work incorporated in the present thesis entitled, “**Phenomenological Studies of Strongly Interacting Matter Under Extreme Conditions**” is my own work and is original. This work (in part or in full) has not been submitted to any University for the award of a Degree or a Diploma. I have properly acknowledged the material collected from secondary sources wherever required. I solely own the responsibility for the originality of the entire content.*

**Date:**

(Guruprasad Prakash Kadam)



# ***CERTIFICATE***

I feel great pleasure in certifying that the thesis entitled, **“Phenomenological Studies of Strongly Interacting Matter Under Extreme Conditions”** embodies a record of the results of investigations carried out by Mr. Guruprasad Prakash Kadam under my guidance. He has completed the following requirements as per Ph.D regulations of the University.

- (a) Course work as per the university rules.
- (b) Residential requirements of the university.
- (c) Regularly submitted six monthly progress reports.
- (d) Presented his work in the departmental committee.
- (e) Published minimum of one research papers in a referred research journal.

I am satisfied with the analysis, interpretation of results and conclusions drawn. I recommend the submission of thesis.

**Date:**

Prof. Hiranmaya Mishra  
(Thesis Supervisor)  
Professor, THEPH,  
Physical Research Laboratory,  
Ahmedabad - 380 009

Countersigned by  
Head of the Department



---

## Acknowledgements

*Human beings are social animals and it would be difficult for them to survive without bunch of other humans around. Being an anti-social is thus anomalous. I have lived my life being highly anti-social, solitude, comfortable with the company of not more than three persons around; a critical point for me. Nevertheless, without support and help of few of those around it would have been impossible to be in the social state that I am in. So it would be utterly unethical not to acknowledge those people who made small or large contribution in my “the PURSUIT of HAPPYNESS”.*

*I would also like to express my most sincere and deep gratitude to my supervisor Prof. Hiranmaya Mishra, for his invaluable guidance, encouragement and support throughout the course of this work. I immensely benefited from his insight and expertise in the subject. Discussion with him was a great pleasure as he always gave importance to my views and was always friendly and patient with me. He is the sole reason that I have become an independent researcher in my Ph.D period itself, a necessary step to survive in today’s scientific competition. I would like to thank Dr. Namit Mahajan for his invaluable insights during casual discussions we made on various topics of my interests. I should admire his expertise on quantum field theory as well as up to date information of the scientific literature in my fields of interests. I would also like to thank Prof. Jitesh Bhatt for his viewpoints in the casual discussions and I regret of not starting any project on common research interests. I would like to thank Prof. S. Mohanty, Prof. S. Goswami, Prof. D. Angom, Prof. R. Rangarajan, Dr. Partho Konar, Dr. Navinder Singh, Dr. B. Sahu and Dr. N. Mahajan for taking stimulating courses in theoretical physics during my Ph.D tenure.*

*I would like to express my foremost deep gratitude to my father, Prakash Kadam and my wife, Swapnali, who are the constant inspirations of my life. Their support helped me a lot in my pursuit of Ph.D.*

*Being an anti-social it is legitimate to have very few friends. When I searched for the definition of the word “friend“ I found too many, but the one that I per-*

sonally liked and thought pertinent is the following: A friend is a person known well to another and regarded with liking, affection, and loyalty. So I would say I got many good friends during my Ph.D tenure at PRL. The foremost close to me are all my batch mates: Arun, Ikshu, Manu, Sanjay, Alok, Shraddha, Girish, Tanmoy, Kuldeep, Abhaya, Chitrabhanu, Anirban and Gaurav. I appreciate great social environment they made around me which I lacked during my undergraduate and graduate period. I would especially like to thank my seniors, Avdhesh, Gulab, Girish Chakravorty, Monojit and Arko for their help for various purposes. I would also like to acknowledge Mansi, Ananta Mishra, Aman and Abhishek Atreya for an illuminating physics discussions on various topics. Apart from those whom I specifically mentioned for acknowledgement there are more others whom I cannot acknowledge due to lack of space but they have certainly contributed to my success in some way. I express gratitude for them and apologize for not mentioning explicitly for the credit.

**Guru**

---

## ABSTRACT

This thesis deals with the phenomenological studies of hot and dense matter created in relativistic heavy ion collision experiments (HICs). Quantum chromodynamics (QCD) is perturbative at high energies due to phenomenon of asymptotic freedom, but the strong coupling constant is no more a small parameter at the energy scale ( $\sim 0.2$  GeV) involved in HICs. Thus, perturbative QCD fails due to lack of any small parameter which would be used to exploit full strength of quantum field theory. First principle lattice quantum chromodynamics (LQCD), which is non-perturbative formulation of QCD has been used to study such matter. Albeit successful at zero baryon density, LQCD suffers from so called the sign problem at finite baryon density especially in the hadronic phase where the non-perturbative effects are very strong. There has been attempt to solve this problem by using various mathematical tricks, but these methods have their own limitations and the results are not quite reliable except at small chemical potential. In this thesis, we study the thermodynamics of hadronic matter at zero as well as finite baryon density using hadron resonance gas model (HRG) as an effective theory of QCD describing hadronic matter. We confront HRG estimates with the lattice QCD simulations at zero baryon density as well as available finite baryon density simulations. In ideal HRG the properties of hadrons enter through mass spectrum which can either be taken as a sum over discrete states which are experimentally well established or continuum mass spectrum which is consistent with discrete spectrum and also take into account heavier mass states which are not experimentally established but make contribution to the thermodynamics of HRG. We observe that the ideal HRG model with only discrete mass spectrum with finite upper mass cut-off agrees with the LQCD simulations up to temperature ( $T$ )  $\sim 0.140$  GeV, while HRG with continuum mass spectrum agrees with the LQCD up to  $T \sim 0.160$  GeV. We further extend the ideal HRG with the discrete mass spectrum up to mass cut-off  $\sim 2$  GeV and continuum mass spectrum all the way up to infinity but with lower limit  $\sim 2$  GeV. We study such hybrid HRG model at zero as well as finite baryon density and confront the

thermodynamics with the LQCD simulations. We observe that the hybrid HRG model agrees with the LQCD up to  $T \sim 0.160$  GeV as opposed to the ideal HRG with only discrete mass spectrum which agrees with the LQCD up to  $T \sim 0.140$  GeV within error bars, while at finite baryon density, we observe that the ideal HRG with the discrete mass spectrum is sufficient to describe LQCD simulations.

Further, we make possible improvements in non-interacting HRG model so as to explain certain other aspects of hadronic matter that has been produced during the evolution of the matter created in HICs. These include hadron multiplicities, the nuclear liquid-gas phase transition and the effects of chiral symmetry of QCD. First couple of aspects can be explained by accounting repulsive interaction between the hadrons which can be accommodated in the ideal HRG model by Van-der-Waals inspired excluded volume correction. Such interacting HRG model termed as an excluded volume HRG model (EHRG) not only accounts for the hadron multiplicities observed in HICs and the nuclear liquid-gas phase transition but also agrees with the LQCD data quite well. Further, EHRG get rid of implicit assumption of the dilute gas approximation in the ideal HRG model which is quite erroneous around the QCD transition temperature where gas is quite dense. We further extend EHRG model to incorporate the effects of chiral symmetry of QCD. We achieve this by including medium dependent hadron masses which is upshot of the chiral symmetry. We use  $2 + 1$  flavor Nambu-Jona-Lasinio model to compute medium dependent masses of approximate Goldstone modes as well as that of constituent quarks. For other hadrons we use linear scaling rule based on constituent quark model. We observe that EHRG with medium dependent hadron masses is in agreement with the LQCD simulation up to  $T \sim 0.170$  GeV.

We estimate transport properties like shear ( $\eta$ ) and bulk ( $\zeta$ ) viscosities of hadronic matter at finite temperature and density using two formalisms, *viz.*, the Kubo's formalism and the relativistic kinetic theory. We estimate these coefficient within ambit of HRG model and its extensions. We observe that the bulk viscosity to entropy density ratio ( $\zeta/s$ ) computed using Kubo's formalism rises very rapidly with temperature. Further, the ratio is higher at higher baryon den-

sity. Unlike Kubo's formalism, ratio  $\zeta/s$  estimated using kinetic theory decreases with temperature and vanishes at higher temperature. The shear viscosity to entropy density ratio  $\eta/s$  also decreases in kinetic theory and approaches perfect fluid limit ( $= \frac{1}{4\pi}$ ) called Kovtun-Son-Starinets bound (KSS). Thus, hadronic matter created in the evolution of matter created in HICs itself behave close to perfect fluid. This result is consistent with the estimations based on other approaches like Chapman-Enskog theory. Further, at finite baryon density, ratio  $\eta/s$  approaches more closer to KSS bound.

Finally, we estimate the transport properties, *viz.*, shear ( $\eta$ ) and bulk ( $\zeta$ ) as well as thermal conductivity ( $\lambda$ ), of hot and dense quark matter by solving the Boltzmann kinetic equation within relaxation time approximation. The thermodynamical quantities as well as medium dependent quark and meson masses are estimated within two flavor NJL model. To estimate the relaxation time we have consider the quark-antiquark two body scatterings through exchange of pion and sigma resonances. Since the meson masses are minimum at the Mott transition temperatures beyond which they are degenerate and increase linearly with temperature, we find that the meson propagator occurring in the transition amplitude leads to a large contribution to the cross section for the quark-antiquark scattering at the Mott transition temperature for the pions. This eventually leads to a smaller relaxation time which, in turn, lead to a minimum in the temperature dependence of the relaxation time. This behavior of relaxation time is reflected in all the transport coefficients,  $\eta/s$ ,  $\zeta/s$  and  $\lambda/T^2$  which shows minimum at Mott temperature.

**Keywords** : Heavy ion collisions, Hadron resonance gas model, Nambu-Jona-Lasinio model, shear viscosity, bulk viscosity



---

## LIST OF PUBLICATIONS

1. *Bulk and shear viscosities of hot and dense hadron gas,*  
**Guru Prakash Kadam** and H. Mishra, Nucl. Phys. A **934**, 133 (2014).
2. *Transport properties of hadronic matter in magnetic field,*  
**Guru Prakash Kadam**, Mod. Phys. Lett. A **30**, no. 10, 1550031 (2015).
3. *Dissipative properties of hot and dense hadronic matter in an excluded-volume hadron resonance gas model,*  
**Guru Prakash Kadam** and H. Mishra, Phys. Rev. C **92**, no. 3, 035203 (2015).
4. *Medium modification of hadron masses and the thermodynamics of hadron resonance gas model,*  
**Guru Prakash Kadam** and H. Mishra, Phys. Rev. C **93**, no. 2, 025205 (2016).
5. *Curing the acausal behavior of the sound velocity in an excluded volume hadron resonance gas model,*  
**Guru Prakash Kadam**, arXiv:1510.04371 [hep-ph].
6. *Estimating transport coefficients in hot and dense quark matter,*  
Paramita Deb, **Guru Prakash Kadam**, H. Mishra, arXiv:1603.01952 [hep-ph].



---

## List of Abbreviations

AGS	Alternating Gradient Synchrotron
CBM	Compressed Baryonic Matter
CERN	Conseil Europeen pour la Recherche Nucleaire
EHRG	Excluded volume Hadron Resonance Gas
FAIR	Facility for Antiproton and Ion Research
HIC	Heavy Ion Collision
HRG	Hadron Resonance Gas
KSS	Kovtun-Son-Starinets
LQCD	Lattice Quantum Chromodynamics
NICA	Nuclotron-based Ion Collider fAility
NJL	Nambu-Jona-Lasinio
PHSD	Parton Hadron String Dynamics
PNJL	Polyakov-Nambu-Jona-Lasinio
RHIC	Relativistic Heavy Ion Collider
SPS	Super Proton Synchrotron
STAR	Solenoidal Tracker at RHIC
UrQMD	Ultrarelativistic Quantum Molecular Dynamics
VDW	Van-der-Waals



# Contents

<b>Acknowledgements</b>	<b>i</b>
<b>Abstract</b>	<b>iii</b>
<b>List of Publications</b>	<b>vii</b>
<b>List of Abbreviations</b>	<b>ix</b>
<b>Contents</b>	<b>xi</b>
<b>List of Tables</b>	<b>xv</b>
<b>List of Figures</b>	<b>xvii</b>
<b>1 Introduction</b>	<b>1</b>
1.1 Phases of QCD . . . . .	2
1.1.1 QCD vacuum . . . . .	2
1.1.2 QCD at finite temperature and density . . . . .	3
1.2 Heavy-ion collisions . . . . .	6
1.3 Transport properties of strongly interacting matter . . . . .	8
1.3.1 Relativistic hydrodynamics . . . . .	9
1.3.1.1 Ideal hydrodynamics . . . . .	10
1.3.1.2 Viscous hydrodynamics . . . . .	11
1.3.2 Transport coefficients: Shear and bulk viscosities . . . . .	12
1.3.2.1 Physics of shear and bulk viscosities . . . . .	12

1.3.2.2	The status of transport coefficients in the context of heavy-ion collisions . . . . .	14
1.4	Organization of the thesis . . . . .	18
<b>2</b>	<b>Thermodynamics of hadron resonance gas model</b>	<b>21</b>
2.1	Hadron resonance gas model . . . . .	21
2.1.1	Non interacting hadron resonance gas model . . . . .	21
2.1.2	Excluded volume hadron resonance gas model . . . . .	28
2.1.3	Hadron resonance gas model with medium dependent hadron masses . . . . .	31
2.1.4	Hadron resonance gas model in magnetic field . . . . .	38
2.2	Conclusion . . . . .	42
<b>3</b>	<b>Transport properties of hot and dense hadronic matter</b>	<b>45</b>
3.1	Transport coefficients in kinetic theory . . . . .	45
3.1.1	Relativistic Boltzmann equation . . . . .	45
3.1.2	Boltzmann equation in relaxation time approximation . . . . .	49
3.1.3	Transport coefficients in relaxation time approximation . . . . .	50
3.2	Transport coefficients in Kubo's formalism . . . . .	54
3.2.1	Kubo's formula for bulk viscosity . . . . .	54
3.2.2	Anisotropic bulk viscosity in presence of strong magnetic field . . . . .	56
3.3	Results and discussion . . . . .	58
3.4	Conclusion . . . . .	68
<b>4</b>	<b>Transport properties of hot and dense quark matter</b>	<b>69</b>
4.1	Thermodynamics of two flavor NJL model and meson masses . . . . .	69
4.2	Boltzmann equation in relaxation time approximation and trans- port coefficients revisited . . . . .	72
4.2.1	Transition rates and thermal averaging . . . . .	83
4.3	Results and discussion . . . . .	85
4.4	Conclusion . . . . .	92

**5 Summary and outlook** **95**

**Bibliography** **99**

**Publications attached with the thesis** **xiii**



# List of Tables

2.1 Parameters defining continuum density of states. . . . .	25
--------------------------------------------------------------	----



# List of Figures

1.1	Proposed phase diagram of QCD. . . . .	3
1.2	Evolution of the matter created in heavy ion collision experiments. . . . .	7
1.3	Origin of shear and bulk viscosities. . . . .	13
1.4	Collision or beam axis is perpendicular to the plane of the figure. Impact parameter $b$ =length AB. $z$ is the longitudinal direction, $xy$ is the transverse or azimuthal plane, $xz$ is the reaction plane, and $\phi$ is the azimuthal angle of one of the outgoing particles and $\Phi_R$ is reaction plane angle. Figure has been taken from Ref. [1]. . . . .	15
2.1	Thermodynamics of hadron resonance gas. Left panel (a) shows scaled pressure as a function of temperature for $\mu = 0$ (blue) and $\mu = 0.3$ GeV (green) with the exponential Hagedorn spectrum given by Eq. (2.1.10). The dotted line corresponds to discrete spectrum for hadron resonance gas. The right panel shows the same quantities but with the power law spectrum as given in Eq. (2.1.11). . . . .	26
2.2	Trace anomaly of HRG with and without inclusion of Hagedorn density of states at two different chemical potentials. . . . .	27
2.3	Speed of sound in HRG with and without inclusion of Hagedorn density of states at two different chemical potentials. . . . .	27
2.4	Results for thermodynamical quantities at $\mu = 0$ GeV in EHRG- I and EHRG-II models with the mass dependent excluded vol- ume parametrization. Black dashed curve corresponds to non- interacting hadron resonance gas model. . . . .	33

2.5	Scaled pressure as a function of temperature at two different chemical potentials in EHRG-I and EHRG-II with mass dependent excluded volume parametrization. . . . .	34
2.6	Results of thermodynamical estimated using HRG model at different chemical potential and magnetic field. . . . .	41
2.7	Speed of sound in HRG at different chemical potentials and magnetic fields. . . . .	42
3.1	Comparison of shear viscosity to entropy density ratio estimated within various other models with our model. . . . .	59
3.2	Left panel: Shear viscosity to entropy density ( $\eta/s$ ) ratio of temperature for different chemical potentials for $r_h = 0.3$ fm. Middle panel: $\eta/s$ for $r_h = 0.5$ fm. Right panel: Shear viscosity coefficient for $r_h = 0.5$ fm. . . . .	59
3.3	Comparison of fluidity measures in our model with Ref. [2] at two different chemical potentials. . . . .	60
3.4	Fluidity measure $\frac{\eta T}{(\epsilon+P)}$ at different chemical potentials for $r_h = 0.3$ fm and 0.5 fm. . . . .	61
3.5	Left panel: Bulk viscosity to entropy density ( $\zeta/s$ ) ratio of temperature for different chemical potentials for $r_h = 0.3$ fm. Middle panel: $\zeta/s$ for $r_h = 0.5$ fm. Right panel: Bulk viscosity coefficient for $r_h = 0.5$ fm. . . . .	62
3.6	Comparison of bulk viscosity to entropy density ratio estimated within SHMC model [3] with our model. . . . .	62
3.7	Viscosity coefficients along the chemical freeze-out curve. . . . .	63
3.8	Left panel shows shear viscosity coefficient estimated within EHRG-I and EHRG-II models. Right panel shows shear viscosity to entropy density ratio. . . . .	64
3.9	Bulk viscosity to entropy density in Kubo's formalism (Eq. 3.2.8) at different chemical potentials estimated within HRG model with discrete and exponential mass spectrum. . . . .	65

3.10	Left panel: Bulk viscosity in Kubo's formalism (Eq. 3.2.15) at different magnetic field and chemical potentials. Right panel: Bulk viscosity to entropy density in Kubo's formalism at different magnetic fields. . . . .	66
4.1	Temperature dependence of the constituent quark mass $M$ , and pion and sigma meson masses at $\mu = 0$ [Fig. (1a)] and temperature derivative of the constituent quark mass for $\mu = 0$ MeV and $\mu = 100$ MeV [Fig. (1b)]. . . . .	86
4.2	Temperature dependence of square of the velocity of sound [Fig. (2a)] and $C_v/T^2$ [Fig. (2b)] for $\mu = 0$ MeV and $\mu = 100$ MeV and temperature derivative of the constituent quark mass for $\mu = 0$ MeV and $\mu = 100$ MeV. . . . .	87
4.3	Fig. (3a) shows relaxation time as a function of temperature for $\mu = 0$ MeV and for $\mu = 100$ MeV. In Fig. (3b), shear viscosity to entropy density ratio is shown for $\mu = 0$ MeV and $\mu = 100$ MeV. . . . .	88
4.4	Ratio of bulk viscosity to entropy density for $\mu = 0$ MeV and for $\mu = 100$ MeV. . . . .	89
4.5	the violation of conformality measure $C_1 1 - 3V_n^2$ [Fig. (5a)] and $C_2 = M^2 - TM \frac{dM}{dT}$ [Fig. (5b)] as a function of temperature for $\mu = 0$ MeV and for $\mu = 100$ MeV. . . . .	90
4.6	Thermal conductivity in units of $T^2$ for $\mu = 100$ MeV. . . . .	91



# Chapter 1

## Introduction

Among the four fundamental interactions governing the physics of elementary particles the strong nuclear force is of prime importance due to its rich structure. The theory that describes the strong interaction between the elementary particles at a fundamental level is quantum chromodynamics (QCD) where the fundamental degrees of freedom are quarks and gluons. There are six known flavors of quarks, namely, up (u), down (d), strange (s), charm (c), bottom (b) and top (t), and eight kinds of (bi-)colored gluons. The QCD is an example of a quantum field theory based on so called gauge principle [4, 5]. It is a remarkable theory and has been successfully used to explain wide range of phenomena; from the hadron mass spectrum [6] to the deep inelastic scattering (DIS) experiments [7, 8]. One peculiar feature of QCD is the asymptotic freedom [9, 10]. Because of the non-abelian nature of the fundamental gauge group, the behavior of the coupling constant of QCD is exactly opposite to that of quantum electrodynamics (QED); the QCD coupling constant is small at high energies (short distance) while it becomes large at small energies (large distance). In fact it can be shown that, at one loop, the strong coupling constant runs with the energy scale as

$$g^2(q^2) = \frac{16\pi^2}{b \log(\frac{q^2}{\Lambda_{QCD}^2})}; \quad b = \frac{11N_c}{3} - \frac{2N_f}{2} \quad (1.0.1)$$

where  $N_c$  and  $N_f$  represents number colors and flavors in the theory.  $\Lambda_{QCD}$  is the scale at which the strong coupling constant becomes non-perturbative and  $q^2$  is the four momentum exchange. Thus we note that at large energies (large momentum transfer) it is possible to use perturbative technique with the coupling constant as a small parameter together with the full strength of quantum field theory to derive the observable quantities. The prime example of the success of perturbative QCD lies in its application to explain DIS experiments. At low energy (low momentum transfer), however, perturbative QCD cannot produce reliable results since the coupling constant is large and it cannot be used as a perturbative expansion parameter. Apart from small quark masses, it has no numerically small parameter and the only intrinsic scale is the dynamically generated confinement scale  $\Lambda_{QCD} \sim 200$  MeV. So, for low energy processes one needs to construct non-perturbative technique which does not depend on small parameter expansion. Lattice QCD is one of the known first principle non-perturbative technique of QCD [11].

## 1.1 Phases of QCD

### 1.1.1 QCD vacuum

QCD vacuum is the example of non-perturbative vacuum characterized by non-vanishing condensates of quarks (and gluons). In 2+1 flavor QCD\*, these condensates are formed when the chiral symmetry ( $SU_L(3) \times SU_R(3)$ ) is spontaneously broken to  $SU_V(3)$  flavor symmetry. The value of these condensates defined by the quantity  $\bar{q}q^\dagger$  turns out to be  $-230 \text{ MeV}^3$  which can be interpreted as number of such pairs per unit volume. The Goldstone's theorem [12] implies that spontaneous breakdown of the chiral symmetry is associated with the appearance of octet of approximately massless pseudo-scalar Goldstone bosons.

This spontaneous chiral symmetry breaking has an important effect on the

---

\*2+1 flavor QCD consist of three quark flavors  $q_a = (u, d, s)$  such that  $u$  and  $d$  are light flavors while  $s$  is heavy flavor.

$^\dagger q = (q_L, q_R)$  and  $q_{L,R} = \frac{1}{2}(1 \mp \gamma_5)q$ .

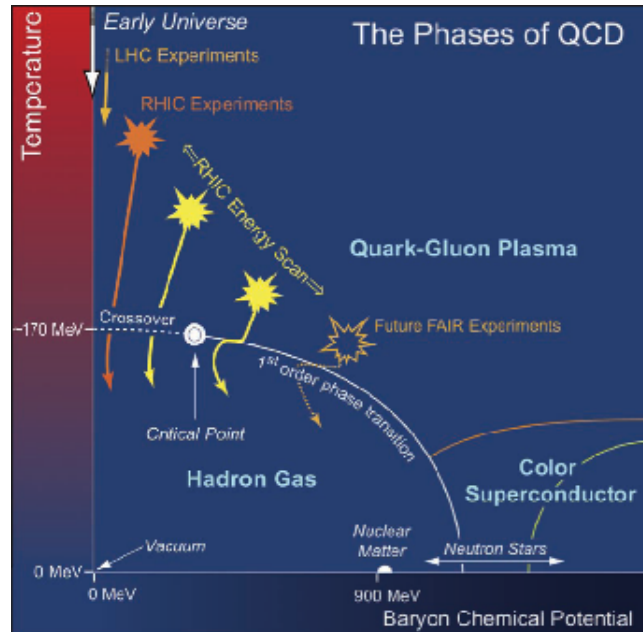


Figure 1.1: Proposed phase diagram of QCD.

dynamics of QCD at low energies. Since  $\langle \bar{q}q \rangle = \langle \bar{q}_L q_R + \bar{q}_R q_L \rangle \neq 0$ , a left handed quark propagating through such vacuum can flip its helicity<sup>‡</sup> and becomes right handed quark. Thus quark behaves as if it has mass. Thus the interaction of quark with vacuum condensates leads to generation of mass. This dynamically generated mass is called constituent quark mass ( $\mathcal{M}_q$ ) as opposed to current quark mass ( $m_q$ ). For light quark flavors (u,d),  $\mathcal{M}_q \sim 350$  MeV and  $m_q \sim 5$  MeV while for the strange quark  $\mathcal{M}_q \sim 550$  MeV and  $m_q \sim 140$  MeV. Thus, most of the mass of the quark (whence the hadron) is due to dynamical breaking of the chiral symmetry.

### 1.1.2 QCD at finite temperature and density

In order to understand the astrophysical compact objects like compact stars and the matter created in the heavy ion collision experiments (HICs), the study of thermodynamics of QCD is essential. The thermodynamical information about a system is often represented in the form of a phase diagram which is just a plot

<sup>‡</sup>Helicity is defined as the projection of spin ( $\vec{S}$ ) in the direction of momentum ( $\vec{p}$ ) i.e  $h = \frac{\vec{S} \cdot \vec{p}}{|\vec{p}|}$ .

of external control parameters, for instance, in case of water, the control parameters are pressure (P) and temperature (T). Depending on these thermodynamic parameters, matter can exhibit different manifestations called phases. In the case of strongly interacting matter described by QCD, the control parameters are temperature (T) and baryon chemical potential ( $\mu$ ) and the proposed phase diagram is as shown in Fig. (1.1). Each point in this phase diagram corresponds to stable thermodynamic state characterized by thermodynamical functions like pressure (P) and energy density ( $\epsilon$ ). It can be noted from Fig. (1.1) that the QCD phase diagram can be broadly divided into two main phases, *viz.*, confined hadronic phase and deconfined quark-gluon matter phase<sup>§</sup>. The confining hadronic phase exist at low temperature and low baryon density where the fundamental degrees of freedom are composite hadrons, while the quark-gluon matter exist at high temperature,  $T \sim 200$  MeV which is of order of intrinsic QCD scale. Since the hadrons are composite objects (made up of quarks and gluons) and QCD is asymptotically free, it is legitimate to anticipate that the QCD matter at high temperature (whence at high energy density) undergo phase transition from the confined hadronic phase to the deconfined quark-gluon matter phase.

It is possible to make very crude estimates of temperature ( $T_c$ ) and energy density ( $\epsilon_c$ ) at which hadron to quark-gluon-plasma (QGP) phase transition would take place. For this purpose we use simplest model of hadron which accommodate two important features of QCD, *viz.*, asymptotic freedom and color confinement. In this so called MIT bag model [13, 14] the massless quarks are assumed to move freely inside the bag of radius  $R$ , but are confined inside due to inward pressure of the bulk vacuum. It turns out that this inward pressure is  $P_{in} = -\Lambda_{bag}^4$ , where  $\Lambda_{bag}$  is the bag constant and is of order of intrinsic QCD scale, i.e 200 MeV. At zero baryon chemical potential and at low temperature, thermal medium of hadrons is mostly dominated by pions ( $\pi^\pm, \pi^0$ ). At moderate temperature ( $> 100$  MeV), the pressure due to gas of pions is approximately

---

<sup>§</sup>There are some exotic QCD phases conjectured to exist at high baryon density, but these phases are not relevant to the study carried out in this thesis.

given by blackbody radiation pressure,

$$P_\pi = g_\pi \times \frac{\pi^4}{90} T^4 \quad (1.1.1)$$

where  $g_\pi$  is the degeneracy factor of pion ( $= 3$ ). For the gas of deconfined quarks and gluons (in 2 flavor QCD),

$$P_{q\bar{q}} = g_q \times \frac{7}{4} \times \frac{\pi^2}{90} T^4; P_g = g_g \times \frac{\pi^2}{90} T^4 \quad (1.1.2)$$

where, factor  $7/4$  arises due Fermi-Dirac statistics of quarks. The degeneracy factors for quarks and gluons are 12 and 16 respectively. At the deconfinement, pressure of the gas of pions and that of quark-gluon matter must be equal. Thus,

$$3 \times \frac{\pi^4}{90} T_c^4 = 37 \times \frac{\pi^4}{90} T_c^4 - \Lambda_{bag}^4 \quad (1.1.3)$$

where, we have subtracted the negative pressure of the bulk vacuum (in MIT bag model) to take into account deconfinement. Thus, one obtain the transition temperature  $T_c \sim 145$  MeV and corresponding energy density turns out to be  $\epsilon_c = 850$  MeV/fm<sup>3</sup>. This estimation is rather crude, but one gets a rough idea about the order of magnitudes involved in hadron-QGP phase transition. Latest first principle lattice QCD (LQCD) simulations tells us that the transition temperature is in range 150 – 160 MeV [15].

Phase transition from hadronic phase to quark gluon plasma phase is usually referred as deconfinement phase transition because there is a release of quark and gluon degrees of freedom above  $T_c$ . There is no well defined order parameter which characterize this phase transition but it is believed that in the massless limit ( $m_q \rightarrow 0$ ) it is the  $Z(3)$  center symmetry which is broken in high temperature quark-gluon-matter phase and corresponding order parameter is Polyakov loop [16]. It can be shown that the natural consequence of confinement is dynamical breaking of chiral symmetry [17]. Thus it is legitimate to conclude that the deconfinement should be accompanied by chiral symmetry restoration. In this chiral restoration phase transition the chiral condensate melts away whence

quarks lose their dynamically generated (constituent) mass. The corresponding order parameter in this case is  $\langle \bar{q}q \rangle$ . The study of deconfinement as well as chiral restoration phase transition are of immense importance. Both the phase transitions, deconfinement as well as chiral symmetry restoration, occur at finite temperature and baryon density and since the the LQCD simulations gives reliable results at zero baryon density only, one has to invoke effective model scenarios which are in conformity with the LQCD simulations at  $\mu = 0$ . Hadron resonance gas model is tremendously successful in this respect whence the cause of motivation to study the hadronic matter in this thesis.

## 1.2 Heavy-ion collisions

Establishing the fact that the strongly interacting matter can manifest itself in at least two phases, *viz.*, the hadronic phase and the quark-gluon-plasma (QGP) phase, it is natural to look for the physical systems where these forms of matter would exist. Our observable universe is dominated by stable hadronic matter (protons and neutrons) while quark-gluon matter cannot be observed directly due to confinement. According to standard cosmological scenario, the quark-gluon-plasma might have existed during the short period of  $10^{-5} - 10^{-4}$  seconds after the big bang. But the physicist across the world are focusing their attention in an attempt to re-create such matter in laboratories under controlled conditions. For this purpose two heavy nuclei (e.g Sulfur (S), Lead (Pb) and gold (Au) etc.) are accelerated to high energies in giant accelerators and then they are allowed to collide with each other. Alternating Gradient Synchrotron (AGS) and Relativistic Heavy Ion Collider (RHIC), both in Brookhavan, Super Proton Synchrotron (SPS) and A Large Ion Collider Experiments (ALICE), both at CERN are the experiments where the physicists are attempting to recreate strongly interacting matter under extreme conditions of high temperature and density. Each experiment is aimed to probe the specific region of the QCD phase diagram as shown in Fig. (1.1) and it depends upon the highest energy achieved (or the center of mass energy).

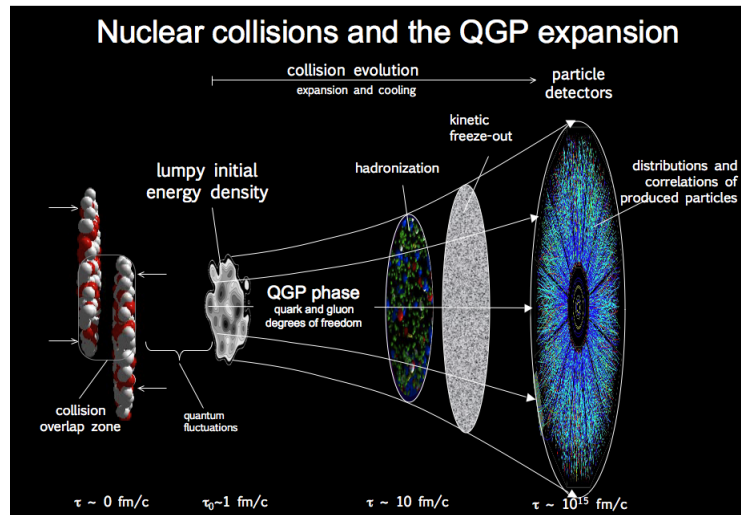


Figure 1.2: Evolution of the matter created in heavy ion collision experiments.

The schematic representation of the evolution of the matter created in HICs is shown in Fig. (1.2). The heavy ion collision scenario can be broadly divided to three temporal regions, *viz.*, the pre-equilibrium phase, the QGP phase and the hadronic phase (chemical and thermal freeze-out). Two colliding nuclei can be imagined as spherical objects in their rest frame but due to Lorentz contraction in the direction of motion in the center of mass frame, they can be imagined as colliding pancake shaped objects as show in left part of Fig. (1.2). When two nuclei collide, many partons are liberated due to inelastic collisions between the nucleons. These partons which are produced in very dense medium ( $\sim n_0$  i.e nuclear matter density) re-scatter many times so as to deposit substantial amount of initial energy in mid-rapidity region ( $y \simeq 0$ <sup>¶</sup>) to produce hot and dense fireball. This fireball thermalize<sup>||</sup> after certain time ( $\tau_0 \sim 1$  fm). In the next stage, this thermalized QGP undergoes an expansion due to excess pressure with respect to vacuum. The thermalised plasma is in local equilibrium whence the evolution of which can be described by relativistic hydrodynamics. After certain time, as the

<sup>¶</sup>Rapidity is a convenient variable used in the relativistic collisions. For a particle of four momentum  $(E, \vec{p})$  it can be defined as  $y = \frac{1}{2} \ln \left( \frac{E+p_z}{E-p_z} \right)$ .

<sup>||</sup>The actual mechanism behind this thermalization is still not understood due to non-Abelian nature of theory describing strongly interacting matter. Certain models like color glass condensate (CGC) [18] attempt to describe this initial thermalization of QGP but with certain drawbacks.

fireball expand and cool, the temperature eventually drops down to the transition temperature ( $T_c$ ) at which the quarks and gluons start reorganizing themselves into hadrons. Below  $T_c$  the hadronization takes place where the abundance of various hadronic species is fixed (akin to nucleosynthesis era in the standard big bang theory). This is known as chemical freeze-out. At this stage the hadronic matter is still in local thermal equilibrium and hydrodynamical theory is still valid. As this chemically freezed hadronic medium further expand and cool the interaction rate become insufficient to maintain the local equilibrium. At this stage, so called thermal freeze-out, the mean free path of hadrons becomes larger than the system size so that the hydrodynamic description breaks down and hadrons fly away freely to be detected in detectors.

### 1.3 Transport properties of strongly interacting matter

Having established the rough physical picture of the phases of the strongly interacting matter and its description in the context of heavy-ion collisions, the natural next step is to give this picture a firm theoretical basis. Matter created in the heavy-ion collision has been successfully described using the hydrodynamics which is the long wavelength and low frequency limit of the microscopic dynamics of multi-particle system that is close to the local equilibrium. In the formulation of the fluid dynamics the identification of the scales involved is very important. System created in heavy-ion collision experiments involve four characteristic length scales, *viz.*, the system size ( $L$ ), the inhomogeneity length scale ( $h$ ), the mean free path ( $\lambda_{mfp}$ ) and the range of interaction ( $R$ ), typically a scattering length. These length scales are typically distinguished as follows. A particle suffers collision with the other particle with the typical length scale which is of order of  $R$ . After the collision particle travel freely without suffering another collision over the distance which is of order of  $\lambda_{mfp}$ . Inside the region which is of order of  $h$ , particle suffers many collisions so that the distribution function becomes approximately equilibrium distribution function characterized by local

variables (hydrodynamical fields), namely, temperature (T), chemical potential ( $\mu$ ) and fluid velocity ( $\mathbf{u}$ ). These local variables are functions of space-time and over the larger time interval smooth out across the whole system (L) to reach the global equilibrium. This hierarchy of scales can be written as

$$R \ll \lambda_{mfp} \ll h \ll L \quad (1.3.1)$$

There are two prominent time scales involved which governs the evolution of the fluid from its initial non-equilibrium state. First, there is fast relaxation from initial non-equilibrium state to local equilibrium state which occur over length scale of  $h$ . This regime is governed by *kinetic theory*. Second, there is slow relaxation from local equilibrium to the global equilibrium which occur over region of several  $h$ . This regime is governed by *hydrodynamics*.

### 1.3.1 Relativistic hydrodynamics

In fluid dynamics the response of a fluid to the external perturbations which are slowly varying is governed by conservation laws. The non-relativistic fluids can be described by the fluid velocity ( $\vec{v}(\vec{x}, t)$ ), the pressure ( $P(\vec{x}, t)$ ) and the mass density  $\rho(\vec{x}, t)$ . For non-relativistic fluids, the mass density cannot be correct degree of freedom because it does not account for kinetic energy which certainly becomes comparable to the rest mass energy close to speed of light [19, 20]. Thus, for relativistic fluids mass density is replaced by energy density  $\epsilon(\vec{x}, t)$ . Similarly, velocity ( $\vec{v}(\vec{x}, t)$ ) is replaced by four velocity  $u^\mu$  defined as

$$u^\mu = \frac{dx^\mu}{d\tau} \quad (1.3.2)$$

where,  $\tau$  is the proper time and  $\mu$  is the Lorentz index. In natural units\*\*,  $u^\mu = \frac{1}{\sqrt{(1-\vec{v}^2)}}(1, \vec{v})$  satisfying the condition  $u^\mu u_\mu = 1$ .

---

\*\*  $\hbar = c = \kappa_B = 1$

### 1.3.1.1 Ideal hydrodynamics

The equations governing the dynamics of relativistic fluid can be obtained from the energy-momentum tensor,  $T^{\mu\nu}$ . The energy-momentum tensor for the ideal relativistic fluid can be defined as

$$T_0^{\mu\nu} = (\epsilon + P)u^\mu u^\nu - P g^{\mu\nu} \quad (1.3.3)$$

where,  $g^{\mu\nu}$  is the Minkowski metric<sup>††</sup>. In the local rest frame ( $u^\mu = (1, \vec{0})$ ) energy-momentum tensor takes the form

$$T_0^{\mu\nu} = \text{diag}(\epsilon, P, P, P) \quad (1.3.4)$$

In the absence of external sources the energy-momentum tensor is conserved,

$$\partial_\mu T_0^{\mu\nu} = 0 \quad (1.3.5)$$

One can rewrite Eq. (1.3.3) by defining a projection operator  $\Delta^{\mu\nu} = g^{\mu\nu} - u^\mu u^\nu$ ,

$$T_{(0)}^{\mu\nu} = \epsilon u^\mu u^\nu - p \Delta^{\mu\nu}. \quad (1.3.6)$$

Projecting Eq. (1.3.5) parallel to  $u^\mu$  we get

$$u_\nu \partial_\mu T_{(0)}^{\mu\nu} = (\epsilon + p) \partial_\mu u^\mu + u^\mu \partial_\mu \epsilon = 0 \quad (1.3.7)$$

and projecting the same equation perpendicular to  $u^\mu$  we get

$$\Delta_\nu^\alpha \partial_\mu T_{(0)}^{\mu\nu} = (\epsilon + p) u^\mu \partial_\mu u^\alpha - \Delta^{\mu\alpha} \partial_\mu p = 0 \quad (1.3.8)$$

One can recast Eqs. (1.3.7) and (1.3.8) as

$$D\epsilon + (\epsilon + p) \partial_\mu u^\mu = 0 \quad (1.3.9)$$

$$(\epsilon + p) D u^\alpha - \nabla^\alpha p = 0. \quad (1.3.10)$$

---

<sup>††</sup> $g^{\mu\nu} = \text{diag}(1, -1, -1, -1)$

where we have defined  $D \equiv u^\mu \partial_\mu$  and  $\nabla^\alpha \equiv \Delta^{\mu\alpha} \partial_\mu$ . Eq. (1.3.9) is the relativistic generalization of fluid continuity equation, while Eq. (1.3.10) is the relativistic generalization of Euler fluid equation.

### 1.3.1.2 Viscous hydrodynamics

The fluids found in nature do not respond to the external perturbations equally. There are fluids which support complicated flow patterns which dissipate over the time. The dissipation may occur very quickly or very slowly. If the dissipation occur slowly we call it good fluid as opposed to poor fluid where the dissipation occur so quickly that they do not support patterns like waves or eddies. The physical quantity which distinguishes good fluid from poor fluid is the viscosity. Viscosity causes the dissipation which convert part of the kinetic energy of the flow into heat. The dissipative effects of the viscosity can be incorporated in the hydrodynamics by defining the energy-momentum tensor of the form

$$T^{\mu\nu} = T_{(0)}^{\mu\nu} + \Pi^{\mu\nu}, \quad (1.3.11)$$

where  $T_{(0)}^{\mu\nu}$  is our old ideal energy-momentum tensor and  $\Pi^{\mu\nu}$  incorporate effects of viscous dissipation. Taking appropriate projections of conservation equations as discussed in the case of ideal hydrodynamics, one can obtain fundamental equations for relativistic viscous hydrodynamics as [19]

$$\begin{aligned} D\epsilon + (\epsilon + p)\partial_\mu u^\mu - \Pi^{\mu\nu}\nabla_{(\mu}u_{\nu)} &= 0, \\ (\epsilon + p)Du^\alpha - \nabla^\alpha p + \Delta_\nu^\alpha \partial_\mu \Pi^{\mu\nu} &= 0. \end{aligned} \quad (1.3.12)$$

Now, the entropy current in equilibrium can be defined as

$$s^\mu = su^\mu \quad (1.3.13)$$

The covariant form of second law of thermodynamics is

$$\partial_\mu s^\mu \geq 0 \quad (1.3.14)$$

Using thermodynamical relation (at zero chemical potential)  $\epsilon + P = Ts$ , Eq. (1.3.14) can be written as

$$\partial_\mu s^\mu = Ds + s\partial_\mu u^\mu = \frac{1}{T}D\epsilon + \frac{\epsilon + p}{T}\partial_\mu u^\mu = \frac{1}{T}\Pi^{\mu\nu}\nabla_{(\mu}u_{\nu)} \geq 0, \quad (1.3.15)$$

One can separate traceless part from  $\Pi^{\mu\nu}$  to write

$$\Pi^{\mu\nu} = \pi^{\mu\nu} + \Delta^{\mu\nu}\Pi \quad (1.3.16)$$

Thus, the entropy conservation law becomes

$$\partial_\mu s^\mu = \frac{1}{2T}\pi^{\mu\nu}\nabla_{\langle\mu}u_{\nu\rangle} + \frac{1}{T}\Pi\nabla_\alpha u^\alpha \geq 0. \quad (1.3.17)$$

where,  $\nabla_{\langle\mu}u_{\nu\rangle} \equiv 2\nabla_{(\mu}u_{\nu)} - \frac{2}{3}\Delta_{\mu\nu}\nabla_\alpha u^\alpha$ . Above inequality can be satisfied if traceless part  $\pi^{\mu\nu}$  is proportional to  $\nabla_{\langle\mu}u_{\nu\rangle}$  and non-vanishing trace part is proportional to  $\nabla_\alpha u^\alpha$ . Thus,

$$\pi^{\mu\nu} = \eta\nabla^{\langle\mu}u^{\nu\rangle}, \quad \Pi = \zeta\nabla_\alpha u^\alpha, \quad (1.3.18)$$

with  $\eta \geq 0$  and  $\zeta \geq 0$ . In the non-relativistic limit, spatial part of viscous stress tensor can be written as

$$\Pi^{ki} = -\eta \left( \frac{\partial v^i}{\partial x^k} + \frac{\partial v^k}{\partial x^i} - \frac{2}{3}\delta^{ki}\frac{\partial v^l}{\partial x^l} \right) - \zeta \delta^{ik}\frac{\partial v^l}{\partial x^l} \quad (1.3.19)$$

where, (i, k, l) are the spatial indices and  $\eta, \zeta$  are the shear and bulk viscosity coefficients respectively.

## 1.3.2 Transport coefficients: Shear and bulk viscosities

### 1.3.2.1 Physics of shear and bulk viscosities

In the fluid dynamics the shear and bulk viscosities govern the dissipative effects where a part of initial kinetic energy of flow converts into heat energy. Conversion of mechanical energy into heat (whence generation of entropy) is directly



Figure 1.3: Origin of shear and bulk viscosities.

proportional to these viscosity coefficients [21]

$$\frac{dE_{mech}}{dt} = -\frac{\eta}{2} \int d\mathbf{x} \left( \frac{\partial v^i}{\partial x^k} + \frac{\partial v^k}{\partial x^i} - \frac{2}{3} \delta_{ik} \nabla \cdot \mathbf{v} \right)^2 - \zeta \int d\mathbf{x} (\nabla \cdot \mathbf{v})^2 \quad (1.3.20)$$

It is not difficult to understand the mechanism of dissipations in the systems as a response to external perturbations. Fig. (1.3) shows the response of the system when subjected to shear stress and uniform compression (or rarefaction). When the fluid is subjected to tangential force the velocity gradients sets up in the fluid. If we imagine a fluid to be composed of parallel layers as shown by blue arrows in the left part of Fig. (1.3) where the direction of the arrows indicate the fluid flow (velocity), while the length of arrows indicate the velocity gradient. Thus, there exist a frictional force ( $F$ ) between adjacent layers of the fluid which turns out to be proportional to velocity gradients ( $\nabla_i u^j$ ,  $i \neq j$ ) where the proportionality constant is independent of velocities and is a measure of dissipation in the fluid and hence fluidity. This is the coefficient of shear viscosity ( $\eta$ ).

Now if the external perturbations are of the form which do not change the shape of the fluid, e.g uniform compression or rarefaction, then the mechanism of the energy dissipation is quite different. If the system is uniformly compressed it leaves equilibrium where the energy density rises but pressure rises by an amount larger than that predicted by equation of state ( $P(\epsilon)$ ). This non-equilibrium pressure is given by

$$P = P_{equi} - \zeta \nabla \cdot \mathbf{u} \quad (1.3.21)$$

where  $\mathbf{u}$  is flow velocity and  $P_{\text{equi}}$  is equilibrium pressure.  $\zeta$ , also called as the bulk viscosity, quantifies (time integral of) extra shift in the pressure. Since  $\zeta$  raises or lowers the pressure in the radial direction, it affects the radial flow in the fluid (right part of Fig. (1.3)).

It may be tempting to conclude that these viscosity coefficients can be measure of fluidity. But the experimental values of viscosity coefficients of water, liquid helium, cold atomic gases and quark-gluon matter vary by order of magnitudes in spite of fact that all of them are termed as good fluids. In order to establish true measure of fluidity we need to invoke hydrodynamical description of the fluid governed by Navier-Stokes equations. In hydrodynamics, the Reynolds number, which is ratio of inertial to viscous force, determines the behavior of the solution of Navier-Stokes equations. This dimensionless number actually characterize the fluidity and large Reynolds number corresponds to good fluids. The Reynolds number is defined as

$$Re = \left( \frac{mn}{\eta} \right) uL \quad (1.3.22)$$

where,  $n$  is the number density,  $u$  is characteristic velocity and  $L$  is characteristic length scale of flow. Since  $Re$  is dimensionless ratio  $\eta/n$  should have dimension of  $muL$ , i.e angular momentum, which can be measured in units of  $\hbar$ . Thus for non-relativistic fluids ratio  $\eta/(\hbar n)$  is the measure of fluidity. For relativistic fluids where the particle number is not conserved, measure of fluidity is ratio  $\eta/s$ , where  $s$  is the entropy density. In this thesis we will focus on the computation and estimation of ratios  $\eta/s$  and  $\zeta/s$  of strongly interacting matter at finite temperature as well as baryon density.

### 1.3.2.2 The status of transport coefficients in the context of heavy-ion collisions

Transport properties like shear and bulk viscosities enter in the hydrodynamical evolution governed by hydrodynamical equations (Eqs. 1.3.12) and therefore essential for studying the near equilibrium evolution of a thermodynamic system.

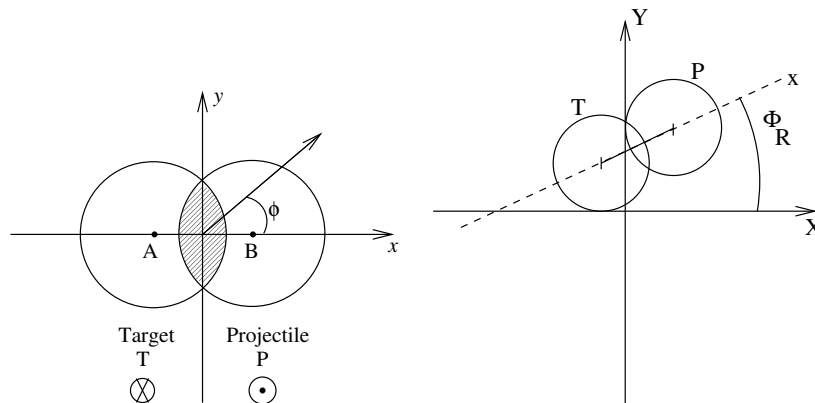


Figure 1.4: Collision or beam axis is perpendicular to the plane of the figure. Impact parameter  $b = \text{length AB}$ .  $z$  is the longitudinal direction,  $xy$  is the transverse or azimuthal plane,  $xz$  is the reaction plane, and  $\phi$  is the azimuthal angle of one of the outgoing particles and  $\Phi_R$  is reaction plane angle. Figure has been taken from Ref. [1].

In the context of heavy ion collisions, the coefficient of shear viscosity perhaps has been the mostly studied transport coefficient. The spatial anisotropy in a nuclear collision gets converted to a momentum anisotropy through a hydrodynamic evolution. As we have discussed earlier, in non-central heavy ion collision the geometry of initial thermalised plasma is almond shaped but the momentum distribution of the particle is almost uniform. This initial spatial anisotropy can potentially affect the momentum anisotropy of final state particles. For this purpose, it is customary to Fourier decompose the triple differential invariant distribution of the particles in the final state as [22]

$$E \frac{d^3 N}{d^3 p} = \frac{d^3 N}{p_T dp_T dy d\phi} = \frac{d^2 N}{p_T dp_T dy} \frac{1}{2\pi} \left\{ 1 + \sum_1^{\infty} 2v_n \cos n(\phi - \Phi_R) \right\} \quad (1.3.23)$$

where  $\phi$  is the azimuthal angle and  $\Phi_R$  is reaction plane angle as shown in Fig.1.4. The first two harmonic coefficients  $v_1$  and  $v_2$  are called directed and elliptic flow coefficients. It is these coefficients that carry information regarding momentum anisotropy of final state particles and the equilibration of momentum anisotropy is mainly controlled by shear viscosity coefficient.

The elliptic flow measurement at RHIC led to  $\eta/s$ , the ratio of shear viscosity ( $\eta$ ) to the entropy density  $s$ , close to  $1/(4\pi)$  which is the smallest for any

known liquid in nature [23]. Indeed, arguments based on ADS/CFT correspondence suggest that the ratio  $\eta/s$  cannot be lower than this 'Kovtun-Son-Starinets' (KSS) bound [24]. Thus the quark gluon plasma (QGP) formed in the heavy ion collision is the most perfect fluid.

In the context of HICs the transport coefficient that relates the momentum flux with a velocity gradient is the bulk viscosity. Generally, it was earlier believed that the bulk viscosity does not play any significant role in the hydrodynamic evolution of the matter produced in heavy ion collision experiments. The argument being that the bulk viscosity  $\zeta$  scales like  $\epsilon - 3p$  and therefore will not play any significant role as the matter might be following the ideal gas equation of state. However, in the course of the expansion of the fire ball the temperature can be near the critical temperature  $T_c$  where  $\epsilon - 3p$  can be large as expected from the lattice QCD simulations [15, 25] leading to a large value for the bulk viscosity. This, in turn, can give rise to phenomenon of cavitation when the pressure vanishes and the hydrodynamic description for the evolution breaks down [26]. Indeed, during last couple of years, there have been quite a few attempts to investigate the effects of the bulk viscosity on the hydrodynamic evolution of hot matter following a heavy ion collision and have found effects on particle spectra as well as flow coefficients [27–29]. The interplay of shear and bulk viscosity on the elliptic flow has also been looked into in Ref. [30] as well as more recently in Ref [31, 32]. Bulk viscosity effects from the hadronic phase on the transverse momentum spectra and elliptic flow has been investigated in Ref [33]. Further, a large bulk viscosity appear to be essential to explain the flow harmonics in ultra central collisions [34].

There have been various attempts to estimate coefficients of bulk viscosity ( $\zeta$ ) for strongly interacting matter. The rise of bulk viscosity coefficient near the transition temperature has been observed in various effective models of strong interaction. These include chiral perturbation theory [35], quasi particle models [36] as well as Nambu-Jona-Lasinio model [37]. One of the interesting ways to extract this coefficient is using symmetry properties of QCD once one realizes that the bulk viscosity characterizes the response to conformal transformation.

According to Kubo's formula bulk viscosity can be expressed as bi-local correlator of the trace of energy momentum tensor. Since trace vanishes for conformally symmetric systems non-zero bulk viscosity implies violation of the conformal symmetry. This was attempted in Ref. [38]. Based on Kubo formula for  $\zeta$  and the low energy theorems [39], the coefficients of bulk viscosity gets related to thermodynamic properties of strongly interacting system.

It may be noted that it is also of both practical and fundamental importance to know the transport coefficients in the hadron phase to distinguish the signatures of QGP matter and hadronic matter. The computation of the transport coefficient of the hadronic mixture is not an easy task. There have been various attempt on this field over last few years involving various approximations like relaxation time approximation, Chapman-Enskog as well as Green Kubo approach to estimate the shear viscosity to entropy ratio using different effective models for hadronic interactions [35, 37, 40–43]. This apart, there have been attempts to estimate the transport coefficients using transport codes. The shear viscosity to entropy ratio in the hadronic phase has been estimated using UrQMD transport code in Ref. [44]. Both the bulk as well as the shear viscosity to entropy ratio has also been estimated using parton hadron string dynamics (PHSD) transport code within a relaxation time approximation [45].

In a different approach,  $\eta/s$  has also been calculated within a hadron resonance gas model in an excluded volume approximation [46] with a molecular kinetic theory approach to relate shear viscosity coefficient to the average momentum transfer. This was used later to include the effects of rapidly rising hadronic density of states near the critical temperature modeled by Hagedorn type exponential rise of density of states [47]. Such a description could describe the lattice data and indicated that the hadronic matter could become almost a perfect fluid where  $\eta/s$  could approach the KSS bound. Later lattice data which, however, indicated a lower pseudo-critical temperature about 160 MeV led to the assertion that the hot hadronic matter described through hadron resonance gas is far from being a perfect fluid [48]. All these studies have been done at zero baryon density.

It has been also known that the basic features of hadronization in heavy ion collisions are well described by the hadron resonance gas models. The multiplicities of particle abundances of various hadrons in these experiments show good agreement with the corresponding thermal abundances calculated in HRG with appropriately chosen values for the temperature and the chemical potentials [49]. In present thesis work we have attempted to studying viscosity coefficients within the ambit of hadron resonance gas model to include finite chemical potential effects. This can possibly have some relevance on the current and planned experiments with heavy ion collisions at beam energy scan at RHIC, Facility for Antiproton and Ion Research (FAIR) and Nuclotron-based Ion Collider fAcility (NICA) at Dubna.

The shear viscosity to entropy ratio at finite baryon density has been estimated using relativistic Boltzmann equations for pion nucleon system using phenomenological scattering amplitude [50]. This leads to the ratio as a decreasing function of chemical potential in the  $T$ - $\mu$  plane. Further, this ratio as a function of chemical potential shows a valley structure at low temperature which was interpreted as a signature of liquid gas phase transition [50]. This has also been studied using an effective nucleon pion system for nuclear matter [51]. Here, the ratio seem to reduce both with temperature as well as chemical potential.

The bulk viscosity at finite chemical potential using low energy theorems of QCD has been studied in Ref. [52]. This was estimated using a Schwinger-Dyson approach to calculate the dressed quark propagator at finite chemical potential to use it for calculation of thermo dynamical quantities needed to estimate bulk viscosity.

## 1.4 Organization of the thesis

The thesis is organized as follows:

After brief introduction in Chapter 1, we introduce the hadron resonance gas model (HRG) in Chapter 2 as an effective model describing the hadronic phase of QCD. We discuss the equation of state of HRG model and its reliability to

describe the hot and dense hadronic matter by confronting it with existing first principle lattice QCD simulations. Because the non-interacting HRG model has certain limitations when certain aspects of strongly interacting matter are concerned, we make possible improvements in ideal HRG model so as to incorporate these aspects without losing simplicity and success of HRG model.

In Chapter 3 we discuss the transport properties of hadronic matter using two formalisms, *viz.*, Kubo's formalism and the relativistic kinetic theory. After deriving basic formulas for transport coefficients in these formalisms we estimate them within ambit of HRG model and its extensions. Further, we make connection of these transport coefficients with the heavy-ion collision experiments.

In Chapter 4 we discuss the the transport properties of quark matter using relativistic kinetic theory within ambit of Nambu-Jona-Lasinio model.

Finally, in Chapter 5, we summarize the results and also discuss the scope for further studies.



# Chapter 2

## Thermodynamics of hadron resonance gas model

### 2.1 Hadron resonance gas model

#### 2.1.1 Non interacting hadron resonance gas model

The hadronic phase of quantum chromodynamics at low temperature ( $T$ ) and zero baryon density ( $\mu_B$ ) is essentially consist of pions ( $\pi^0, \pi^\pm$ ), while at higher temperature and baryon density, it consist other light mesons ( $K, \eta, \eta'$ ) and heavy baryons apart from pions which interact with each other via residual strong force. So, any effective model of the strong interaction describing hadronic matter should account for all the mesonic and baryonic degrees of freedom with appropriate form of interactions. The hadron resonance gas model (HRG) is the simplest effective model of QCD describing the hadronic matter. It rests on the premise that the interacting hadron resonance matter can be approximated by that of non-interacting gas of hadrons and all the resonances [53]. Thus, the hadron resonance gas model can be defined by summed partition function

$$\ln Z(T, \mu, V) = \int dm [\rho_M(m) \ln Z_M(m, V, T, \mu) + \rho_B(m) \ln Z_B(m, V, T, \mu)] \quad (2.1.1)$$

where the gas of hadrons is contained within volume  $V$ , at a temperature  $T$  and chemical potential  $\mu$ .  $Z_M$  and  $Z_B$  are the partition functions of mesons and baryons respectively with mass  $m$ . Further,  $\rho_M$  and  $\rho_B$  are corresponding spectral densities and  $\ln Z_{M,B}$  is the partition functions corresponding to mesons and baryons,

$$\ln Z_{M,B}(m, V, T, \mu) = \pm \frac{1}{V} \int \frac{d^3p}{2\pi^3} \ln(1 \pm \exp[-(E - \mu)/T]) \quad (2.1.2)$$

Before one is able to use the partition function (2.1.1) to compute the thermodynamical quantities, it is necessary to know the form of spectral densities which contain the properties of hadrons. One accustomed approach in an ideal HRG model is to take all the hadrons and their resonances up to a mass cutoff  $\Lambda$  such that

$$\rho_{B/M}(m) = \sum_a^{M_a < \Lambda} g_a \delta(m - M_a) \quad (2.1.3)$$

where the sum is over all the hadrons and resonances states up to a mass cut off  $\Lambda$ .  $M_a$  are the masses of all the experimentally established hadrons and  $g_a$  is corresponding degeneracy factor (spin, isospin etc.).

Using partition function given by Eq. (2.1.1) together with discrete mass spectrum defined by Eq. (2.1.3), it is straightforward to compute all the thermodynamical quantities. Pressure ( $P$ ), baryon number density ( $n_B$ ), entropy density ( $s$ ), energy density ( $\epsilon$ ) and speed of sound ( $C_s^2$ ) are calculated as:

$$\begin{aligned} P(T, \mu) &= \lim_{V \rightarrow \infty} \frac{T}{V} \ln Z(T, \mu, V) \\ &= \sum_a \frac{g_a}{6\pi^2} \int_0^\infty dp \frac{p^4}{E_a} \frac{1}{\exp[(E_a - \mu)/T] \pm 1} \end{aligned} \quad (2.1.4)$$

$$\begin{aligned} n_B(T, \mu) &= \left. \frac{\partial P(T, \mu)}{\partial \mu} \right|_T \\ &= \sum_a \frac{g_a}{2\pi^2} \int_0^\infty dp \frac{p^2}{\exp[(E_a - \mu)/T] + 1} \end{aligned} \quad (2.1.5)$$

$$\begin{aligned}
s(T, \mu) &= \left. \frac{\partial P(T, \mu)}{\partial T} \right|_{\mu} \\
&= \sum_a \frac{g_a}{2\pi^2} \int_0^\infty dp p^2 \left\{ \ln(1 \pm \exp[-(E_a - \mu)/T]) \right. \\
&\quad \left. \pm \frac{(E_a - \mu)}{T(\exp[(E_a - \mu)/T] + 1)} \right\} \tag{2.1.6}
\end{aligned}$$

$$\begin{aligned}
\epsilon(T, \mu) &= Ts - P + \mu n_B \\
&= \sum_a \frac{g_a}{2\pi^2} \int_0^\infty dp E_a \frac{p^2}{\exp[(E_a - \mu)/T] \pm 1} \tag{2.1.7}
\end{aligned}$$

$$C_s^2 = \frac{dP(T, \mu)}{d\epsilon(T, \mu)} \tag{2.1.8}$$

where,  $E_a = \sqrt{p^2 + M_a^2}$  is the free particle dispersion relation. For relativistic gas of hadrons there will be contribution of antiparticles also.

LQCD which acts as a benchmark for any effective model of QCD also constrain the equation of state predicted by it. It has been observed that the HRG model with only hadrons and resonances up to certain mass cut-off can describe the lattice data up to  $T \sim 0.140$  GeV. But, if one extend the HRG model by including exponentially increasing mass spectrum above 2 GeV, this extended HRG agrees with LQCD up to  $T \sim 0.155$  GeV [54]. Such exponentially rising mass spectrum of form  $\rho(m) = m^{-\frac{5}{2}} e^{\frac{m}{T_H}}$  was first proposed by Hagedorn back in 1965 [55] to explain the experimental data of multi-particle production in proton-proton collisions. In (2+1) flavor QCD one can take all the hadrons and resonances up to 2 GeV. One can then extend this model by taking continuum mass spectrum. Such hybrid HRG model can be defined by the spectral density of the form

$$\rho(m) = \rho_{B/M}(m) + \rho_{conti}(m) \tag{2.1.9}$$

where  $\rho_{B/M}(m)$  is the discrete part of spectral density given by Eq. (2.1.3) and

$\rho_{conti}(m)$  is the continuum part. We shall consider two forms for the continuum part of the spectral density given as

$$\rho_{conti}^{exp}(m) = \frac{A_1}{(m^2 + m_0^2)^{\frac{5}{2}}} e^{\frac{m}{T_H}} \quad (2.1.10)$$

and

$$\rho_{conti}^{power}(m) = \frac{A_2}{T_H} \left( \frac{m}{T_H} \right)^\alpha \quad (2.1.11)$$

The exponential density of states satisfy statistical bootstrap condition\* and reflects the underlying string picture of hadrons, while the power law spectrum do not satisfy bootstrap condition but provides an alternative to describe the rapid rise of density of states at high temperature. The parameters in Eqs. (2.1.10) and (2.1.11) are specified so as to reproduce the lattice QCD results.

With the spectral density defined by Eq. (2.1.9) pressure of the gas of mesons and baryons can be obtained as:

$$P_M = \frac{1}{2\pi^2} \left[ - \sum_a g_a \int p^2 dp \ln(1 - \exp(-E_a/T)) + \int_\Lambda^\infty \rho_{conti}(m) dm m^2 T^2 K_2(m/T) \right], \quad (2.1.12)$$

$$P_B = \frac{1}{2\pi^2} \left[ - \sum_a g_a \int p^2 dp \left( \ln(1 - \exp(-(E_a - \mu)/T)) + \ln(1 - \exp(-(E_a + \mu)/T)) \right) + 2 \int_\Lambda^\infty \rho_{conti}(m) dm m^2 T^2 K_2(m/T) \cosh(\mu/T) \right]. \quad (2.1.13)$$

Other thermodynamical quantities can be obtained using thermodynamical relations (2.1.4)-(2.1.8).

To estimate different thermodynamic quantities using HRG model, for the discrete part of the spectral density in Eq. (2.1.9), we take all the hadrons and their resonances with mass up to the cutoff 2 GeV [56]. Specifically, for baryons

---

\*In the statistical bootstrap model hadron is considered to be made of 2 or 3 constituent which freely roam within volume V. Density of states of each hadron should be consistent with that of constituent which themselves are hadrons.

the mass cut-off is 2.252 GeV while for mesons it is 2.011 GeV. The parameters defining the continuum part of the spectral density are given in Table 2.1.

$\rho$	$T_H(\text{GeV})$	$A_1$	$A_2$	$m_0(\text{GeV})$	$\alpha$
$\rho_{exp}$	0.210	0.63 ( $\text{GeV}^{3/2}$ )	-	0.5	-
$\rho_{power}$	0.180	-	0.51	-	3

Table 2.1: Parameters defining continuum density of states.

Fig. (2.1) shows scaled pressure as a function of temperature at two different values of baryonic chemical potential,  $\mu = 0$  and  $\mu = 0.3$  GeV. The lattice points with the error bars have been taken from Table 4 of Ref. [57] corresponding to the continuum extrapolation. The dotted lines in Fig. (2.1) correspond to considering only the discrete part of the spectral density in Eq. (2.1.9). Left panel corresponds to exponential form of spectral density for continuum part while right panel corresponds to power law form of spectral density. As can be noted in this figure, at  $\mu = 0$ , the discrete spectrum coupled with continuum spectrum describes the lattice data quite well up to  $T = 170$  MeV with the parameterization given in Table 2.1 within the error bars of the lattice simulations, while at finite  $\mu$ , HRG with only discrete spectrum is sufficient to describe the lattice data over wide range of temperatures.

In Fig. 2.2 we have plotted the dimensionless scale anomaly  $(\epsilon - 3p)/T^4$  as a function of temperature at two different chemical potentials. As can be noted from both the Figs. (2a) and (2b), the discrete part of the spectral density does not give a good fit to the lattice data beyond 0.140 GeV for zero chemical potential, but when coupled with continuum part as in Eq.(2.1.10) gives good fit to lattice data up to 0.150 GeV. It is also observed that, for higher chemical potential, the range of the trace anomaly that can be described including the Hagedorn states diminishes. The lattice data for the trace anomaly for  $\mu=0.3$  GeV could be described by the hadron gas alone up to  $T= 0.160$  GeV while including the Hagedorn states, the same could be described up to  $T= 0.150$  GeV within the error bars of the lattice calculations. This could be an artifact of the assumption of having the same spectral density for mesons and baryons.

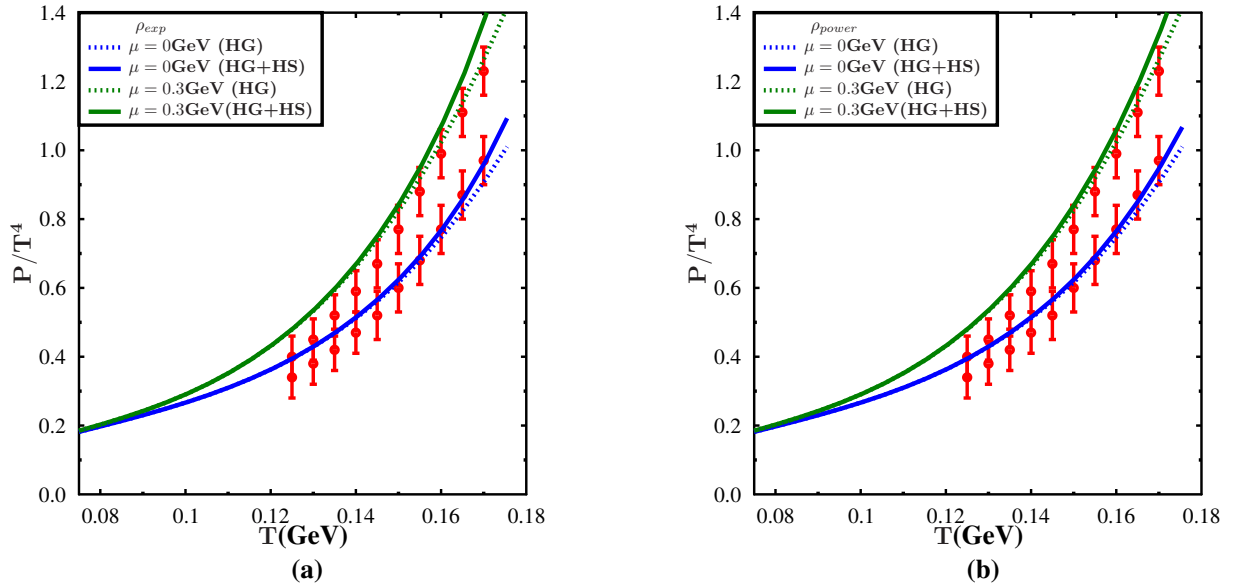


Figure 2.1: Thermodynamics of hadron resonance gas. Left panel (a) shows scaled pressure as a function of temperature for  $\mu = 0$  (blue) and  $\mu = 0.3$  GeV (green) with the exponential Hagedorn spectrum given by Eq. (2.1.10). The dotted line corresponds to discrete spectrum for hadron resonance gas. The right panel shows the same quantities but with the power law spectrum as given in Eq. (2.1.11).

However, while making this observation, it ought to be kept in mind that the lattice data of Ref. [57] is estimated at order  $\mu^2$ . We have taken a higher  $T_H$  value compared to Ref. [48] that was required to fit the lattice data [57]. This is because, in Ref. [48], the lattice data was taken for  $N_t = 10$  lattice data of Ref. [58] while we have fitted with the continuum extrapolation of for  $\mu = 0$  the lattice data in Ref. [57].

Fig 2.3 shows speed of sound squared ( $C_s^2$ ) as a function of temperature at fixed values of chemical potential along with the lattice simulation results. As can be noted from the figure, keeping only the discrete part of the spectral density, does not fit the lattice results although the same could fit the lattice result for pressure and the scale anomaly results. On the other hand the power law parameterization for the continuum part of spectral density along with the discrete part leads to a reasonable fit to lattice data up to 0.150 GeV both at  $\mu = 0$  and

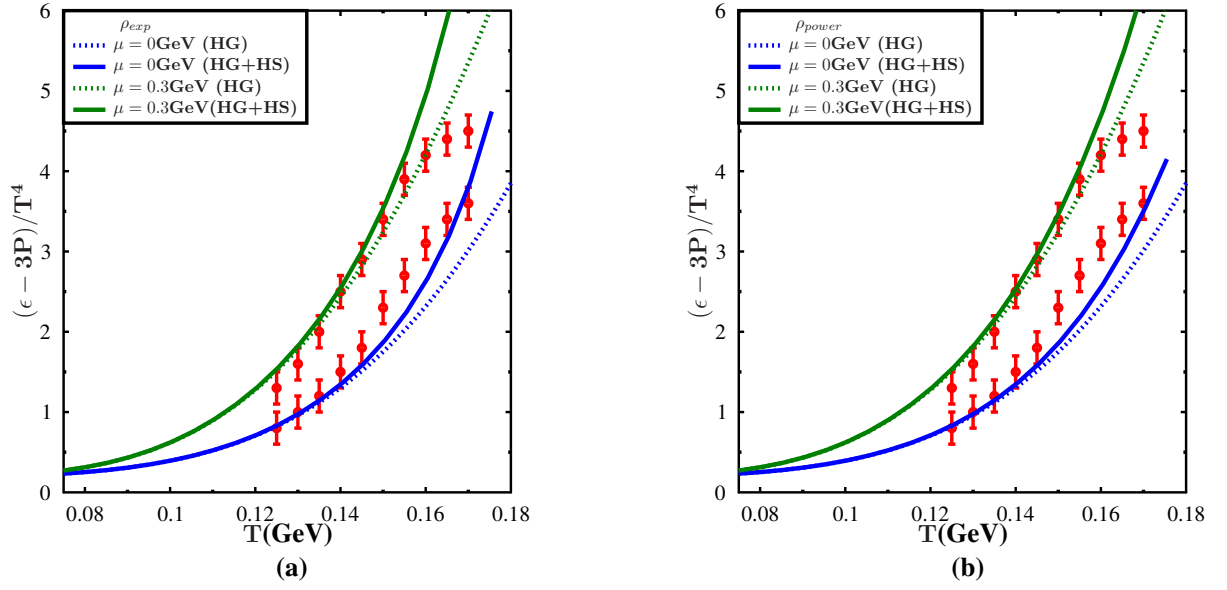


Figure 2.2: Trace anomaly of HRG with and without inclusion of Hagedorn density of states at two different chemical potentials.

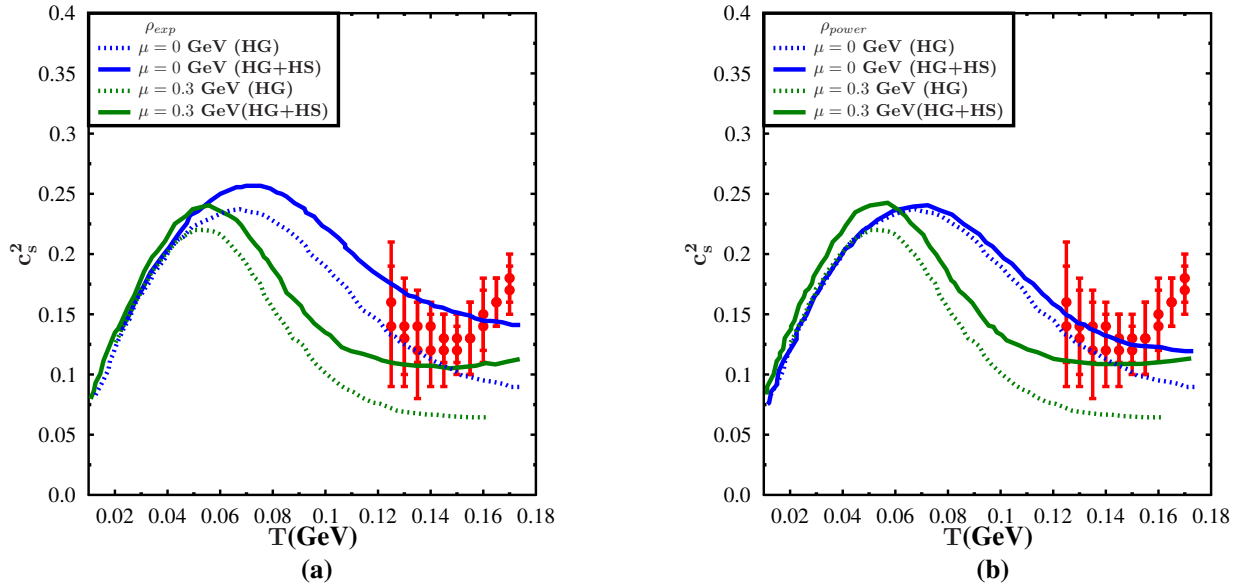


Figure 2.3: Speed of sound in HRG with and without inclusion of Hagedorn density of states at two different chemical potentials.

$\mu = 0.3$  GeV. The initial rise in sound velocity with temperature is reflection of the fact that the light degrees of freedom are excited easily at low temperature and contribute to pressure and energy. But at larger temperatures when baryons are excited, they contribute significantly to energy density but almost nothing to pressure. This leads to decrease of sound velocity with temperature seen at higher temperatures ( $T > 0.08$  GeV). As chemical potential increases, heavier baryonic channels opens up at low temperature and contribute to energy density significantly but nothing to pressure. This leads to lower values of  $C_s^2$  as the chemical potential is increased.

### 2.1.2 Excluded volume hadron resonance gas model

Albeit non-interacting HRG model agrees with LQCD for wide range of temperatures, it misses one important feature of hadronic interactions; the repulsive interactions. It has been conformed experimentally that the nucleons undergo short-range repulsive interactions and hence one can attribute them with small hard-core radius based on N-N scattering data. Further necessity to include short range repulsive interaction comes from heavy ion collision experiments. It has been observed that the chemical freeze-out parameters ( $T_{freezeout}, \mu_{freezeout}$ ) obtained from fitting the particle number ratios at AGS and SPS energies lead to large values of total particle number densities. The total particle number density at the chemical freeze-out within non-interacting HRG is  $n \approx 4n_0$  for the AGS and  $8n_0$  for the SPS,  $n_0$  being the normal nuclear density. To suppress large values of particle number densities, Van-der-Waals inspired excluded volume procedure is used, which is elegant way to account for short range repulsive in interactions. While there are many ways in which one can introduce the volume corrections in non-interacting HRG model, we will describe the thermodynamically consistent excluded volume formulation [59].

Consider a gas of (single species of) hadrons at temperature ( $T$ ) and baryon chemical potential ( $\mu$ ). The pressure is related to grand partition function by

Eq. (2.1.4). The grand partition function for an ideal gas can be defined as

$$Z(T, \mu, V) = \sum_{N=0}^{\infty} e^{\frac{\mu N}{T}} \mathcal{Z}(T, N, V) \quad (2.1.14)$$

If the hadrons are assumed to be hard spheres of radius  $r_h$ , the available volume for hadrons is just a reduced volume  $V - vN$ . Here,  $v$  is the parameter which fix the volume excluded by pair of hadrons. Thus, the partition function (2.1.14) becomes

$$Z^{EV}(T, \mu, V) = \sum_{N=0}^{\infty} e^{\frac{\mu N}{T}} \mathcal{Z}(T, N, V - vN) \theta(V - vN) \quad (2.1.15)$$

Since the available volume is depends on varying number of particles the sum is difficult to compute. This difficulty can be overcame by taking Laplace's transform of Eq. (2.1.15).

$$\begin{aligned} \tilde{Z}^{EV}(T, \mu, y) &= \int_0^{\infty} dV e^{-yV} Z^{EV}(T, \mu, V) \\ &= \sum_{N=0}^{\infty} \int_0^{\infty} dV e^{-yV} e^{\frac{\mu N}{T}} \mathcal{Z}(T, N, V - vN) \\ &= \sum_{N=0}^{\infty} \int_0^{\infty} d\tilde{V} e^{-y\tilde{V}} e^{\frac{\tilde{\mu} N}{T}} \mathcal{Z}(T, N, \tilde{V}) \\ &= \int_0^{\infty} d\tilde{V} e^{-y\tilde{V}} Z(T, \tilde{\mu}, \tilde{V}) \end{aligned} \quad (2.1.16)$$

where, we have used Eq. (2.1.15). Further, we have defined new variables,  $\tilde{\mu} = \mu - vTy$  and  $\tilde{V} = V - vN$ . From the definition of pressure (Eq. (2.1.4))  $Z$  approaches (in the limit  $V \rightarrow \infty$ )

$$Z(T, \mu, V) \xrightarrow{V \rightarrow \infty} \exp\left[\frac{P(T, \mu)V}{T}\right] \quad (2.1.17)$$

Thus, the integrand in Eq. (2.1.16) diverge at its upper limit if  $y < \frac{P}{T}$ . Thus,  $\tilde{Z}^{EV}$  has an extreme right singularity at some point  $y^*$ . This extreme right

singularity gives system pressure,

$$P^{EV}(T, \mu) = Ty^*(T, \mu) \quad (2.1.18)$$

Since  $\tilde{Z}^{EV}$  has only one singular point, i.e when integral over  $y$  in Eq. (2.1.16) diverge at its upper limit, we get

$$y^* = \lim_{y \rightarrow \infty} \frac{\ln Z(T, \tilde{\mu}^*, y)}{y} \quad (2.1.19)$$

where,  $\tilde{\mu}^* = \mu - vTy^*$ . Finally, using Eqs. (2.1.4) and (2.1.19) to eliminate  $y^*$  from Eq. (2.1.18) to get transcendental equation for pressure,

$$P(T, \mu) = P_{ideal}(T, \tilde{\mu}) \quad (2.1.20)$$

Once the pressure is known all the thermodynamical quantities can be readily obtained. The number density, energy density and entropy density are

$$n^{EV}(T, \mu) = \sum_a \frac{n_a^{id}(T, \tilde{\mu})}{1 + \sum_a v_a n_a^{id}(T, \tilde{\mu})} \quad (2.1.21)$$

$$\epsilon^{EV}(T, \mu) = \sum_a \frac{\epsilon_a^{id}(T, \tilde{\mu})}{1 + \sum_a v_a n_a^{id}(T, \tilde{\mu})} \quad (2.1.22)$$

$$s^{EV}(T, \mu) = \sum_a \frac{s_a^{id}(T, \tilde{\mu})}{1 + \sum_a v_a n_a^{id}(T, \tilde{\mu})} \quad (2.1.23)$$

The quantity ( $\Gamma^{-1} = 1 + \sum_a v_a n_a^{id}(T, \tilde{\mu}_B)$ ) is the suppression factor typical of any excluded volume model and is always less than one. Thus, any thermodynamical quantity computed within so called excluded volume hadron resonance gas model (EHRG) is always less than that of non interacting HRG model. For the temperature range in which we are interested, the Boltzmann approximation is rather a good approximation. In classical Boltzmann approximation this prescription is equivalent to additional factor of  $\exp(-vP/T)$  to the pressure. Thus, the pressure in excluded volume hadron resonance gas in Boltzmann approximation is

$$P(T, \mu) = \exp(-vP(T, \mu_B)/T)P_{ideal}(T, \mu) \quad (2.1.24)$$

where  $P_{ideal}$  in Boltzmann approximation can be written as

$$P_{ideal}(T, \mu) = \sum_a \frac{g_a}{2\pi^2} M_a^2 T^2 K_2\left(\frac{M_a}{T}\right) \cosh\left(\frac{\mu}{T}\right) \quad (2.1.25)$$

where  $g_a$  is degeneracy of  $a^{th}$  hadron species and  $K_2$  is the modified Bessel's function [60].

### 2.1.3 Hadron resonance gas model with medium dependent hadron masses

Since HRG is a statistical model, the essential starting point is to find the partition function which in this case is just the partition function of an ideal gas summed over all the hadronic states and their resonances. While calculating the partition function it is the zero temperature (and baryon chemical potential) hadron masses ( $M_h$ ) that enters the Boltzmann factor,  $\text{Exp}(-M_h/T)$ . It is well established fact that the chiral symmetry is an essential feature of QCD, the spontaneous breaking of which is responsible for the large part of the quark mass called constituent quark mass, whence the hadrons. Further, LQCD as well as other effective model calculations at finite temperature shows that this symmetry is restored above so called chiral transition temperature ( $T_c$ ) which renders all the Goldstone modes massless. Thus, since hadrons are made of quarks whose mass depends on temperature and chemical potential, it is  $T$  (and  $\mu$ ) dependent hadron mass that should enter the partition function of HRG before computing any thermodynamical quantity. As we will see, taking into account this effect drastically changes the thermodynamics of hadronic matter at moderately high temperature. Since the HRG model has been used to calculate the transport properties as well, they are also non trivially affected. Thus, it is possible to further improve HRG model further by including temperature and baryon density dependent hadron masses in the partition function. Since it is rather difficult to

obtain  $T$  and  $\mu$  dependent masses of all the hadrons and their resonances except for light mesons, we use the linear scaling rule for mesons and baryons in terms of their constituent quarks [61,62]. Since hadrons are made of either two or three quarks, we write the scaling rule for hadron masses as

$$M_h(T, \mu) = (N_q - N_s)\mathcal{M}_q(T, \mu) + N_s\mathcal{M}_s(T, \mu) + \kappa_h \quad (2.1.26)$$

Here,  $\mathcal{M}$  is the constituent quark mass,  $N_q$  is the number of light quarks in a given hadron and  $N_s$  is the measure of strangeness content of the hadron.  $\kappa_h$  is the constant depends on the state but not on the current quark masses.

We further separate zero temperature and zero density part  $M(T = 0, \mu = 0)$  in Eq. (2.1.26) and absorb  $\kappa_h$  in it to get

$$M_h(T, \mu) = M_h(T = 0, \mu = 0) + (N_q - N_s)\mathcal{M}'_q(T, \mu) + N_s\mathcal{M}'_s(T, \mu) \quad (2.1.27)$$

where  $\mathcal{M}'_{q,s}$  is only medium ( $T$  and  $\mu$ ) dependent part of the constituent quark mass. The scaling rule given by Eq.(2.1.27) is used for all the hadrons but Goldstone mesons. The  $T$  and  $\mu$  dependence of (approximate) Goldstone mesons as well as that of constituent quarks (u,d,s) can obtained using Nambu-Jona-Lasinio (NJL) formalism at finite temperature and density. For general reviews on NJL model, see [63,64].

Above discussion may tempts us to conclude that the non-interacting HRG model is sufficient to describe the hadronic phase of QCD since it is in good agreement with LQCD over wide range of temperatures. But as we discussed in subsection 2.1.3, it is logical necessity to include repulsive interactions as well as temperature and density dependent hadron masses in non-interacting HRG model. It is now interesting to see how the results of ideal HRG model are modified if we include these effects. For that purpose we use the parameter set of Ref. [63] to compute the masses of constituent quarks and light mesons using NJL model which enters in Eq. (2.1.27) to compute  $T$  and  $\mu_B$  dependent hadron masses. The parameter which fixes the excluded volume HRG is the hardcore radius  $r_h$  or the proper volume parameter  $v$ . It is customary in the literature

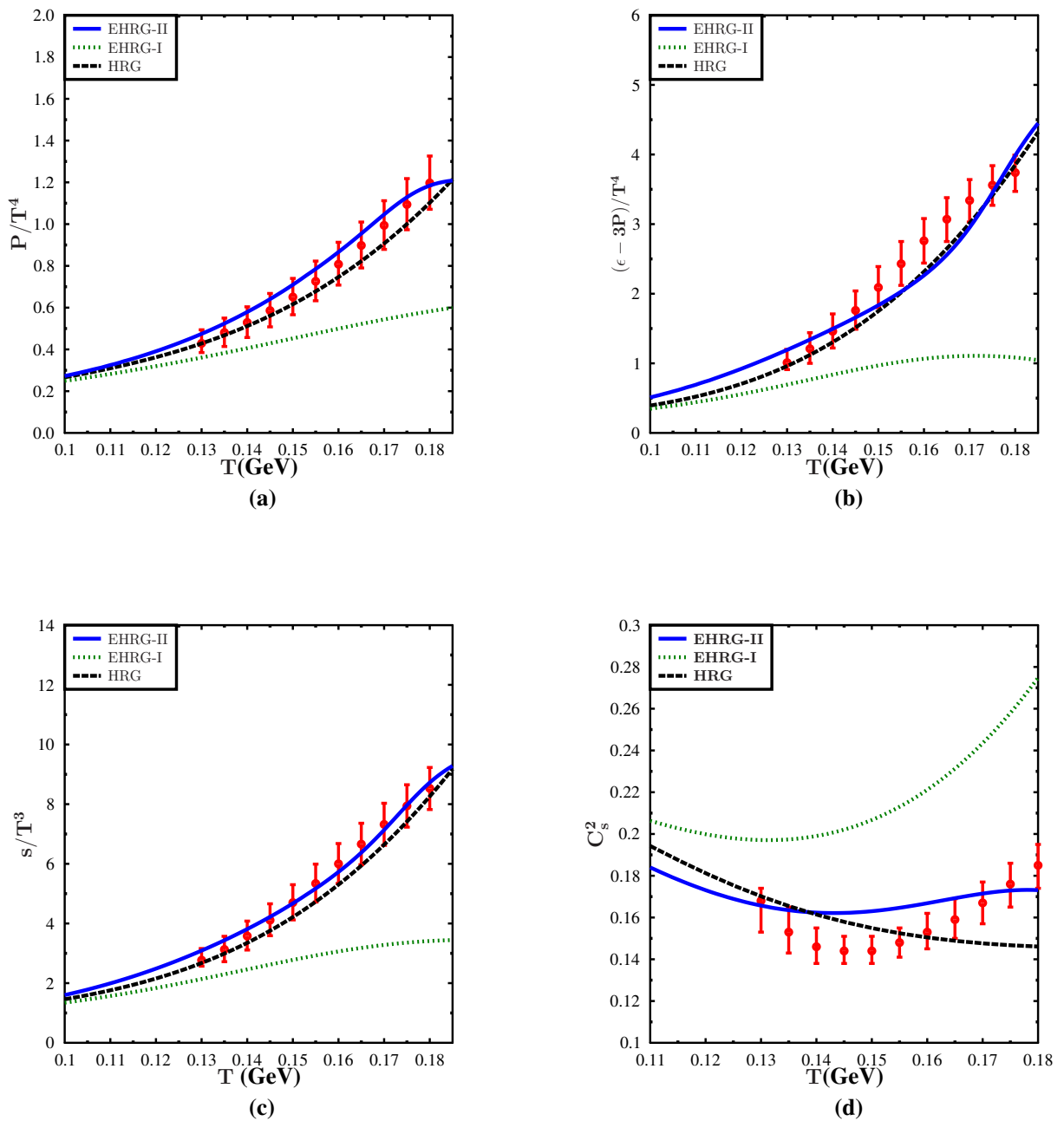


Figure 2.4: Results for thermodynamical quantities at  $\mu = 0$  GeV in EHRG-I and EHRG-II models with the mass dependent excluded volume parametrization. Black dashed curve corresponds to non-interacting hadron resonance gas model.

to use uniform values of hardcore radius for all the hadrons [65, 66]. Baryonic hard core radius can be extracted from the short range repulsive interactions in nucleon-nucleon scattering processes. While it is legitimate to set hard core

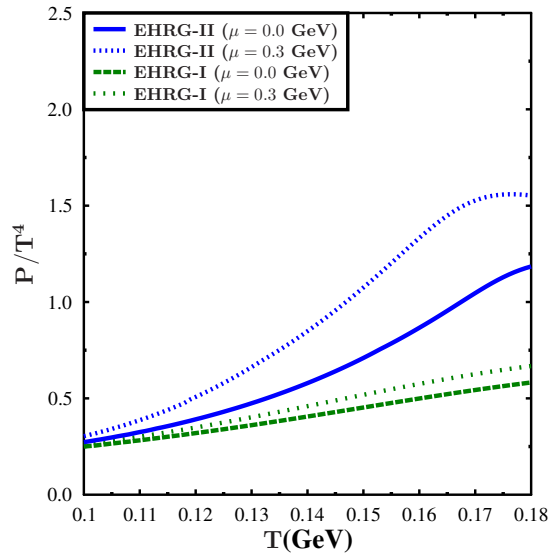


Figure 2.5: Scaled pressure as a function of temperature at two different chemical potentials in EHRG-I and EHRG-II with mass dependent excluded volume parametrization.

radius of all the baryons equal, detailed information regarding short range interaction between mesons is absent. Nevertheless, one can set same hard core radius to all mesons as that of baryons since meson charge radii are similar to the baryons [67]. But for our purpose we use the mass dependent hardcore radius as in Ref. [68]. In this scheme of parametrization,  $v$  is chosen to be proportional to the mass of each hadron;  $v = M/\epsilon_0$ ,  $\epsilon_0$  is a constant which we fix to the value  $0.9 \text{ GeVfm}^{-3}$ . We further generalize this scheme by taking into account  $T$  and  $\mu$  dependent hadron masses.

Results of the thermodynamical quantities are shown in Fig. (2.4). We call EHRG without  $T$ ,  $\mu$  dependent hadron masses as EHRG-I and that with  $T$ ,  $\mu$  dependent hadron masses as EHRG-II. We note that the thermodynamical quantities computed within EHRG-II start deviating from EHRG-I at  $T \sim 0.11 \text{ GeV}$  and this deviation is more pronounced above  $T \sim 0.14 \text{ GeV}$ . All the thermodynamical quantities are numerically larger in EHRG-II than in EHRG-I. This observation can be explained by simply considering Boltzmann factor  $\text{Exp}(-$

$M_h(T, \mu)/T$ ). This factor is a measure of probability that the specific hadronic species of mass  $M$  is thermally excited at given temperature whence making a contribution to the thermodynamical quantities. Since masses of all the hadrons but pions, kaons and eta mesons decreases with temperature, they can be thermally excited abundantly with ease. The masses of the (approximately) Goldstone bosons do not change much around  $T_c$ , but the constituent quark masses do change significantly at this temperature. In fact it drops down to its current quark mass at  $T_c$ . Since we expressed the heavy mesons and baryons masses in terms of constituent quarks [Eq. (2.1.27)] which contribute significantly at higher temperatures, we see the effect of  $T$  (and  $\mu$ ) dependent hadron masses on the thermodynamics only at higher temperatures especially around transition temperature, while this effect is small at low temperatures where the pions and kaons are the dominating degrees of freedom.

We note from Fig. 2.4 that the thermodynamical quantities computed within conventional non-interacting hadron resonance gas (HRG) model better fits the lattice data than EHRG-I model. Such non-interacting HRG model corresponds to  $v = 0$ . Thus, the lattice data seems to prefer zero excluded volume parameter, whence the point particle picture of hadrons. But this observation does not invalidate EHRG-I model altogether. It has been shown in Ref. [65] that non-interacting HRG model is problematic since the thermodynamical quantities rises very rapidly with temperature and ultimately shows sign of Hagedorn divergence around  $T_c$ , while in EHRG-I thermodynamical quantities rise less steeply than that in free HRG. Further, the better agreement of HRG model over EHRG-I with the LQCD may be mere coincidence since we know from the experiments that nucleons, at least, are not point particles but they do have finite spatial extension [67]. There is another experimental evidence that goes in favor of EHRG-I model. The analysis of the data for particle number ratios of Au+Au (AGS) and Pb+Pb (SPS) collisions suggest necessity to include excluded volume corrections in free HRG model [69]. By including repulsive interactions via excluded volume corrections in free HRG model and with the proper choice of excluded volume parameter, it is observed that EHRG-I agrees with lattice data

up to  $T \sim 0.14$  GeV [65]. Inclusion of medium modification of hadron masses in the excluded volume models, the agreement of EHRG-I model with LQCD is observed at higher temperatures too as may be noted from Fig. 2.4(a) where the pressure (normalized by  $T^4$ ) computed with medium dependent hadron masses agrees with lattice data up to  $T \sim 0.2$  GeV. Fig. (2.5) shows scaled pressure at finite chemical potential. Pressure rises more rapidly even at finite  $\mu$  in EHRG-II than in EHRG-I.

Fig. 2.4(b) shows trace anomaly (interaction measure) computed within EHRG-I and EHRG-II. We note that the trace anomaly rises rapidly in EHRG-II as compared to EHRG-I at high temperatures. Trace anomaly in EHRG-I shows decreasing behavior at high temperatures. The reason behind this is twofold. First, the suppression factor  $\frac{1}{1+vn(T,\mu)}$  which decreases as temperature and chemical potential increases and hence all the thermodynamical quantities in EHRG-I are numerically smaller than that in ideal HRG. Since there is no such suppression factor in HRG trace anomaly rises monotonically. Further, due to finite size of hadrons the pressure of hadron gas rises more rapidly as compare to energy density whence the interaction measure decreases at high temperature in EHRG-I. Strong suppression of thermodynamical quantities has also been observed earlier in Ref. [70] where the authors studied EHRG with uniform hard core radius for all the hadrons. Although we have used different scheme of parametrization for hard core radius, suppression effect is still there. But in case of EHRG-II, since hard core radius is itself depend on temperature, the suppression effect is somehow diluted. Rapid rise of trace anomaly has also been observed in HRG model as well as extended HRG model which include continuum spectrum of hadrons (Hagedorn states) along with discrete spectrum [48].

Although our main purpose of this study is not to fit the lattice data, this observation is rather crucial because as mentioned earlier, EHRG-I fails to explain the lattice data above  $T \sim 0.14$  GeV [65]. In our previous work in Ref. [71], we studied the extension of HRG model by including the Hagedorn density of states at finite temperature and density. We found rather good agreement with the lattice data of Ref. [57] below  $T = 0.15$  GeV. In Ref. [70] authors studied the

two extensions of HRG model, *viz.*, HRG model with excluded volume effects (EHRG) and HRG with continuum mass spectrum (Hagedorn states) along with discrete mass spectrum of the hadrons. They observed that two models are not in agreement with the lattice QCD results of Ref. [25] when considered separately. But when considered together, the suppression effects in EHRG and the enhancement effects due to Hagedorn states in HRG leads to better agreement with LQCD. From our observation that merely including the medium effects of hadrons in EHRG fit the LQCD quit well, it may be tempting to conclude that the effects of Hagedorn states can be alternatively simulated by including  $T$  and  $\mu$  dependent hadron masses in EHRG.

Fig. 2.4(d) shows behavior of speed of sound in EHRG-I and EHRG-II. We note that the sound velocity computed within EHRG-II agrees with the lattice quantum chromodynamics quit well over wide range of temperatures. We further note that although the general behavior of  $C_s^2$  is same in two models at low temperatures, it differs quit significantly at high temperatures. In EHRG-I sound velocity rises very rapidly while it flattens out in EHRG-II at high temperatures. As it has been pointed out in Ref. [72], such large and steady rise in sound velocity is sufficient to indicate the acausal behavior typical of all excluded volume models. This acausal behavior of sound speed in excluded volume is not difficult to understand. Physically, the speed of sound is a measure of the efficiency of the medium to propagate the small disturbances as a longitudinal wave. In excluded volume models at low temperatures and low density where the system is dominated by light mesons, gas of hadrons can be treated as an compressible fluid which renders small and finite value of the speed of sound. While at high temperatures and baryon densities, huge number of hadrons are thermally excited which tends to occupy the system volume more due to their finite size. Thus, at high temperatures and densities the gas of hadrons approach towards its incompressible liquid phase where the compressibility of the gas of hadrons approaches close to zero due to their close packing. Since speed of sound is inversely proportional to the compressibility, it rises very rapidly with temperature and even exceeds the speed of light whence violating causality. In contrast, although

the hadrons are abundantly excited thermally in IEHRG model, their hardcore radius decreases with temperature due to our mass dependent parametrization of the proper volume. Whence, at high temperatures the gas of hadrons still remains compressible thus avoiding liquid-gas phase transition which renders small and finite value of sound speed.

#### 2.1.4 Hadron resonance gas model in magnetic field

It is rather straightforward to extend non-interacting HRG model in presence of external magnetic field. The thermodynamic potential of hadronic matter in presence of external magnetic field ( $B$ ) is

$$\frac{\Omega}{V} = \varepsilon - Ts - Bm_B - \mu n_B \quad (2.1.28)$$

Where  $m_B$  is magnetization density. In thermodynamic limit,  $V \rightarrow \infty$ , thermodynamic pressure can be written as

$$P = -\frac{\Omega}{V} = -f = -(f_{vacuum} + f_{thermal}) \quad (2.1.29)$$

Where  $f_{vacuum}$  is vacuum contribution ( $T, \mu = 0, B \neq 0$ ) to free energy. Hence energy density can be written as

$$\varepsilon = Ts + Bm_B + \mu n_B - P \quad (2.1.30)$$

For the ideal gas of hadrons, free energy for charged component of the gas can be written as

$$f_c = \pm \sum_h \sum_{s_z} \sum_{k=0}^{\infty} \frac{eB}{4\pi^2} \int dp_z \left( \frac{E(p_z, k, s_z)}{2} + T \log(1 \pm e^{-E(p_z, k, s_z)/T}) \right) \quad (2.1.31)$$

where  $E = \sqrt{p_z^2 + m^2 + 2eB(k + 1/2 - s_z)}$  is the energy of charged particle moving freely under external magnetic field pointing in  $z$  direction.

Free energy for neutral component of the gas is

$$f_n = \pm \sum_h \int d^3p \left( \frac{E_0}{2} + T \log(1 \pm e^{-E_0/T}) \right) \quad (2.1.32)$$

where  $E_0 = \sqrt{\mathbf{p}^2 + m^2}$ .

Vacuum terms in Eq. (2.1.31) and (2.1.32) are UV divergent and can be regularized by dimensional regularization and renormalization of  $B > 0$  free energy can be carried out by subtracting  $B = 0$  part. Renormalized vacuum free energies for different spin channels in magnetic field are given by [73]

$$\Delta f^{vac,r}(spin0) = \frac{(eB)^2}{8\pi^2} \left[ \zeta'(-1, x+1/2) + x^2/4 - \frac{x^2}{2} \log(x) + \frac{\log(x) + 1}{24} \right] \quad (2.1.33)$$

$$\Delta f^{vac,r}(spin1/2) = -\frac{(eB)^2}{4\pi^2} \left[ \zeta'(-1, x) + \frac{x}{2} \log(x) + x^2/4 - \frac{x^2}{2} \log(x) - \frac{\log(x) + 1}{12} \right] \quad (2.1.34)$$

$$\begin{aligned} \Delta f^{vac,r}(spin1) &= \frac{3(eB)^2}{8\pi^2} \left[ \zeta'(-1, x-1/2) + \frac{1}{3}(x+1/2)\log(x+1/2) \right. \\ &+ \frac{2}{3}(x-1/2)\log(x-1/2) + x^2/4 - \frac{x^2}{2}\log(x) \\ &\left. - \frac{7(\log(x) + 1)}{24} \right] \end{aligned} \quad (2.1.35)$$

where  $x = \frac{m_h^2}{2eB}$  and  $\zeta(-1, x)$  is Hurwitz zeta function [60] whose asymptotic ( $x \gg 1$ ) expression is given by

$$\zeta'(-1, x) = \frac{1}{12} - \frac{x^2}{4} - \left( \frac{1}{12} - \frac{x}{2} + \frac{x^2}{2} \right) \quad (2.1.36)$$

To see the behavior of thermodynamical quantities of HRG model in presence of magnetic field we need to know the gyromagnetic ratios of charged hadrons apart from their masses and other quantum numbers. Since experimental gyromagnetic ratios ( $g_h$ ) are known with small error bars only for lightest hadrons, we take,  $g_h = 2q_h/e$  where  $q_h$  is the charge of given hadron species. We take all the hadrons up to mass cut-off  $\lambda = 1.2$  GeV. Fig. (2.6) shows the thermody-

namical quantities estimated using HRG model in presence of external magnetic field. Note that we do not plot scaled thermodynamical quantities since pressure is non-zero at  $T=0$ , and thus scales thermodynamical quantities diverges. From Fig. (2.6a) we note that pressure is increased by magnetic field. At zero temperature this increase is attributed to the vacuum term in Eq. (2.1.29) which is proportional to magnetic field, while at finite temperature it may be attributed to the value of effective mass  $M_h^{eff} = M_h + eB(1 - 2s)$  which is larger for pions ( $\pi^\pm, \pi^0$ ), smaller for  $\rho^\pm$  and remain unchanged for spin half baryons. Accordingly, the Boltzmann factor ( $e^{-\frac{M_h^{eff}}{T}}$ ) is smaller for pions, larger for  $\rho^\pm$  and remain unchanged for baryons.

Fig. (2.6c) shows that entropy is practically unaffected by presence of magnetic field. At zero temperature there is no vacuum contribution to the entropy density, while at finite temperature the effects of magnetic field are small due to range of magnetic fields under consideration. Further, from Fig. (2.6d) we note that magnetization is positive indicating that the hadronic matter is paramagnetic.

From Fig. (2.7) we note that the dip in the plot of speed of sound against temperature is more pronounced and shifts towards lower temperature. Such dip has been interpreted as deconfinement phase transition from hadronic to quark matter. Decrease in transition temperature  $T_c$  in presence of magnetic field has also been observed in LQCD simulations [74].

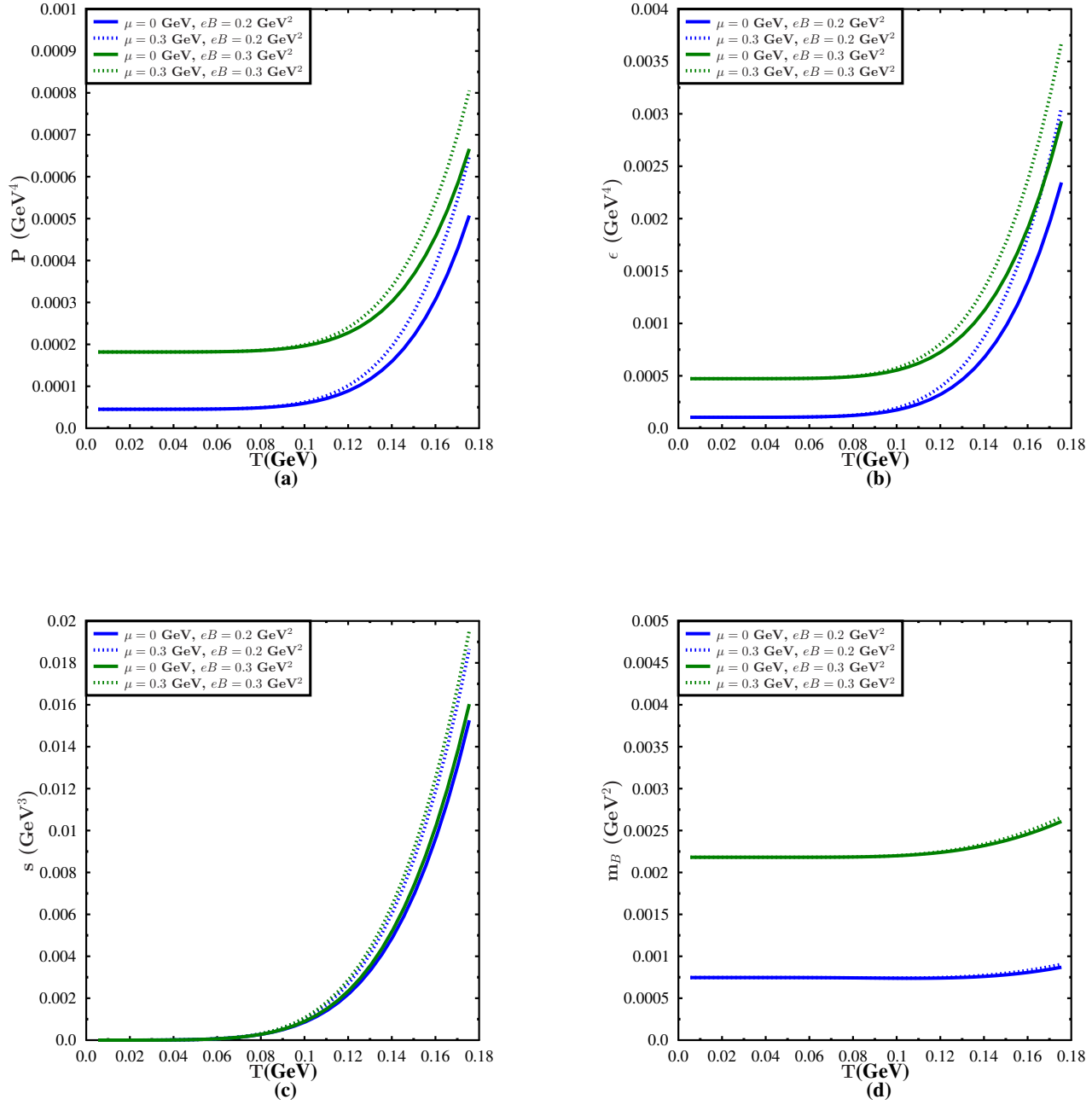


Figure 2.6: Results of thermodynamical estimated using HRG model at different chemical potential and magnetic field.

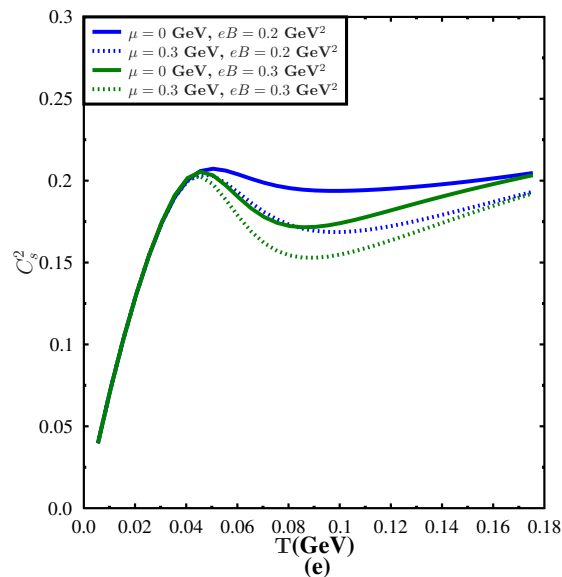


Figure 2.7: Speed of sound in HRG at different chemical potentials and magnetic fields.

## 2.2 Conclusion

In this chapter we discussed the hadron resonance gas model and its extensions, namely excluded volume HRG and HRG with medium dependent hadron masses. HRG model is the simplest effective model of QCD describing the hadronic phase of strongly interacting matter. Although HRG model is in good agreement with LQCD simulations of Ref. [57] at low temperature and zero baryonic chemical potential, inclusion of continuum mass spectrum (Hagedorn states) along with discrete mass spectrum in HRG leads to good agreement with LQCD up to  $T=0.150$  GeV. Further, the speed of sound estimated within HRG with Hagedorn states agrees with LQCD over wide range of temperatures.

Further, we motivated the necessity to include the repulsive interactions between hadrons as well as medium dependent hadron masses. Repulsive interactions can be included in non-interacting HRG model via excluded volume corrections, while medium dependent hadron masses can be computed using Nambu-Jona-Lasinio model. Including these effects in HRG model can simulate

the effects of Hagedorn density of states whence leads to better agreement with LQCD up to  $T = 0.180$  GeV. Further, sound velocity computed within this improved HRG does not rise rapidly at high temperature. Since this rapid rise of sound speed, observed in all excluded volume HRG models, indicates acausal behavior, inclusion of medium dependent hadron masses in excluded volume models suggest possibility of curing such acausal behavior.

Finally, we explored the HRG model in presence of magnetic field. Pressure picks up non-zero contribution from vacuum term whence it is non-zero at zero temperature, while entropy density is not affected much by presence small and moderate magnetic fields. Magnetization of hadronic matter is positive indicating the paramagnetic behavior. Another interesting result is that the dip in the curve of sound speed as a function of temperature shifts towards low temperature with increasing magnetic field; a result consistent with LQCD simulations in magnetic field.



# Chapter 3

## Transport properties of hot and dense hadronic matter

### 3.1 Transport coefficients in kinetic theory

#### 3.1.1 Relativistic Boltzmann equation

In the kinetic theory the system consisting huge number of particles can be described by the phase-space distribution function  $f(\vec{x}, \vec{p}, t)$  defined such that

$$dN(t) = d^3\vec{x}(t)d^3\vec{p}(t)f(\vec{x}, \vec{p}, t) \quad (3.1.1)$$

gives number of particles in phase-space volume element  $d^3\vec{x}d^3\vec{p}$  at time  $t$ . Boltzmann equation is the fundamental equation of kinetic theory which describe the evolution of this distribution function in phase-space. This number is same for any observer in an arbitrary inertial reference frame. Further, this number do not change if there are no collision among the particles and if there is no external unbalanced force. But if either of these two is present, number of particles in a given phase-space volume will change. This change is reflected in change in phase-space volume element as well as the distribution function. So, after an infinitesimal time interval  $dt$ , we have

$$dN(t + dt) = d^3\vec{x}(t + dt)d^3\vec{p}(t + dt)f(\vec{x}(t + dt), \vec{p}(t + dt), t + dt) \quad (3.1.2)$$

The change in distribution function can be readily obtained using rules of partial differentiation as

$$df_p = \left( \frac{\partial f_p}{\partial t} + \frac{d\vec{x}}{dt} \cdot \frac{\partial f_p}{\partial \vec{x}} + \frac{d\vec{p}}{dt} \cdot \frac{\partial f_p}{\partial \vec{p}} \right) dt \quad (3.1.3)$$

The phase space volume element at  $t + dt$  can be expressed in terms of that at time  $t$  with the help of Jacobian as

$$d^3\vec{x}(t+dt)d^3\vec{p}(t+dt) = \det \left( \frac{\partial(\vec{x}(t+dt), \vec{p}(t+dt), t+dt)}{\partial(\vec{x}(t), \vec{p}(t), t)} \right) d^3\vec{x}(t)d^3\vec{p}(t) \quad (3.1.4)$$

Thus, the change in number of particles in a given phase-space volume element due to collisions is

$$dN(t+dt) - dN(t) = d^3\vec{x}(t)d^3\vec{p}(t)dt \left( \frac{\partial f_p}{\partial t} + \frac{\vec{p}}{E_p} \cdot \frac{\partial f_p}{\partial \vec{x}} + \frac{\partial(f_p \vec{F})}{\partial \vec{p}} \right) \quad (3.1.5)$$

where we have used the fact that for particle moving in external force  $\vec{F}$ ,  $\frac{d\vec{x}}{dt} = \frac{\vec{p}}{E_p}$  and  $\vec{F} = \frac{d\vec{p}}{dt}$ . Since the left hand side of above equation is Lorentz invariant, so do the right hand side. In fact, one can shed the whole equation in manifestly covariant form as

$$\frac{d}{dt}dN = \frac{d}{dt}(dN_{gain} - dN_{loss}) = \frac{d^3\vec{x}d^3\vec{p}}{E_p} \left[ p^\mu \frac{\partial f_p}{\partial x^\mu} + m \frac{\partial(K^\mu f_p)}{\partial p^\mu} \right] \quad (3.1.6)$$

where  $p^\mu$  is four-momentum-vector and  $K^\mu$  is Minkowski four-force-vector. If there is no interaction among the particles, for arbitrary phase-space volume element, the term inside square bracket vanishes and we get the Boltzmann equation in the absence of collisions.

$$p^\mu \frac{\partial f_p}{\partial x^\mu} + m \frac{\partial(K^\mu f_p)}{\partial p^\mu} = 0 \quad (3.1.7)$$

If there exist interaction among the particles, at position  $\vec{x}$ , within infinitesimal time interval  $dt$  there is certain number of particles which scatter off from initial momentum  $\vec{p}$  to some other final momentum  $\vec{p}'$ , while there is also certain amount of particles which scatter from initial momentum  $\vec{p}'$  into the final momentum  $\vec{p}$ . Former is called the “loss term” while later is called the “gain term”. To calculate

these two terms one needs to consider following postulates known as Boltzmann's Stoßzahlansatz\*.

**I.** The gas is assumed to be dilute enough so that only binary collisions are relevant. The tertiary collisions are assumed to be extremely rare.

**II.** Two incoming particles with momenta  $\vec{p}_1$  and  $\vec{p}_2$  are uncorrelated. The number of particles at instant  $t$  in a given volume element  $d^3\vec{x}$  with momenta  $\vec{p}_1$  and  $\vec{p}_2$  are then

$$dN = d^3\vec{x}d^3\vec{p}_1f(\vec{x},\vec{p}_1)d^3\vec{x}d^3\vec{p}_2f(\vec{x},\vec{p}_2) \quad (3.1.8)$$

Same is assumed to be true for two outgoing particles with momenta  $\vec{p}'_1$  and  $\vec{p}'_2$ . This is known as postulate of molecular chaos.

**III.** The interaction between the particles is short range. This assumption implies that the phase-space distribution function varies very slowly over the time interval which is small compared to time interval between two successive collisions but large compared to collision time. Now, consider binary scattering process  $a(p_1) + b(p_2) \rightarrow c(p'_1) + d(p'_2)$  where the argument represent the four momentum of respective particle. The four momentum conservation is

$$p_1 + p_2 = p'_1 + p'_2 \quad (3.1.9)$$

The number of elastic collisions happening in infinitesimal time interval  $dt$  constrained by above four momentum conservation is

$$dN_{coll} = d^4x \frac{d^3\vec{p}_1}{E_{p_1}} \frac{d^3\vec{p}_2}{E_{p_2}} \frac{d^3\vec{p}'_1}{E_{p'_1}} \frac{d^3\vec{p}'_2}{E_{p'_2}} f_{p_1} f_{p_2} W(p'_1 + p'_2 \leftarrow p_1 + p_2) \quad (3.1.10)$$

where  $W$  represent the transition rate per unite volume which captures the dynamics of the particles. Thus, the gain term is

$$\frac{d}{dt}dN_{gain} = d^3\vec{x} \frac{d^3\vec{p}}{E_p} \int_{\mathbb{R}^3} \frac{d^3\vec{p}_2}{E_{p_2}} \int_{\mathbb{R}^3} \frac{d^3\vec{p}'_1}{E_{p'_1}} \int_{\mathbb{R}^3} \frac{d^3\vec{p}'_2}{E_{p'_2}} f_{p'_1} f_{p'_2} W(p + p_2 \leftarrow p'_1 + p'_2) \quad (3.1.11)$$

---

\*Stoßzahlansatz is a German word which means "collision number assumption".

and the loss term is

$$\frac{d}{dt}dN_{loss} = d^3\vec{x} \frac{d^3\vec{p}}{E_p} \int_{\mathbb{R}^3} \frac{d^3\vec{p}_2}{E_{p_2}} \int_{\mathbb{R}^3} \frac{d^3\vec{p}'_1}{E_{p'_1}} \int_{\mathbb{R}^3} \frac{d^3\vec{p}'_2}{E_{p'_2}} f_p f_{p_2} W(p'_1 + p'_2 \leftarrow p + p_2) \quad (3.1.12)$$

Here, we have redefined the momentum variable  $p_1 \rightarrow p$ . Substituting Eqs. (3.1.11) and (3.1.12) in Eq. (3.1.6) we get

$$\begin{aligned} p^\mu \frac{\partial f_p}{\partial x^\mu} + m \frac{\partial(K^\mu f_p)}{\partial p^\mu} &= \int_{\mathbb{R}^3} \frac{d^3\vec{p}_2}{E_{p_2}} \int_{\mathbb{R}^3} \frac{d^3\vec{p}'_1}{E_{p'_1}} \int_{\mathbb{R}^3} \frac{d^3\vec{p}'_2}{E_{p'_2}} \\ &\quad [f_{p'_1} f_{p'_2} W(p + p_2 \leftarrow p'_1 + p'_2) \\ &\quad - f_p f_{p_2} W(p'_1 + p'_2 \leftarrow p + p_2)] \end{aligned} \quad (3.1.13)$$

Using the principle of detailed balance in above equation

$$W(p + p_2 \leftarrow p'_1 + p'_2) = W(p'_1 + p'_2 \leftarrow p + p_2) \quad (3.1.14)$$

we finally get the relativistic Boltzmann equation.

$$p^\mu \frac{\partial f_p}{\partial x^\mu} + m \frac{\partial(K^\mu f_p)}{\partial p^\mu} = \frac{1}{2} \int_{\mathbb{R}^3} \frac{d^3\vec{p}_2}{E_{p_2}} \int_{\mathbb{R}^3} \frac{d^3\vec{p}'_1}{E_{p'_1}} \int_{\mathbb{R}^3} \frac{d^3\vec{p}'_2}{E_{p'_2}} W(p + p_2 \leftarrow p'_1 + p'_2) [f_{p'_1} f_{p'_2} - f_p f_{p_2}] \quad (3.1.15)$$

where the factor 1/2 is due to indistinguishability of the particles. The right hand side of Eq. (3.1.15) is called collision term which we denote by  $C[f_p]$  for brevity. Thus, the relativistic Boltzmann equation can be written as

$$p^\mu \frac{\partial f_p}{\partial x^\mu} + m \frac{\partial(K^\mu f_p)}{\partial p^\mu} = C[f_p] \quad (3.1.16)$$

The Boltzmann equation is complicated integro-differential equation and it is rather very difficult to solve exactly especially when dealing with the collision term. Nevertheless, based on some legitimate assumptions pertaining to the system under study one can make simplest approximation of this collision term for the purpose of extracting the transport properties.

### 3.1.2 Boltzmann equation in relaxation time approximation

When the system is perturbed from the equilibrium state characterized by single particle distribution function  $f_p^0$ , the particles in the system undergo collisions taking the system out of equilibrium leading to the transport of conserved quantities, *viz.*, energy and momentum. The single particle distribution function  $f_p$  in such non-equilibrium state will in general be different from  $f_p^0$ . We assume that the effect of collision is always to bring the system towards local equilibrium state. Further, we assume that this equilibration occurs exponentially with time  $\tau$ , called relaxation time which is of order of time interval between successive collisions. Thus, in this approximation Boltzmann equation can be written as

$$p^\mu \frac{\partial f_p}{\partial x^\mu} + m \frac{\partial(K^\mu f_p)}{\partial p^\mu} \simeq -\frac{(f_p - f_p^0)}{\tau(E_p)} \quad (3.1.17)$$

This approximation is valid only if the departure from the equilibrium is small such that

$$f_p = f_p^0 + \delta f_p \quad (3.1.18)$$

and  $\delta f_p \ll f_p^0$ . Mathematically, in this so called relaxation time approximation (RTA), all the non-zero eigenvalues of the collision term  $C[f_p]$  are taken to have common eigenvalue equal to  $-1/\tau(E_p)$ . Thus, substituting Eq. (3.1.18) in Eq. (3.1.17) and neglecting the space-time derivatives of  $\delta f_p$  which is very small, we finally get the Boltzmann equation in relaxation time approximation.

$$p^\mu \frac{\partial f_p^0}{\partial x^\mu} + m \frac{\partial(K^\mu f_p^0)}{\partial p^\mu} \simeq -\frac{\delta f_p}{\tau(E_p)} \quad (3.1.19)$$

Few points are to be noted here:

- I) Negative sign on the r.h.s of Eq. (3.1.19) ensures that the system in non-equilibrium state decays down to the equilibrium state.
- II) The relaxation time  $\tau$  is in general energy dependent. But for the sake of simplicity, it is also customary to use energy independent as well as averaged partial relaxation time as will be discussed in next sub-section.

### 3.1.3 Transport coefficients in relaxation time approximation

The energy-momentum tensor is the 2nd moment of the distribution function.

$$T^{\mu\nu} = \int \frac{d^3p}{E_p} p^\mu p^\nu f_p \quad (3.1.20)$$

The spatial part (momentum flow or pressure tensor) is

$$T^{ij} = \int \frac{d^3p}{E_p} p^i p^j f_p \quad (3.1.21)$$

From Eq. (3.1.18) above equation can be written as

$$T^{ij} = T_0 + \int \frac{d^3p}{E_p} p^i p^j \delta f_p \quad (3.1.22)$$

The second term on the r.h.s of above equation governs the dissipation in the system.

$$T_{dissi}^{ij} = \int \frac{d^3p}{E_p} p^i p^j \delta f_p \quad (3.1.23)$$

where  $T_0$  is the ideal part of energy-momentum tensor. In the absence of external force Eq. (3.1.17) can be written as

$$\delta f_p = -\tau(E_p) \left( \frac{\partial}{\partial t} + v_p^i \frac{\partial}{\partial x^i} \right) f_p^0 \quad (3.1.24)$$

Thus, Eq. (3.1.23) can be written in terms of equilibrium distribution function as

$$T_{dissi}^{ij} = - \int \frac{d^3p}{E_p} p^i p^j \tau(E_p) \left( \frac{\partial}{\partial t} + v_p^i \frac{\partial}{\partial x^i} \right) f_p^0 \quad (3.1.25)$$

In the hydrodynamics, shear and bulk viscosities enters in the dissipative part ( $T_{dissi}^{\mu\nu}$ ) of stress energy tensor.

$$T^{\mu\nu} = T_0^{\mu\nu} + T_{dissi}^{\mu\nu} \quad (3.1.26)$$

where  $T_0^{\mu\nu}$  is ideal part of stress tensor. In the local Lorentz frame in which the

momentum density  $T^{i0}$  is small, dissipative part of stress energy tensor can be written as

$$T_{dissi}^{ij} = -\eta \left( \frac{\partial u^i}{\partial x^j} + \frac{\partial u^j}{\partial x^i} \right) - \left( \zeta - \frac{2}{3}\eta \right) \frac{\partial u^i}{\partial x^j} \delta^{ij} \quad (3.1.27)$$

Assuming steady flow of the form  $u^i = (u_x(y), 0, 0)$  above equation simplifies to

$$T^{xy} = -\eta \frac{\partial u_x}{\partial y} \quad (3.1.28)$$

Also for such flow Eq. (3.1.25) can be written as

$$T^{xy} = \left\{ -\frac{1}{T} \int \frac{d^3p}{(2\pi)^3} \tau(E_p) \left( \frac{p_x p_y}{E_p} \right)^2 f_p^0 \right\} \frac{\partial u_x}{\partial y} \quad (3.1.29)$$

Thus, comparing the coefficient  $\partial u_x/\partial y$  in Eqs. (3.1.28) and (3.1.29) we get the shear viscosity coefficient for a single component of hadronic matter.

$$\eta = \frac{1}{15T} \int \frac{d^3p}{(2\pi)^3} \tau(E_p) \frac{p^4}{E_p^2} f_p^0 \quad (3.1.30)$$

For multicomponent hadronic matter the shear viscosity coefficient is just a sum of contribution from each hadronic species [75]

$$\eta = \frac{1}{15T} \sum_a \int \frac{d^3p}{(2\pi)^3} \frac{p^4}{E_a^2} (\tau_a f_a^0 + \bar{\tau}_a \bar{f}_a^0) \quad (3.1.31)$$

Similarly, the bulk viscosity coefficient of the hadronic matter is [75]

$$\begin{aligned} \zeta &= \frac{1}{T} \sum_a \int \frac{d^3p}{(2\pi)^3} \left\{ \tau_a f_a^0 \left[ E_a C_{n_B}^2 + \left( \frac{\partial P}{\partial n_B} \right)_\epsilon - \frac{p^2}{3E_a} \right]^2 \right. \\ &\quad \left. + \bar{\tau}_a \bar{f}_a^0 \left[ E_a C_{n_B}^2 - \left( \frac{\partial P}{\partial n_B} \right)_\epsilon - \frac{p^2}{3E_a} \right]^2 \right\} \end{aligned} \quad (3.1.32)$$

where  $E_a^2 = p^2 + m_a^2$  and  $(\partial P/\partial n_B)_\epsilon = n_B/(\partial n_B/\partial \mu) + C_{n_B}^2 T^2 \partial(\mu/T)/\partial T$ .

In above expressions bar stands for contribution of antiparticles.

Energy dependent relaxation time is defined by expression

$$\tau^{-1}(E_a) = \sum_{bcd} \int \frac{d^3 p_b}{(2\pi)^3} \frac{d^3 p_c}{(2\pi)^3} \frac{d^3 p_d}{(2\pi)^3} W(a, b \rightarrow c, d) f_b^0 \quad (3.1.33)$$

where the transition rate  $W(a, b \rightarrow c, d)$  is defined by

$$W(a, b \rightarrow c, d) = \frac{(2\pi)^4 \delta(p_a + p_b - p_c - p_d)}{2E_a 2E_b 2E_c 2E_d} |\mathcal{M}|^2 \quad (3.1.34)$$

with  $|\mathcal{M}|$  being transition amplitude. In the center of mass frame Eq. (3.1.33) can be simplified as

$$\tau^{-1}(E_a) = \sum_b \int \frac{d^3 p_b}{(2\pi)^3} \sigma_{ab} \frac{\sqrt{S - 4m^2}}{2E_a 2E_b} f_b^0 \equiv \sum_b \int \frac{d^3 p_b}{(2\pi)^3} \sigma_{ab} v_{ab} f_b^0 \quad (3.1.35)$$

where  $v_{ab}$  is relative velocity and  $\sqrt{S}$  is center of mass energy.  $\sigma_{ab}$  is the total scattering cross section for the process,  $a(p_a) + b(p_b) \rightarrow a(p_c) + b(p_d)$ .

For the simplicity we can use averaged relaxation time ( $\tilde{\tau}$ ) which is rather a good approximation as energy dependent relaxation time [76]. One can obtain  $\tilde{\tau}$  as follows. Averaging over  $f_a^0$  Eq. (3.1.35) becomes

$$\frac{\int \frac{d^3 p_a}{(2\pi)^3} \tau^{-1}(E_a) f_a^0}{\int \frac{d^3 p_a}{(2\pi)^3} f_a^0} = \sum_b \frac{\int \frac{d^3 p_a}{(2\pi)^3} \frac{d^3 p_b}{(2\pi)^3} \sigma_{ab} v_{ab} f_a^0 f_b^0}{\int \frac{d^3 p_a}{(2\pi)^3} f_a^0} \quad (3.1.36)$$

Thus averaged partial relaxation time is given by

$$\tilde{\tau}_a^{-1} = \sum_b n_b \langle \sigma_{ab} v_{ab} \rangle \quad (3.1.37)$$

where  $n_b = \int \frac{d^3 p_b}{(2\pi)^3} f_b^0$  is the number density of  $b^{th}$  hadronic species.

In this work we will use equilibrium Maxwell-Boltzmann distribution (in the local rest frame) given by

$$f_a^0 = \exp\left(-\frac{E_a - \mu}{T}\right) \quad (3.1.38)$$

The thermal average of total cross section times relative velocity i.e  $\langle \sigma v \rangle$  for

the scattering of hard sphere particles (having constant cross section,  $\sigma$ ) of the same species at zero baryon density can be calculated as follows [77, 78]. With Maxwell-Boltzmann distribution  $f^0(E) = \exp(-E/T)$ , the thermal average  $\langle \sigma v \rangle$  for the process  $a(p_a) + a(p_b) \rightarrow a(p_c) + a(p_d)$  can be written as

$$\langle \sigma_{ab} v_{ab} \rangle = \frac{\sigma \int d^3 p_a d^3 p_b v_{ab} e^{-E_a/T} e^{-E_b/T}}{\int d^3 p_a d^3 p_b e^{-E_a/T} e^{-E_b/T}} \quad (3.1.39)$$

Momentum space volume elements  $d^3 p_a d^3 p_b$  can be written in terms of scattering angle  $\theta$  as

$$d^3 p_a d^3 p_b = (4\pi)^2 p_a p_b E_a dE_a E_b dE_b \frac{1}{2} d\cos\theta \quad (3.1.40)$$

Changing integration variables from  $E_a, E_b, \theta$  to  $E_-, E_+, S$  we get

$$d^3 p_a d^3 p_b = 2\pi^2 E_a E_b dE_- dE_+ dS \quad (3.1.41)$$

where  $S = (p_a + p_b)^2$  is usual Mandelstam variable and  $E_{\pm} = E_a \pm E_b$ . With this change in variables the integration region transform as

$$E_- \leq \sqrt{1 - \frac{4m^2}{S}} \sqrt{E_+^2 - S} \quad (3.1.42)$$

with  $E_+ \geq \sqrt{S}$  and  $S \geq 4m^2$ . Thus numerator in Eq. (3.1.39) becomes

$$\int d^3 p_a d^3 p_b v_{ab} e^{-E_a/T} e^{-E_b/T} = 2\pi^2 T \int dS \sqrt{S} (S - 4m^2) K_1(\sqrt{S}/T) \quad (3.1.43)$$

Similarly denominator of Eq. (3.1.39) can be evaluated as

$$\int d^3 p_a d^3 p_b e^{-E_a/T} e^{-E_b/T} = [4\pi m^2 T K_2(m/T)]^2 \quad (3.1.44)$$

where  $K_n$  is modified Bessel function of order  $n$ . Thus the thermal average becomes

$$\langle \sigma_{ab} v_{ab} \rangle = \frac{\sigma}{8m^4 T K_2^2(m/T)} \int_{4m^2}^{\infty} dS \sqrt{S} (S - 4m^2) K_1(\sqrt{S}/T) \quad (3.1.45)$$

For scattering between different species of the particles  $(a(p_a) + b(p_b) \rightarrow a(p_c) +$

$b(p_d)$ ) one can generalize above equation to get

$$\langle \sigma_{ab} v_{ab} \rangle = \frac{\sigma}{8T m_a^2 m_b^2 K_2(\frac{m_a}{T}) K_2(\frac{m_b}{T})} \int_{m_a+m_b}^{\infty} dS \frac{[S - (m_a - m_b)^2]}{\sqrt{S}} [S - (m_a + m_b)^2] K_1(\sqrt{S/T}) \quad (3.1.46)$$

Computing the thermal averaged cross section as above, one can relate it to the relaxation time in Eq. (3.1.37). The viscosities can then be calculated using Eq. (3.1.31) and Eq. (3.1.32) once the thermodynamic quantities are estimated using EHRG model. It is very difficult or rather tedious task to compute all the cross section in hadronic matter. Further, since we will be using HRG model to estimate the thermodynamical quantities, there is no direct way to compute these cross sections. For simplicity, we introduce interactions among hadrons through hard sphere repulsion. The non-relativistic expression for hard sphere scattering cross section is simply  $4\pi r_h^2$ . Thus, taking phenomenological values for hard-sphere radius of hadrons, one can readily estimate the viscosity coefficients.

## 3.2 Transport coefficients in Kubo's formalism

### 3.2.1 Kubo's formula for bulk viscosity

Bulk viscosity corresponds to the response of the system to conformal transformations. According to Kubo's formula it can be written as a bilocal correlation function of energy-momentum tensor [38]

$$\zeta = \lim_{\omega \rightarrow 0} \frac{1}{9\omega} \int_0^{\infty} dt \int d\mathbf{x} \exp(i\omega t) [\theta_{\mu}^{\mu}(x), \theta_{\mu}^{\mu}(0)] \equiv \int d^4x iG^R(x) \quad (3.2.1)$$

with  $G^R(x)$  being the retarded function for the trace of energy momentum tensor. One can introduce a spectral function which is related to the retarded Green's function by relation,  $\rho(\omega, \mathbf{p}) = -(1/\pi)\text{Im}G(\omega, \mathbf{p})$ . Assuming Lorentzian ansatz for the spectral function at low energy [38] as

$$\rho(\omega, 0)/\omega = (9\zeta/\pi)(\omega_0^2/(\omega_0^2 + \omega^2)), \quad (3.2.2)$$

where,  $\omega_0$  is a scale above which perturbation theory becomes valid. Thus, the bulk viscosity can be written as

$$9\zeta\omega_0 = 2 \int_0^\infty du \frac{\rho(u, 0)}{u} du = \int d^4x \langle \theta_\mu^\mu(x) \theta_\mu^\mu(0) \rangle \equiv \Pi \quad (3.2.3)$$

The trace of stress-energy tensor for massless QCD at tree level vanishes due to conformal symmetry. But for QCD with non-zero current quark mass conformal symmetry is explicitly broken. This breaking is further assisted by higher order quantum corrections to energy-momentum tensor. Thus, trace of energy momentum tensor for massive QCD with quantum corrections is

$$\theta_\mu^\mu = m\bar{q}q + \frac{\beta(g)}{2g} G_{\mu\nu}^a G^{a\mu\nu} \equiv \theta_q + \theta_g \quad (3.2.4)$$

In the above  $g$  is the strong coupling and  $\beta(g)$  is the QCD beta function that decides the running of the QCD coupling. Thus, the evaluation of the bulk viscosity boils down to evaluation of the energy-momentum correlator. This is done by using the low energy theorems of QCD generalized to finite temperature and density. The lowest in the chain of relations is [39]

$$\int d^4x \langle \theta_g(x) \hat{O} \rangle = (\hat{D} - d) \langle \hat{O} \rangle (T, \mu), \quad (3.2.5)$$

where,  $\hat{D} = T\partial/\partial T + \mu\partial/\partial\mu$ , and with  $d$  being the canonical dimension of the operator  $\hat{O}$ . LET for gluon and quark fields can be written as

$$\int d^4x \langle \theta_{\mu\mu}^g(x) \theta_{\mu\mu}^g(0) \rangle = (\hat{D} - 4) \langle \theta_{\mu\mu}^g \rangle \quad (3.2.6)$$

$$\int d^4x \langle \theta_{\mu\mu}^q(x) \theta_{\mu\mu}^q(0) \rangle = (\hat{D} - 2) \langle \theta_{\mu\mu}^q \rangle \quad (3.2.7)$$

Using Eqs.(3.2.6) and (3.2.7) in Eq.(3.2.3) we get

$$\begin{aligned}
9\zeta\omega_0 &= (\hat{D} - 4)\langle\theta_\mu^\mu\rangle + (\hat{D} - 2)\langle\theta^{q\mu}\rangle \\
&= 16|\epsilon_{vac}^g| + 6(f_\pi^2 m_\pi^2 + f_K^2 m_K^2) \\
&+ Ts\left(\frac{1}{c_s^2} - 3\right) + \left(\mu\frac{\partial}{\partial\mu} - 4\right)(\epsilon^* - 3P^*) + (\hat{D} - 2)m_q\langle\bar{q}q\rangle_* \quad (3.2.8)
\end{aligned}$$

In the above we have used  $\langle\theta_\mu^\mu\rangle = \epsilon - 3P$  and the thermodynamic relations  $c_v = \partial\epsilon/\partial T$ ,  $\partial P/\partial T = s$  and  $c_s^2 = s/c_v$  for the velocity of sound of the medium. We have also separated the contributions to the correlators in terms of the vacuum and the medium. In Eq.(3.2.8) we have neglected terms quadratic in the current quark masses and have used PCAC relations<sup>†</sup> to express vacuum condensates ( $\langle m\bar{q}q\rangle_0$ ) to the masses and decay widths of pions ( $m_\pi, f_\pi$ ) and kaons ( $m_K, f_K$ ).

### 3.2.2 Anisotropic bulk viscosity in presence of strong magnetic field

In presence of strong magnetic field, the rotational symmetry breaks down and hence the transport properties become anisotropic. In this sub-section, we again use Kubo's formalism to obtain the bulk viscosity in presence of strong magnetic field. QCD low energy theorems given by Eq. (3.2.5) can be generalized in presence of magnetic field as [79]

$$\int d^4x \langle\theta_g(x)\hat{O}\rangle = (\tilde{D} - d)\langle\hat{O}\rangle(T, \mu), \quad (3.2.9)$$

where,  $\tilde{D} = T\partial/\partial T + \mu\partial/\partial\mu + 2B\frac{\partial}{\partial B}$ . In presence of magnetic field,  $SO(3)$  rotational symmetry is broken and pressure in the direction perpendicular to the magnetic field may be different from that of pressure in longitudinal direction. For the thermodynamic system at finite  $T$ ,  $\mu$  and  $B$ , longitudinal thermodynamic pressure in limit  $V \rightarrow \infty$  can be written in terms of energy density ( $\varepsilon$ ),

---

<sup>†</sup> $\langle m\bar{q}q\rangle_0 = -m_\pi f_\pi - m_K f_K$

magnetization ( $M$ ), baryon density ( $\rho_b$ ) and entropy density ( $s$ ) as

$$P_* = Ts + BM + \mu\rho_b - \varepsilon \quad (3.2.10)$$

Also the trace of stress tensor in longitudinal direction is

$$\langle\theta_\mu^\mu\rangle = 4\varepsilon_v + (\varepsilon - 3P)_* + BM_* \quad (3.2.11)$$

Thus, using Eqs. (3.2.9), (3.2.10) and (3.2.11) in Eq. (3.2.3) we get

$$\begin{aligned} 2 \int_0^\infty du \frac{\rho(u, 0)}{u} du &= -16\varepsilon_v - 2 \sum_q m_q \langle \bar{q}q \rangle_0 + \left( T \frac{\partial}{\partial T} + \sum_q \mu_q \frac{\partial}{\partial \mu_q} + 2B \frac{\partial}{\partial B} - 2 \right) \sum_q m_q \langle \bar{q}q \rangle_* \\ &+ Ts \left( \frac{1}{C_s^2} - 3 \right) + \left( \sum_q \mu_q \frac{\partial}{\partial \mu_q} - 4 \right) (\varepsilon - 3P)_* + 2B^2 \chi - 4BM \\ &+ B \left( T \frac{\partial}{\partial T} + \sum_q \mu_q \frac{\partial}{\partial \mu_q} \right) M \end{aligned} \quad (3.2.12)$$

where  $\chi = \partial M / \partial B$  is magnetic susceptibility and  $C_s^2 = \partial P / \partial \varepsilon$  is sound velocity at constant magnetic field and chemical potential. Note that we haven't used any specific form of spectral density to compute bulk viscosity yet. Instead of Lorentzian form of spectral density (3.2.2) we use Gaussian ansatz of the form

$$\frac{\rho(\omega, \mathbf{0})}{\omega} = \frac{9\zeta}{\pi} e^{-\left(\frac{\omega}{\pi\omega_0}\right)^2} \quad (3.2.13)$$

This ansatz satisfy the definition of bulk viscosity in terms of spectral function.

$$\zeta = \frac{\pi}{9} \lim_{\omega \rightarrow 0} \frac{\rho(\omega, \mathbf{0})}{\omega} \quad (3.2.14)$$

Further, it is odd under parity as required by parity properties of retarded Greens function, whence of spectral function. Apart from this, Gaussian ansatz reduces to Lorentzian form in small frequency limit. Because the large frequency modes are suppressed in Gaussian form of spectral function,  $\zeta/s$  will have lower value as compared to that with Lorentz form of spectral function. Thus, using spectral function (3.2.13) in Eq. (3.2.12) we get the expression for the bulk viscosity in

longitudinal direction as

$$\begin{aligned}
9\sqrt{\pi}\zeta\omega_0 &= -16\varepsilon_v - 2\sum_q m_q \langle \bar{q}q \rangle_0 + \left( T \frac{\partial}{\partial T} + \sum_q \mu_q \frac{\partial}{\partial \mu_q} + 2B \frac{\partial}{\partial B} - 2 \right) \sum_q m_q \langle \bar{q}q \rangle_* \\
&+ Ts \left( \frac{1}{C_s^2} - 3 \right) + \left( \sum_q \mu_q \frac{\partial}{\partial \mu_q} - 4 \right) (\varepsilon - 3P)_* + 2B^2 \chi - 4BM \\
&+ B \left( T \frac{\partial}{\partial T} + \sum_q \mu_q \frac{\partial}{\partial \mu_q} \right) M
\end{aligned} \tag{3.2.15}$$

Thus, once the thermodynamical quantities are estimated the bulk viscosity coefficient can be easily estimated using Eq. (3.2.15.)

### 3.3 Results and discussion

Viscosity coefficients can be readily estimated using formulas derived in the previous section once the thermodynamical quantities are estimated for the hadronic phase. For this purpose we use hadron resonance gas model and its extended versions discussed in chapter 2. We use non-interacting HRG model to estimate the viscosity coefficients obtained using Kubo's formalism, while we use EHRG model to estimate the viscosity coefficients obtained using relativistic kinetic theory.

Results for shear viscosity coefficient estimated using relativistic kinetic theory are shown in Fig. (3.1). The general behavior of  $\eta/s$  is similar to that observed in Ref. [46] where the authors considered EHRG within relativistic molecular kinetic theory unlike relaxation time approximation scheme used in this work. We also compare our results of  $\eta/s$  with other model calculations like Chapman-Enskog theory [2], scaling hadron masses and couplings (SHMC) model [3] and chiral perturbation theory [80] at zero baryon chemical potential as shown in Fig. (3.1). We note that the general behavior of  $\eta/s$  is in conformity with these models. We also note that at low temperature ( $\sim 0.120\text{GeV}$ ) where the pions are dominating degrees of freedom, our results matches with Ref. [80] where the authors estimates  $\eta/s$  for the gas of pions using chiral perturbation theory while at high temperature (above  $0.120\text{ GeV}$ ) our results matches with

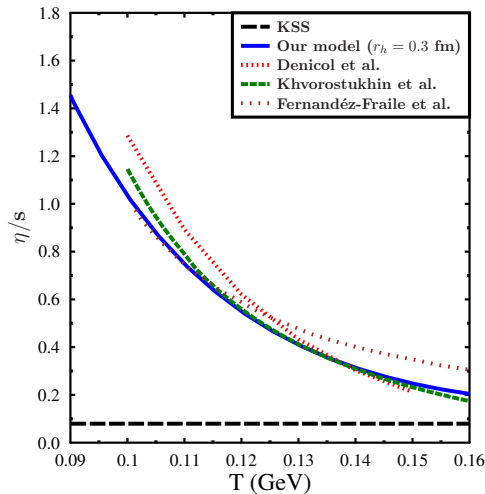


Figure 3.1: Comparison of shear viscosity to entropy density ratio estimated within various other models with our model.

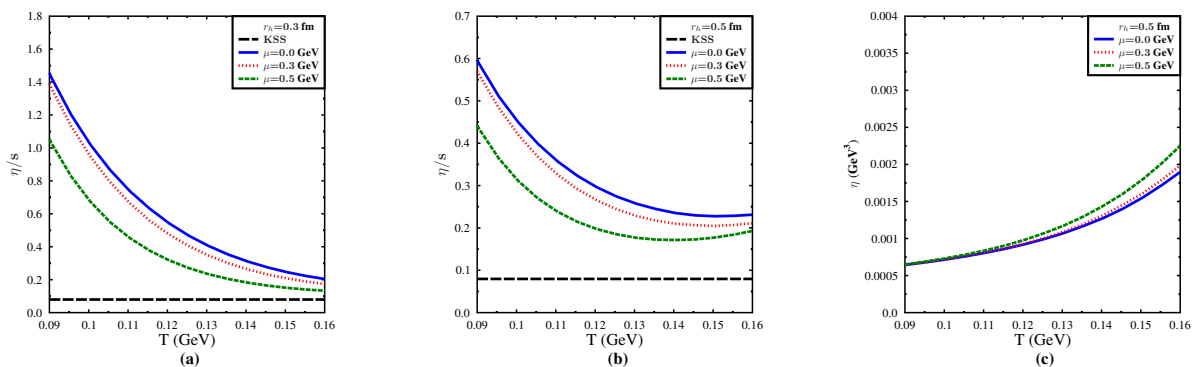


Figure 3.2: Left panel: Shear viscosity to entropy density ( $\eta/s$ ) ratio of temperature for different chemical potentials for  $r_h = 0.3$  fm. Middle panel:  $\eta/s$  for  $r_h = 0.5$  fm. Right panel: Shear viscosity coefficient for  $r_h = 0.5$  fm.

Ref. [3] where the authors estimated this ratio in SHMC model for hadronic matter. Further we observe that at finite chemical potential, although the general behavior of the ratio is similar as a function of temperature, ratio is smaller than that at  $\mu = 0$  GeV and approaches closer to KSS bound. Thus finite baryon chemical potential significantly affect  $\eta/s$ . Although the shear viscosity itself increases with  $\mu$  as shown in Fig. 3.2(c), decrease in ratio  $\eta/s$  at finite  $\mu$  is solely

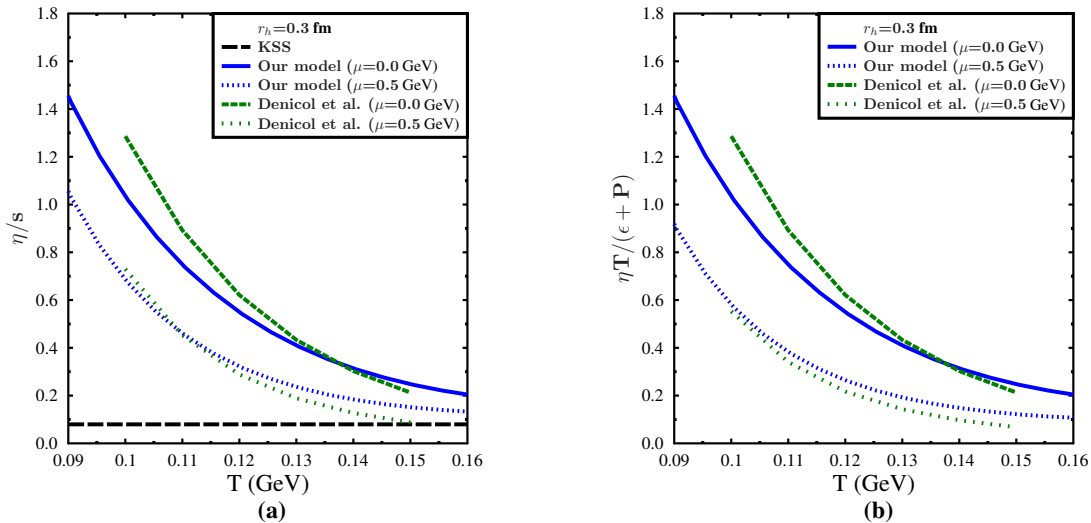


Figure 3.3: Comparison of fluidity measures in our model with Ref. [2] at two different chemical potentials.

due to rapid increase in entropy density. This behavior of  $\eta/s$  at finite baryon density is consistent with Ref. [2] where the authors have estimated  $\eta/s$  using Chapman-Enskog theory within hadron resonance gas model. We compare our results with the results of Ref. [2] at zero and finite  $\mu$  as shown in Fig. 3.3(a). We note that the general behavior of  $\eta/s$  is similar except the fact that the value approaches closer to KSS bound in Chapman-Enskog theory.

It is important to note that at finite chemical potential,  $\eta/s$  cannot be inferred as a measure of fluidity [81]. Also this ratio can be shown to violate KSS bound in kinetic theory. Based on crude kinetic theory argument one can show that  $\eta \approx \frac{1}{3} \sum_a (n \langle p \rangle \lambda)_a$ , where  $n$  is number density,  $\langle p \rangle$  is thermal momentum and  $\lambda$  is mean free path. Kinetic theory is valid only for those gases for which mean free path is much smaller than the typical size of the system ( $L$ ) i.e,  $\lambda \ll L$  and for those gases for which  $\lambda$  must be larger than inter particle spacing. Then uncertainty relation  $\lambda \langle p \rangle \geq 1$  implies that there is a lower bound to shear viscosity,  $\eta \gtrsim 2T^3$  [82]. Further, in the non-relativistic limit one can show that the shear viscosity of the gas of hard spheres is independent of number of particle species [41]. On the other hand, entropy density of the gas consisting

multiple hadronic species (which also goes as  $T^3$ ) can be made very large so that ratio  $\eta/s$  can be made arbitrarily small. In fact at sufficiently high chemical potential mixing entropy of multicomponent hadron gas overwhelms and hence ratio  $\eta/s$  can go below KSS bound. This fact has been used in Ref. [83] to give counterexample to KSS bound.

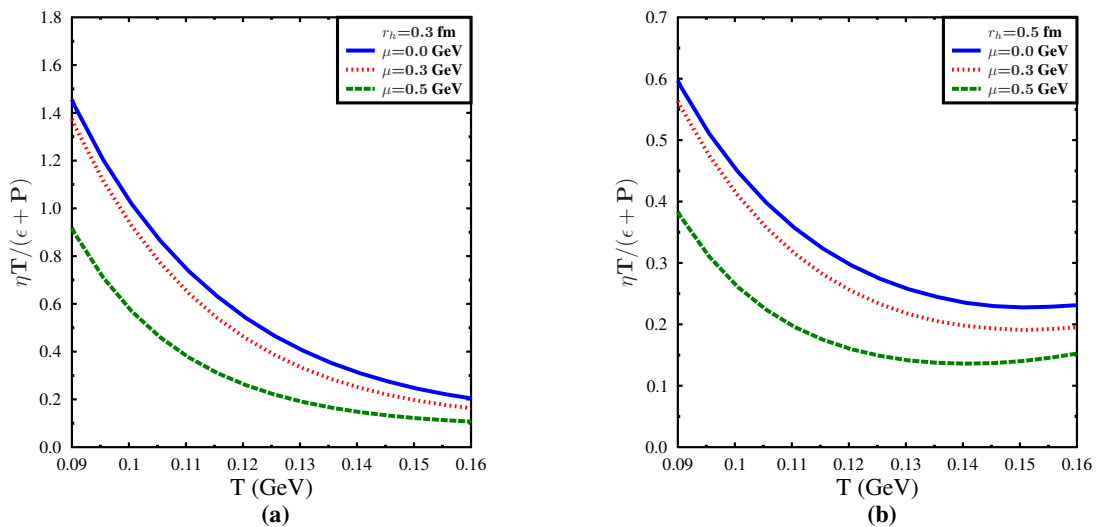


Figure 3.4: Fluidity measure  $\frac{\eta T}{(\epsilon + P)}$  at different chemical potentials for  $r_h = 0.3$  fm and 0.5 fm.

At finite  $\mu$ , it is the ratio  $\eta T/(\epsilon + P)$  which is correct measure of fluidity [81]. Quantity  $\epsilon + P$  is called enthalpy and as per thermodynamical relation,  $\epsilon + P = Ts + \mu n_B$ , we note that at  $\mu = 0$  we get back  $\eta/s$  as a fluidity measure. From Fig. (3.4) we note that effect of finite chemical potential is more pronounced in ratio  $\eta T/(\epsilon + P)$ . This can again be attributed to rapid rise in enthalpy at finite  $\mu$ . The general behavior of the ratio  $\eta T/(\epsilon + P)$  is again in conformity with Ref. [2] as shown in Fig. 3.3(b) except the fact that for given chemical potential the ratio is smaller in Chapman-Enskog theory.

Fig.(3.5) shows results for the bulk viscosity. We note that ratio  $\zeta/s$  decreases with temperature at zero chemical potential. As shown in Fig.(3.6), the general behavior of  $\zeta/s$  is similar to that observed in Ref. [3] where the authors estimated the bulk viscosity using SHMC model. At finite chemical potential although

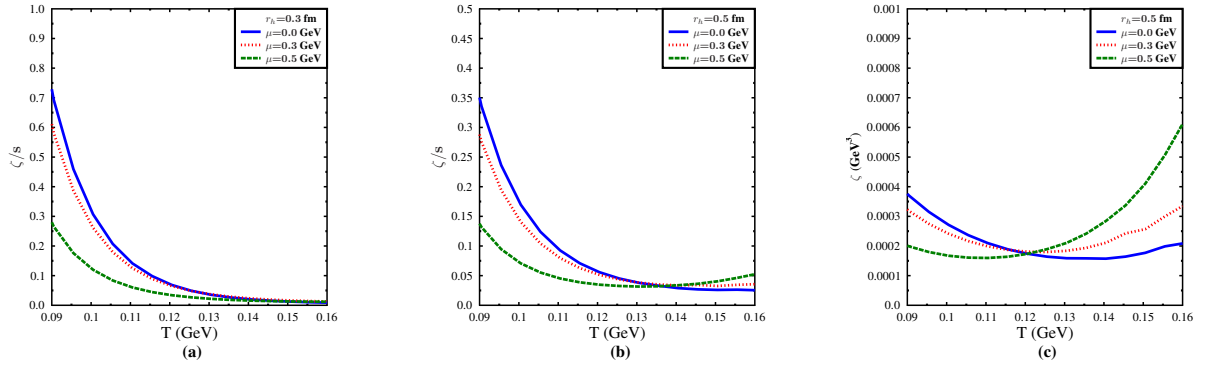


Figure 3.5: Left panel: Bulk viscosity to entropy density ( $\zeta/s$ ) ratio of temperature for different chemical potentials for  $r_h = 0.3$  fm. Middle panel:  $\zeta/s$  for  $r_h = 0.5$  fm. Right panel: Bulk viscosity coefficient for  $r_h = 0.5$  fm.

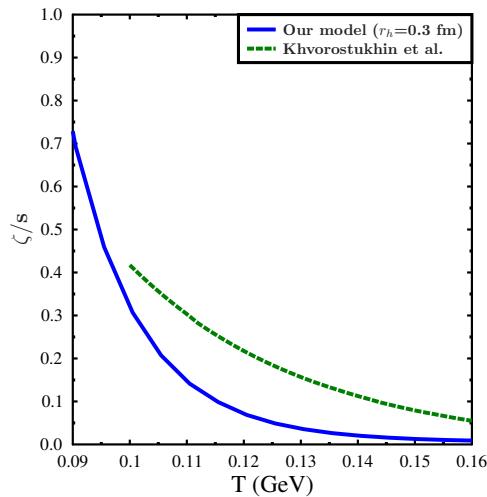


Figure 3.6: Comparison of bulk viscosity to entropy density ratio estimated within SHMC model [3] with our model.

the ratio  $\zeta/s$  decreases at low temperature, it increases in the window  $T = 0.120 - 0.160$  GeV. This is because bulk viscosity itself increases very rapidly in this window as shown in Fig.(3.5c). This rise may be attributed to the explicit scale symmetry violation by finite chemical potential and hence the massive nucleon excitations which contribute more at finite baryon chemical potential [71]. We might mention here that although the inelastic scattering processes

needs to be taken into account for the precise estimation of the bulk viscosity [84], authors in Ref. [85] showed that inelastic processes are irrelevant in the bulk viscosity computation at low and moderate temperatures. In Fig. (3.6) we compare  $\zeta/s$  estimated in our model with SHMC model [3]. We note that our  $\zeta/s$  curve vanishes faster at high temperature.

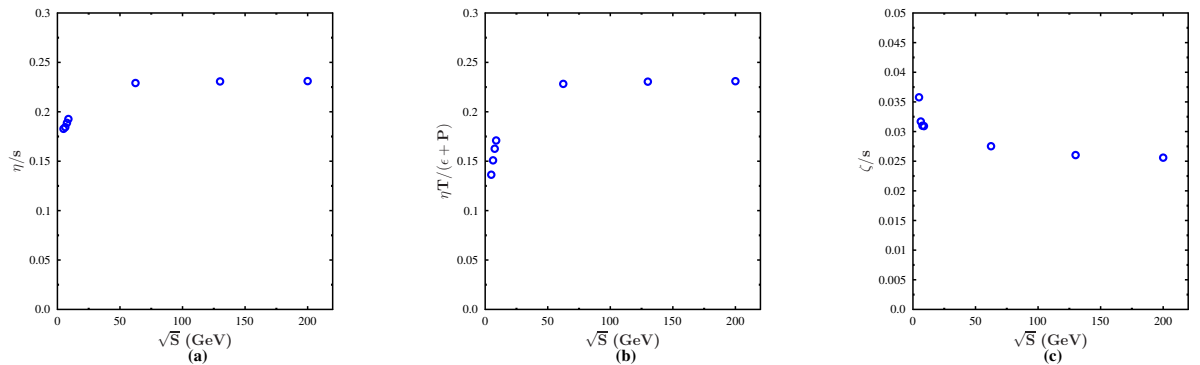


Figure 3.7: Viscosity coefficients along the chemical freeze-out curve.

One can make connection with heavy ion collision experiments by finding the beam energy ( $\sqrt{S}$ ) dependence of the temperature and chemical potential. This is extracted from a statistical thermal model description of the particle yield at various  $\sqrt{S}$  [86]. The freeze out curve  $T(\mu)$  is parametrized by  $T(\mu) = a - b\mu^2 - c\mu^4$ , where,  $a = 0.166 \pm 0.002$  GeV,  $b = 0.139 \pm 0.016$  GeV $^{-1}$  and  $c = 0.053 \pm 0.021$  GeV $^{-3}$ . The energy dependence of the baryon chemical potential is given as  $\mu = d/(1 + e\sqrt{S})$ , with,  $d = 1.308 \pm 0.028$  GeV, and  $e = 0.273 \pm 0.008$  GeV $^{-1}$ . From Fig. 3.7(a) we observe that ratio  $\eta/s$  is well above KSS bound at low center of mass energy and increases monotonically to become constant at higher  $\sqrt{S}$  along freeze-out curve. This is legitimate since low  $\sqrt{S}$  corresponds to low temperature and high chemical potential along freeze-out curve at which shear viscosity is smaller. Fig. 3.7(b) shows ratio  $\eta T/(\epsilon+P)$  along chemical freeze-out. We observe that this ratio again remains constant apart from initial rise. Since ratio  $\eta T/(\epsilon+P)$  is a true measure of fluidity at finite baryon chemical potential, we conclude that in chemical freeze-out transition the fluid behavior of hadron gas does not change. Further, along freeze-out curve ratio  $\zeta/s$  decreases monotonically first

and then becomes independent at higher center of mass energies as shown in Fig. 3.7(c).

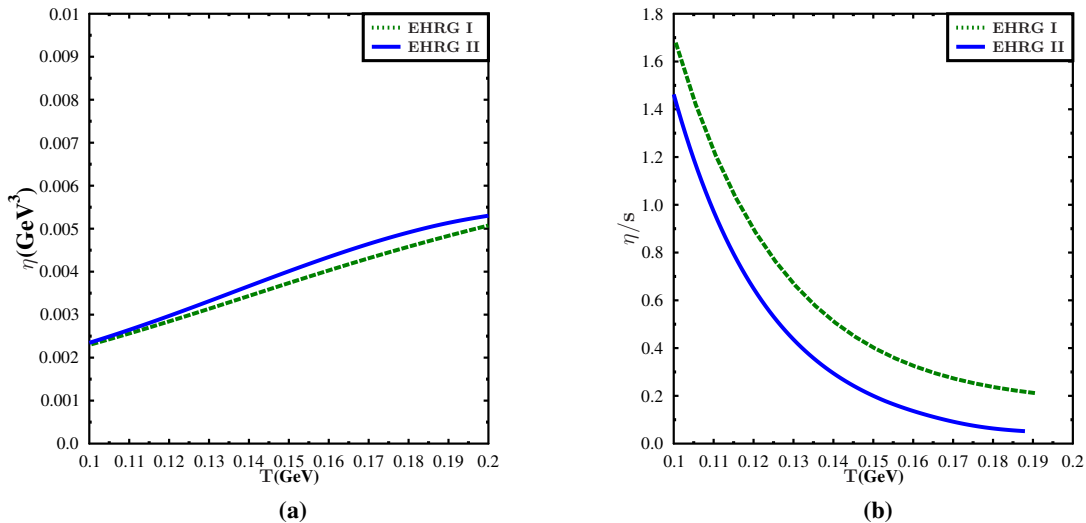


Figure 3.8: Left panel shows shear viscosity coefficient estimated within EHRG-I and EHRG-II models. Right panel shows shear viscosity to entropy density ratio.

Fig. 3.8(b) shows shear viscosity to entropy density ratio estimated in two models, EHRG-I and EHRG-II. We note that the effect  $T$  (and  $\mu$ ) dependent hadron masses is also reflected in transport properties. Shear viscosity is proportional to average thermal momentum which is certainly affected by temperature dependent hadronic species in the system. Nevertheless, the shear viscosity itself does not change much [Fig. 3.8(a)], but the ratio  $\eta/s$  is smaller in EHRG-II model than in EHRG-I due to more rapid increase in the entropy density in former. This effect is more important around transition temperature since the shear viscosity shows peculiar behavior around this temperature. It may be interesting to compare these results with the results of Ref. [47] where the authors estimated  $\eta/s$  within EHRG model extended by inclusion of exponentially rising Hagedorn density of states. They observed that the inclusion of Hagedorn density of states significantly lowers  $\eta/s$  and this ratio approaches close to the KSS bound near  $T_c$ . Thus, they argued that the inclusion of Hagedorn states could explain the low value of shear viscosity in the hadronic phase. Since we observed the same

behavior of  $\eta/s$  near  $T_c$  but with the inclusion of medium dependent hadronic states, it may be again tempting to conclude that the effects of Hagedorn states can be alternatively simulated by including  $T$  and  $\mu$  dependent hadron masses in EHRG.

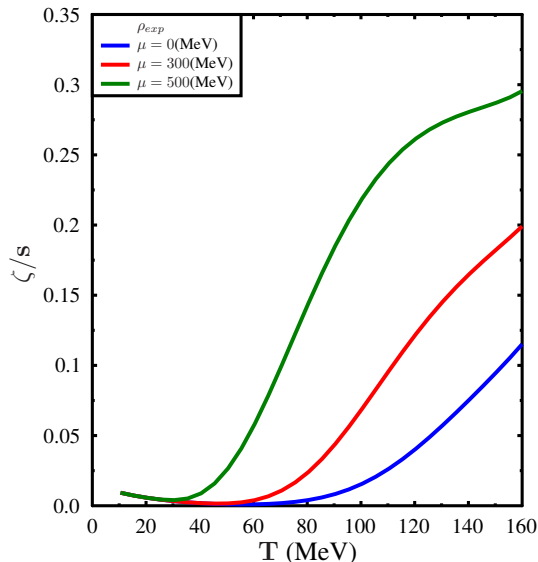


Figure 3.9: Bulk viscosity to entropy density in Kubo's formalism (Eq. 3.2.8) at different chemical potentials estimated within HRG model with discrete and exponential mass spectrum.

Fig. (3.9) shows bulk viscosity to entropy density ratio in Kubo's formalism estimated within HRG model which include discrete as well as continuum exponential mass spectrum. We note that the ratio decrease with temperature at low temperature followed by a sharp increase and finally flattens out at temperatures around 160 MeV. This behavior is connected with the behavior of velocity of sound with temperature through Eq.(3.2.8). The initial decrease of  $\zeta/s$  with temperature is due to increase of sound velocity at low temperature due to excitation of light hadrons. At temperature  $T > 60$  MeV, the sharp rise is related to the decrease of velocity of sound with excitations of heavier hadrons leading to decrease of sound velocity which finally flattens out at temperatures around 155 MeV (see Fig. 2.3). The larger bulk viscosity to entropy ratio at higher chem-

ical potential is again related to decrease of velocity of sound due to excitation of heavier baryons. Such a behavior of rising of  $\zeta/s$  with temperature on the hadronic side is in contrast to decreasing behavior of the same within the PHSD transport code. On the other hand, in Ref. [87], the increasing behavior of  $\zeta/s$  with temperature was observed on the hadronic side.

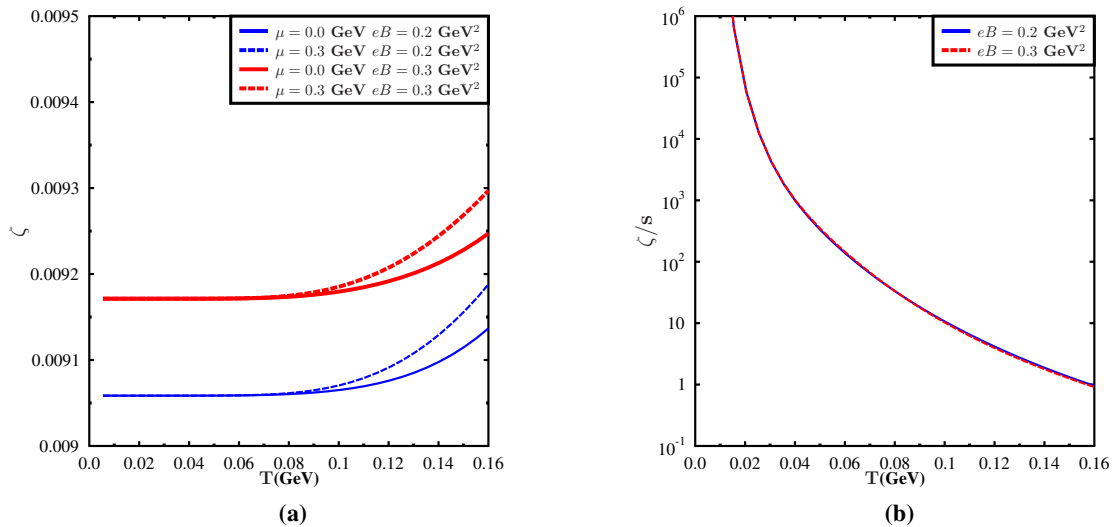


Figure 3.10: Left panel: Bulk viscosity in Kubo's formalism (Eq. 3.2.15) at different magnetic field and chemical potentials. Right panel: Bulk viscosity to entropy density in Kubo's formalism at different magnetic fields.

Fig. 3.10(a) shows bulk viscosity as a function of temperature at two different magnetic fields and chemical potentials. We note that vacuum contribution due to finite magnetic field dominates the bulk viscosity up to 0.1 GeV. This behavior may be interpreted as follows. The effective mass of the charged particle in magnetic field is given by

$$m_*^2 = m^2 + B(1 - 2s) \quad (3.3.1)$$

where  $s$  is total spin of the particle. This effective mass increases with magnetic field for spin 0 channel but decreases for spin 1 channel and remains same for spin 1/2 channel. Thus statistical weight factor,  $\exp(-\beta m_*)$  is larger for spin 1 chan-

nel than for spin 0 channel. At low temperature where the system is dominated by pions, thermal contribution to thermodynamic quantities (pressure, energy density, magnetization, susceptibility) is very small. Hence these quantities are dominated by vacuum part due to finite magnetic field. At finite magnetic field, as the bulk viscosity is proportional to magnetic susceptibility, bulk viscosity has dominant contribution from vacuum susceptibility. Above  $T \simeq 0.1$  GeV, due to thermal excitation of  $\rho^\pm$  mesons and other heavier hadrons, bulk viscosity rises. Also at finite chemical potential we note that bulk viscosity rises more rapidly as compared to  $\mu = 0$  case and thermal contribution to the bulk viscosity starts at lower temperature. This is due to thermal excitation of baryons at lower temperature.

Fig. 3.10(b) shows bulk viscosity in units of entropy density at finite magnetic field ( $eB$ ). We note that behavior of  $\zeta/s$  in magnetic field is opposite to that of  $eB = 0$  case. This is a reflection of the fact that bulk viscosity is non-zero even at  $T = 0$  while entropy density is zero so that ratio  $\zeta/s$  blows up. As temperature increases, entropy density increases while bulk viscosity remains constant to its vacuum value, whence  $\zeta/s$  decreases.

### 3.4 Conclusion

In this chapter we estimated the bulk and shear viscosities of hadronic matter. To estimate bulk viscosity coefficient we used two different formalisms, *viz.*, Kubo formalism and relativistic kinetic theory. The thermodynamical quantities were estimated using HRG and its extensions. Shear viscosity coefficient was estimated using kinetic theory only.

The bulk viscosity to entropy density ratio ( $\zeta/s$ ) estimated using Kubo's formalism rises with temperature, while at finite chemical potential, the  $\zeta/s$  become higher as compared to  $\mu = 0$  and is related to the fact that the velocity of sound becomes smaller due to finite chemical potential with excitation of heavier baryons contributing more to the energy density as compared to the pressure. Unlike Kubo formalism, ratio  $\zeta/s$  estimated using relativistic kinetic theory decreases with temperature and almost vanishes near transition temperature.

The shear viscosity to entropy density ratio estimated using relativistic kinetic theory shows decreasing behavior with temperature. Further, at finite chemical potential  $\eta/s$  shows same behavior as a function of temperature but ratio is smaller as compared to  $\mu = 0$ . This decrease is solely due to rapid increase in entropy density at finite  $\mu$ . At finite baryon density  $\eta T/(\epsilon + P)$  is correct measure of fluidity. We find that effect of finite  $\mu$  is more pronounced for  $\eta T/(\epsilon + P)$  and this is again attributed to rapid rise in enthalpy.

In order to make connection with heavy ion collision experiments we computed both  $\eta/s$  and  $\zeta/s$  along chemical freeze-out line. Along chemical freeze-out curve both the ratios  $\eta/s$  and  $\eta T/(\epsilon + P)$  remains constant apart from initial rise. This suggest that fluid behavior of hadron gas does not change along chemical freeze-out transition. Further, the ratio  $\zeta/s$  decreases monotonically and then becomes independent of center-of-mass energy along freeze-out.

# Chapter 4

## Transport properties of hot and dense quark matter

### 4.1 Thermodynamics of two flavor NJL model and meson masses

We summarize here the thermodynamics of the simplest NJL model with two flavors with a four point interaction in the scalar and pseudo scalar channels with Lagrangian given as

$$\mathcal{L} = \bar{\psi}(i\gamma_{\mu}\partial^{\mu} - m_0)\psi - G((\bar{\psi}\psi)^2 + (\bar{\psi}i\gamma^5\mathbf{t}^a\psi)^2). \quad (4.1.1)$$

Here,  $\psi$  is the doublet of u and d quarks. We also have assumed isospin symmetry and have taken the same (current)mass  $m_0$  for both the flavors. Using the standard methods of thermal field theory, one can write down the thermodynamic potential within a mean field approximation corresponding to the Lagrangian

Eq.(4.1.1) as [88]

$$\begin{aligned}\Omega(\beta, \mu) &= -\frac{2N_c N_f}{(2\pi)^3} \int \sqrt{\mathbf{k}^2 + M^2} d\mathbf{k} \\ &\quad - \frac{2N_c N_f}{(2\pi)^3 \beta} \int d\mathbf{k} (\ln(1 + \exp(-\beta(E - \mu))) + \ln(1 + \exp(-\beta(E + \mu)))) \\ &\quad + \frac{(M - m_0)^2}{4G},\end{aligned}\tag{4.1.2}$$

where,  $\beta$  is inverse of temperature and  $\mu$  is the quark chemical potential and  $E(\mathbf{k}) = \sqrt{\mathbf{k}^2 + M^2}$  is the on shell single particle energy with 'constituent' quark mass  $M^*$ . The constituent quark mass satisfies the self consistent gap equation

$$M = m_0 - 2G\rho_s = m_0 + \frac{2N_c N_f}{(2\pi)^3} \int \frac{M}{E(\mathbf{k})} (1 - f_-(\mathbf{k}, \beta, \mu) - f_+(\mathbf{k}, \beta, \mu)) d\mathbf{k}\tag{4.1.3}$$

where, we have introduced the scalar density  $\rho_s$  given as

$$\rho_s = \langle \bar{\psi}\psi \rangle = -\frac{2N_c N_f}{(2\pi)^3} \int d\mathbf{k} \frac{M}{E(\mathbf{k})} (1 - f_-(\mathbf{k}) - f_+(\mathbf{k})).\tag{4.1.4}$$

In the above  $f_{\mp}(\mathbf{k}, \beta, \mu) = (\exp(\beta(E \mp \mu)) + 1)^{-1}$  is the fermion distribution function for quarks and anti-quarks respectively with a constituent mass  $M$  that are related to the quark number density in the standard way

$$\rho = \frac{2N_c N_f}{(2\pi)^3} \int d\mathbf{k} [f_-(\mathbf{k}, \beta, \mu) - f_+(\mathbf{k}, \beta, \mu)]\tag{4.1.5}$$

Within random phase approximation (RPA), the meson propagator can be calculated as

$$D_M(\omega, \mathbf{p}) = \frac{2iG}{1 - 2G\Pi_M(\omega, \mathbf{p})}\tag{4.1.6}$$

where,  $M = \sigma, \pi$  for scalar and pseudo scalar channel mesons respectively and  $\Pi_M$  is the corresponding polarization function. The mass of the meson is given by the pole position of the meson propagator at zero momentum specified by the

---

\*Notations in this chapter will be quite different from that in Chapter 2 in the context of NJL model.

equation

$$1 - 2G\Pi_M(m_M, 0) = 0 \quad (4.1.7)$$

Explicitly,

$$\Pi_\pi(m_\pi, \mathbf{0}) = I_1 - m_\pi^2 I_2(m_\pi, 0) \quad (4.1.8)$$

$$\Pi_\sigma(m_\sigma, \mathbf{0}) = I_1 - (m_\sigma^2 - 2M^2)I_2(m_\sigma) \quad (4.1.9)$$

where,

$$I_1 = \frac{2N_c N_f}{(2\pi)^3} \int d\mathbf{q} \frac{\mathbf{q}}{E_q} (1 - f_-(\mathbf{q}, \beta, \mu) - f_+(\mathbf{q}, \beta, \mu)) \quad (4.1.10)$$

and,

$$I_2(m_{\pi/\sigma}) = \frac{2N_c N_f}{(2\pi)^3} \int d\mathbf{q} \frac{\mathbf{q}}{E_q} (1 - f_-(\mathbf{q}, \beta, \mu) - f_+(\mathbf{q}, \beta, \mu)) \frac{1}{m_{\pi/\sigma}^2 - 4E(\mathbf{q})^2} \quad (4.1.11)$$

so that the masses of the pion and sigma mesons are given, using the gap equation Eq.(4.1.3) by

$$\frac{m_0}{M} + 2Gm_\pi^2 I_2(m_\pi) = 0 \quad (4.1.12)$$

for pions and

$$\frac{m_0}{M} + 2G(m_\sigma^2 - 4M^2)I_2(m_\sigma) = 0 \quad (4.1.13)$$

for the mass of the sigma meson. The medium dependent masses of these mesons, so obtained, will be used later to estimate the relaxation time of from the scattering of quarks and anti quarks through exchange of mesons. In the following we look into the Boltzmann equation to derive the transport coefficients in terms of the relaxation time.

## 4.2 Boltzmann equation in relaxation time approximation and transport coefficients revisited

Within a quasi particle approximation, a kinetic theory treatment for calculation of transport coefficient can be a reasonable approximation that we shall be following similar to as done in Refs. [3, 36, 43]<sup>†</sup>. The plasma can be described by a phase space density for for each species of particle. Near equilibrium, the distribution function can be expanded about a local equilibrium distribution function for the quarks as,

$$f(\mathbf{x}, \mathbf{p}, t) = f^0(\mathbf{x}, \mathbf{p}, t) + f^1(\mathbf{x}, \mathbf{p}, t)$$

where, the local equilibrium distribution function  $f^0$  is given as

$$f^0(\mathbf{x}, \mathbf{p}, t) = [\exp(\beta(x)(u_\nu(x)p^\nu \mp \mu(x))) + 1]^{-1} \quad (4.2.1)$$

Here,  $\mathbf{u}$  is the flow velocity,  $\mu$  is the chemical potential associated with a conserved charge like baryon number.  $\mp\mu$  corresponds to particle and antiparticle distribution functions. Further,  $E = \sqrt{\mathbf{p}^2 + M^2}$  with a mass  $M$  which in general is medium dependent. The departure from the equilibrium is described by the Boltzmann equation

$$\frac{df_a}{dt} = \frac{\partial f_a}{\partial t} + \mathbf{v}_a \cdot \nabla f_a - \nabla E_a \cdot \nabla_p f_a = -C^a[f] \quad (4.2.2)$$

where, we have introduced the species index 'a' on the distribution function. With a medium dependent mass, the last term on the left hand side can be written as  $(M/E_a)(\partial m/\partial x^i)(\partial f^a/\partial p^i)$  and the Eq. (4.2.2) can be rewritten as

$$\frac{df_a}{dt} = \frac{p^\mu}{E_a} \partial_\mu f^a - \frac{M}{E_a} \frac{\partial m}{\partial x^i} \frac{\partial f^a}{\partial p^i} = -C^a[f] \quad (4.2.3)$$

---

<sup>†</sup>In this chapter we will use slightly different method as well as notations to derive transport coefficients.

To study the transport coefficients, one is interested in small departure from equilibrium in the hydrodynamic limit of slow spatial and temporal variations. In the collision term on the right hand side we shall be limiting ourselves to  $2 \rightarrow 2$  scatterings only. Within the relaxation time approximation, in the collision term for species, all the distribution functions are given by the equilibrium distribution function except the distribution function for particle 'a'. The collision term, to first order in the deviation from equilibrium function will be then proportional to  $f_1$ , realizing the fact that  $C^a[f_{eq}] = 0$  by local detailed balance. In that case, the collision term is given by

$$C[f] = -f_a^1/\tau_a \quad (4.2.4)$$

$\tau^a$ , the relaxation time for particle 'a', in general is a function of energy but one can define a mean relaxation time taking a thermal average of the scattering cross sections which we shall spell out in the following subsection.

We shall next use the Boltzmann equation to calculate the transport coefficients in this relaxation time approximation. The departure from equilibrium for the distribution function is used to estimate the departure of the equilibrium energy momentum tensor to define the transport coefficients. Let us consider now the structure of the energy momentum tensor  $T^{\mu\nu}$  and of the quark current  $J_\mu$ .  $T^{\mu\nu}$  and  $J_\mu$  can be written in terms of chemical potential, temperature and the four velocity  $u_\mu$  as

$$T^{\mu\nu} = -Pg^{\mu\nu} + wu^\mu u^\nu + \Delta T^{\mu\nu}, \quad (4.2.5)$$

and,

$$J_\mu = nu_\mu + \Delta J_\mu, \quad (4.2.6)$$

where,  $P(T, \mu)$  is the pressure,  $\epsilon$  is the energy density,  $w = \epsilon + P$  is the enthalpy,  $u_\mu$  is the four velocity of the fluid. The dissipative parts are given by

$$\Delta T^{\mu\nu} = \eta \left( D^\mu u^\nu + D^\nu u^\mu + \frac{2}{3} \Delta^{\mu\nu} \partial_\alpha u^\alpha \right) - \zeta \partial_\alpha u^\alpha, \quad (4.2.7)$$

and,

$$\Delta J_\mu = \lambda \left( \frac{nT}{w} \right)^2 D_\mu \left( \frac{\mu}{T} \right) \quad (4.2.8)$$

with  $\eta$ ,  $\zeta$  and  $\lambda$  are the coefficients of shear viscosity, bulk viscosity and thermal conductivity respectively. Further, in the above,  $D_\mu = \partial_\mu - u_\mu u^\alpha \partial_\alpha$  is the derivative normal to  $u^\mu$ . It is useful to note that, in the fluid rest frame, which will be used to calculate the transport coefficients,  $D_0 = 0$  and  $D_i = \partial_i$ . We also would like to note that for system without any conserved current, the thermal conductivity is zero [80, 82].

The energy momentum tensor,  $T^{\mu\nu}$  and the current  $J_\mu$  can also be written in terms of the distribution functions as,

$$T^{\mu\nu} = \sum_a \int d\Gamma_a \frac{p^\mu p^\nu}{E_a} f_a + g^{\mu\nu} V, \quad (4.2.9)$$

and,

$$J_\mu = \int \sum_a t_a \int d\Gamma_a \frac{p_\mu}{E_a} f_a, \quad (4.2.10)$$

where, we have introduced the notations  $d\Gamma_a = g_a \frac{d^3 p}{(2\pi)^3}$ ,  $g_a$  being the degeneracy for species  $a$ ;  $p^\mu = (E_a, \mathbf{p})$ , with  $E^a = \sqrt{\mathbf{p}^2 + m_a^2}$ . Further,  $V$  is the mean field or the ‘vacuum’ energy density contribution in terms of the mean field giving a medium dependent mass and  $t^a = \pm 1$  for particles and antiparticles respectively. The non equilibrium part of the distribution function is used to calculate the departure from equilibrium of the energy momentum tensor. The variation of the spatial part of Eq.(4.2.9) is given as

$$\delta T^{ij} = \sum_a \int d\Gamma_a \frac{p^i p^j}{E_a} \left( \delta f_a - f_a^0 \frac{\delta E_a}{E_a} \right) - \delta^{ij} \delta V, \quad (4.2.11)$$

where, the variation of the quasi particle energy is also included to take into account the medium dependence of the mass. The deviation of the distribution function, in general, will have departure from the equilibrium form. In addition it can also change from the change in the single particle energy from its equilibrium value. Defining the equilibrium values of  $T$ ,  $\mu$  and  $E$  with a superscript ‘0’, we

can write

$$\delta f_a = f_a(E_a, T, \mu) - f_a^0(E_a^0, T^0, \mu^0) = \delta \tilde{f}_a - \frac{\delta E_a}{T} (f_a^0(1 - f_a^0)), \quad (4.2.12)$$

where, we have defined  $\delta \tilde{f}_a = f_a(E_a, T, \mu) - f_a(E_a, T_0, \mu_0)$  and have retained up to the linear term in  $\delta E_a$ . Let us note that it is  $\delta \tilde{f}_a$  which determines the transport coefficient as it is defined with the non equilibrium energy, which enters in the energy momentum conservation in the collision term of the Boltzmann equation.

Similarly, using the gap equation, the deviations in the 'vacuum' energy term in Eq.(4.2.9) is given by

$$\delta V = \sum_a \int d\Gamma_a \frac{M}{E_a} f_a \delta M. \quad (4.2.13)$$

This leads to

$$\delta T^{ij} = \sum_a \int d\Gamma_a \frac{p^i p^j}{E_a} \delta \tilde{f} - \sum_a \int d\Gamma_a \frac{M}{E_a} f_a \left( 1 + \frac{p^2(1 - f_a)}{3E_a T} + \frac{\mathbf{p}^2}{3E_a^2} \right) \delta M, \quad (4.2.14)$$

where, we have replaced  $p^i p^j \sim 1/3(\mathbf{p}^2)$  and for the terms involving  $\delta E_a$ , we have used  $\delta E_a = (M/E_a)\delta M$ . The terms involving  $\delta M$  in Eq.(4.2.14) can be shown to vanish by doing an integration by parts leading to

$$\Delta T^{ij} = \sum_a \int d\Gamma_a \frac{p^i p^j}{E_a} \delta \tilde{f}. \quad (4.2.15)$$

In a similar manner, it can be shown that the departure of the quark current due to the non equilibrium part of the distribution function can be written as

$$\Delta J^i = \sum_a t_a \int d\Gamma_a \frac{\mathbf{p}^i}{E_a} \delta \tilde{f} \quad (4.2.16)$$

Next, we compute  $\delta \tilde{f}_a \equiv f^1(x, p)$  using the Boltzmann equation, Eq.(4.2.3), in the relaxation time approximation. This is then used to calculate non equilibrium parts of energy momentum tensor and the quark current to finally relate them to the transport equations using Eqs. (4.2.7) and (4.2.8). To do so, it is convenient

to analyze in a local region choosing an appropriate rest frame. We further note that we shall be working with first order hydrodynamics and hence will keep up to first order in space time gradients only. The left hand side of the Boltzmann equation Eq.(4.2.3), is explicitly small because of the gradients and we therefore may replace  $f^a$  by  $f_a^0$ . In the local rest frame  $u_\mu = (1, 0, 0, 0)$ , but, the gradients of the velocities are nonzero. Further, in the local equilibrium distribution function  $f_a^0$  in Eq.(4.2.1), the flow velocity, temperature and chemical potential all depend upon  $x$ . In addition, the four momentum  $p_a$  also depends upon the coordinate  $x$  through the dependence of mass on the same. We give here some details of the calculations of the left hand side of the Boltzmann equation. To do so, let us calculate the derivative of the equilibrium distribution function Eq.(4.2.1) given as

$$\partial_\mu f_a^0 = -f_a^0(1 - f_a^0) \left[ -\frac{1}{T^2}(E_a - \mu_a) + \frac{1}{T}\partial_\mu(p_\nu u^\nu - \mu^a) \right] \quad (4.2.17)$$

Noting the fact the  $E^a$  also has spatial dependence through its mass dependence, one obtains for the first term in the L.H.S. of Eq.(4.2.3)

$$\frac{p^\mu}{E^a} \partial_\mu f_a^0 = \frac{f_a^0(1 - f_a^0)}{E^a} \left[ \frac{E^a}{T^2} p^\mu \partial_\mu T + p^\mu \partial_\mu \left( \frac{\mu^a}{T} \right) - \frac{1}{T} (p^\mu \partial_\mu E^a + p^\mu p^\nu \partial_\mu u_\nu) \right] \quad (4.2.18)$$

while, the second term is given as

$$\frac{\partial f_a^0}{\partial p^i} = -f_a^0(1 - f_a^0) \frac{p_i}{E^a T} \quad (4.2.19)$$

Next using the fact that  $u^\nu u_\nu = 1$ , one can show that, in the local rest frame,  $\partial_\nu u^0 = 0$ . This can be used to expand the term with gradient of flow velocity Eq.(4.2.18) in terms of spatial and temporal derivatives of the flow velocity  $u_i$ . Combining both Eq.(4.2.18) and Eq.(4.2.19), LHS of Eq.(4.2.3), is given as,

$$\frac{f_a^0(1 - f_a^0)}{E^a} \left[ -E^a \partial_0 \left( \frac{E^a - \mu^a}{T} \right) \frac{E^a p^i}{T} \left( \frac{\partial_i T}{T} - \partial_0 u_i \right) + p^i \partial_i \left( \frac{\mu^a}{T} \right) - p^i p^j \partial_j u_i \right] = -\frac{f_a^1}{\tau}. \quad (4.2.20)$$

Next, we can use the conservation equation  $\partial_\mu T^{\mu\nu} = 0$  to write  $\partial_0 u_i = \partial_i P$  in the rest frame. Using thermodynamic relations  $\partial_i P = s \partial_i T + n \partial_i \mu$  to write

$(\partial_i T)/T - \partial_0 u_i = -(nT/w)\partial_i(\mu/T)$ . Further, the spatial derivative of the flow velocity can be decomposed in to a traceless part and a divergence part in the flow velocity. This leads to

$$\frac{df_a^0}{dt} = \frac{f_a^0(1-f_a^0)}{T} q^a(\beta, \mu) = -\frac{\delta \tilde{f}_a}{\tau_a} \quad (4.2.21)$$

where, we have defined,

$$\begin{aligned} q^a(T, \mu) = & -\left[ \frac{\partial T}{\partial t} \left( \frac{E^a - \mu^a}{T} - \frac{\partial E^a}{\partial T} \right) \right. \\ & - \frac{\partial \mu}{\partial t} \left( \frac{\partial E^a}{\partial \mu} - t^a \right) + \frac{T}{E^a} \left( t^a - \frac{E^a n}{w} \right) p^i \partial_i \left( \frac{\mu}{T} \right) \\ & \left. - \frac{p^i p^j}{2E^a} W_{ij} + \frac{\mathbf{p}^2}{3E^a} \partial_k u^k \right] \end{aligned} \quad (4.2.22)$$

The Boltzmann equation Eq.(4.2.21) thus relates the non equilibrium part of the distribution functions to the variation in fluid velocity, the temperature and the chemical potential. This will be used to calculate the dissipative part of the energy momentum tensor.

Using stress energy conservation  $\partial_\mu T^{\mu\nu} = 0$ ; the baryon number conservation equation  $\partial_\mu J^\mu = 0$ , as well as standard thermodynamic relations, one can relate the temporal derivatives of temperature and chemical potentials with the velocity of sound at constant baryon density and constant entropy density respectively as

$$\partial_0 T = -v_n^2 T \nabla \cdot \mathbf{u} \quad (4.2.23)$$

and

$$\partial_0 \mu = -v_s^2 \mu \nabla \cdot \mathbf{u}. \quad (4.2.24)$$

The velocity of sound at constant density( $n$ ) can be calculated using Jacobian methods as follows.

$$\begin{aligned}
v_n^2 &= \left( \frac{\partial P}{\partial \epsilon} \right)_n \\
&= \frac{\frac{\partial P}{\partial T} \frac{\partial P}{\partial \mu} + \frac{\partial P}{\partial \mu} \frac{d\mu}{dT}}{\frac{\partial \epsilon}{\partial T} \frac{\partial \epsilon}{\partial \mu} + \frac{\partial \epsilon}{\partial \mu} \frac{d\mu}{dT}}
\end{aligned} \tag{4.2.25}$$

Since baryon density has been kept constant we write

$$dn(T, \mu) = \frac{\partial n}{\partial T} dT + \frac{\partial n}{\partial \mu} d\mu = 0 \tag{4.2.26}$$

Thus we get

$$\frac{d\mu}{dT} = - \frac{\partial n / \partial T}{\partial n / \partial \mu} \tag{4.2.27}$$

Using Eqs. (4.2.25) and (4.2.27) we get

$$v_n^2 = \frac{\partial(P, n)}{\partial(\epsilon, n)} = \frac{s\chi_{\mu\mu} - n\chi_{\mu T}}{\frac{\partial \epsilon}{\partial T}\chi_{\mu\mu} - \frac{\partial \epsilon}{\partial \mu}\chi_{\mu T}} \tag{4.2.28}$$

where we have defined  $\chi_{xy} = \frac{\partial^2 P}{\partial x \partial y}$  and have used standard thermodynamical relations. Similarly we can obtain speed of sound at constant entropy density  $s$  as,

$$v_s^2 = \left( \frac{\partial P}{\partial \epsilon} \right)_s = \frac{\partial(P, s)}{\partial(\epsilon, s)} = \frac{s\chi_{\mu T} - n\chi_{TT}}{\frac{\partial \epsilon}{\partial T}\chi_{\mu T} - \frac{\partial \epsilon}{\partial \mu}\chi_{TT}} \tag{4.2.29}$$

In the NJL model one can explicitly calculate the derivatives of the energy density with temperature or chemical potential. On the other hand, using thermodynamic relations one can also rewrite Eq.(4.2.28) and Eq.(4.2.29) as

$$v_n^2 = \frac{s\chi_{\mu\mu} - n\chi_{\mu T}}{T(\chi_{\mu\mu}\chi_{TT} - \chi_{\mu T}^2)} \tag{4.2.30}$$

$$v_s^2 = \frac{n\chi_{TT} - s\chi_{\mu T}}{\mu(\chi_{\mu\mu}\chi_{TT} - \chi_{\mu T}^2)} \tag{4.2.31}$$

Thus, we can have from Eq.(4.2.23) and Eq.(4.2.24), the variation for the distri-

bution function in the relaxation time approximation,

$$\frac{\delta \tilde{f}_a}{\tau_a} = -\frac{f_a^0(1-f_a^0)}{T} q^a(T, \mu), \quad (4.2.32)$$

with  $q^a(T, \mu)$  given as

$$q^a(T, \mu) = -Q_a(T, \mu, \mathbf{p}^2) \nabla \cdot \mathbf{u} + \frac{T}{E_a} p^i \partial_i \left( \frac{\mu}{T} \right) \left( t_a - \frac{E_a n}{w} \right) + \frac{p^i p^j}{2T} W_{ij} \quad (4.2.33)$$

In the above, the coefficient of the divergence in flow velocity part,  $Q_a$ , is given by

$$-Q_a(T, \mu, \mathbf{p}^2) = \left[ v_n^2 \left( -E_a + T \frac{\partial E_a}{\partial T} + \mu \frac{\partial E_a}{\partial \mu} \right) + \left( \frac{\partial P}{\partial n} \right)_\epsilon \left( \frac{\partial E}{\partial \mu} - t^a \right) + \frac{\mathbf{p}_a^2}{3E_a} \right] \quad (4.2.34)$$

Substituting the expression for  $\delta \tilde{f}$  from Eq.(4.2.32) in Eq.(4.2.15), in the local rest frame,

$$\delta T^{ij} = \sum_a \int d\Gamma \frac{p_a^i p_a^j}{T E_a} \tau_a f_a^0 (1 - f_a^0) q_a(\mathbf{p}, \beta, \mu). \quad (4.2.35)$$

The contribution of the the term proportional to gradient of  $(\mu/T)$  term in Eq.(4.2.33) vanishes because of symmetry. On comparison of the resulting expression with the tensor structure of the dissipative part of  $\Delta T^{\mu\nu}$  of Eq.(4.2.15), we have the expressions for the shear viscosity coefficient  $\eta$  as

$$\eta = \frac{1}{15T} \sum_a \int d\Gamma_a \frac{\mathbf{p}_a^4}{E_a^2} (\tau_a f_a^0 (1 - f_a^0)). \quad (4.2.36)$$

Similarly, the bulk viscosity coefficient  $\zeta$  is given as

$$\zeta = -\frac{1}{3T} \sum_a \int d\Gamma_a \frac{\mathbf{p}_a^2}{E_a} (\tau_a f_a^0 (1 - f_a^0) Q_a) \quad (4.2.37)$$

In a similar manner, one can substitute  $\delta \tilde{f}$  in Eq.(4.2.16) to obtain

$$\Delta J_i = \sum_a \int d\Gamma_a p^i \tau_a f_a^0 (1 - f_a^0) q^a(t, \mu). \quad (4.2.38)$$

In the above, on the other hand, the term in  $q^a$  that results in a nonzero contri-

bution is the term with gradient in  $(\mu/T)$ . Comparing this with Eq.(4.2.8), we have the thermal conductivity given as

$$\lambda = \left(\frac{w}{nT}\right)^2 \sum_a \int d\Gamma_a \frac{\mathbf{P}^2 \tau_a}{3E_a^2} \left(1 - \frac{t^a n E^a}{w}\right) \quad (4.2.39)$$

However, the solutions for  $Q^a$  as given in Eq.(4.2.34) for the bulk viscosity is to be supplemented by Landau-Lifshitz matching conditions i.e. the variations of the distribution function should be such that they satisfy the conditions  $u_\mu \Delta J^\mu = 0$  and  $u_\mu \Delta T^{\mu\nu} u_\nu = 0$ . In the local rest frame these conditions reduce to

$$\Delta J_0 = \sum_a \int d\Gamma_a t^a \delta f_a = 0 \quad (4.2.40)$$

$$\Delta T^{00} = \sum_a \int d\Gamma_a E_a \delta f_a = 0. \quad (4.2.41)$$

Using Eq.(4.2.12) relating  $\delta f_a$  and  $\delta \tilde{f}$  one can write the Landau Lifshitz conditions in the relaxation time approximation as

$$\Delta J_0 = \langle \tau^a Q^a(T, \mu) t^a g^a(T, \mu) \rangle = 0 \quad (4.2.42)$$

$$\Delta T_{00} = \langle \tau^a Q^a(T, \mu) E^a g^a(T, \mu) \rangle = 0 \quad (4.2.43)$$

with,

$$g^a(T, \mu) = 1 - \frac{T \left(\frac{\partial E^a}{\partial T}\right)_\sigma}{E^a - \mu^a + T \left(\frac{\partial \mu^a}{\partial T}\right)_\sigma} \quad (4.2.44)$$

where, we have defined the derivative with respect to temperature at fixed entropy per quark as [89]

$$\left(\frac{\partial E^a}{\partial T}\right)_\sigma = \left(\frac{\partial E^a}{\partial T}\right)_\mu + \left(\frac{\partial E^a}{\partial \mu}\right)_T \left(\frac{\partial \mu}{\partial T}\right)_\sigma \quad (4.2.45)$$

and

$$\left(\frac{\partial \mu}{\partial T}\right)_\sigma = \frac{1}{T} \left[ \mu + \frac{1}{v_n^2} \left(\frac{\partial P}{\partial n}\right)_\epsilon \right] \quad (4.2.46)$$

The above arises due to the fact that the variations of temperature and chem-

ical potential are not independent variations. They and are related by the hydrodynamic flow of the matter which occurs at constant entropy per baryon  $\sigma = s/n$  [89]. Further, we have introduced the notation [3]

$$\langle \phi_a(p) \rangle = \int d\Gamma_a [\phi_a(p) f_a^0 (1 - f_a^0)].$$

If the variations as in Eq.(4.2.32) do not satisfy the the Landau-Lifshitz conditions Eq.(4.2.42) and Eq.(4.2.43), one may still fulfill them performing a shift [3, 89]

$$\tau_a Q_a \rightarrow \tau_a Q_a - \alpha_n t^a - \alpha_e E^a \quad (4.2.47)$$

where,  $\alpha_n$  and  $\alpha_e$  are the Lagrange multipliers associated with conservation of baryon number and energy. Performing the substitution Eq.(4.2.47) in Eq.(4.2.42) and Eq.(4.2.43) we have the Landau-Lifshitz conditions given as

$$\sum_a t_a \langle \tau_a Q_a \rangle - \alpha_n \sum_a \langle g^a \rangle - \alpha_e \sum_a \langle t^a E^a g^a \rangle = 0, \quad (4.2.48)$$

$$\sum_a \langle E^a \tau^a Q^a \rangle - \alpha_n \sum_a \langle t^a E^a g^a \rangle - \alpha_e \sum_a \langle E_a^2 g^a \rangle = 0. \quad (4.2.49)$$

One can solve these two equations for the coefficients  $\alpha_e$  and  $\alpha_n$  and calculate the bulk viscosity coefficient  $\zeta$  after performing the replacement Eq.(4.2.47) in Eq.(4.2.37). This leads to

$$\zeta = -\frac{1}{3T} \sum_a \int d\Gamma_a \frac{\mathbf{p}_a^2}{E_a} (\tau_a f_a^0 (1 - f_a^0) Q_a) - \alpha_e w - \alpha_n n. \quad (4.2.50)$$

On the other hand, it is convenient to use Eq.(4.2.48) and Eq.(4.2.49) to obtain

$$\alpha_e w + \alpha_n n = - \sum_a \langle \tau^a Q^a \left( E^a - T \frac{\partial E^a}{\partial T} - \mu \frac{\partial E^a}{\partial \mu} \right) + \left( \frac{\partial P}{\partial n} \right)_\epsilon \left( \frac{\partial E^a}{\partial \mu} - t^a \right) \rangle. \quad (4.2.51)$$

Substituting this back in Eq.(4.2.50), we have

$$\begin{aligned} \zeta &= \frac{1}{9T} \sum_a \int d\Gamma^a \tau^a f_a^0 (1 - f_a^0) \\ &\times \left[ \frac{\mathbf{p}^2}{E^a} - 3v_n^2 \left( E^a - T \frac{\partial E^a}{\partial T} - \mu \frac{\partial E^a}{\partial \mu} \right) + 3 \left( \frac{\partial P}{\partial n} \right)_\epsilon \left( \frac{\partial E^a}{\partial \mu} - t^a \right) \right]^2 \end{aligned} \quad (4.2.52)$$

In a similar manner, putting the constraint  $\Delta T^{0i} = 0$  in the rest frame yields, the expression for thermal conductivity as [89]

$$\lambda = \frac{1}{3} \left( \frac{w}{nT} \right)^2 \sum_a \int d\Gamma \frac{\mathbf{p}^2}{E_a^2} \tau^a \left( t^a - \frac{nE^a}{w} \right)^2 f_a^0 (1 - f_a^0) \quad (4.2.53)$$

In passing, we would like to comment here that the expression for thermal conductivity is identical to as derived in Ref. [80] discussed for a hot pion gas within chiral perturbation theory, when one replaces the rate by inverse of the width and fermion distribution functions for the quarks by the bose distribution functions for pions.

Thus all the dissipative coefficients are explicitly positive definite within the relaxation time approximation. The expression for the bulk viscosity reduces to the expression for the same in the limit of vanishing density to that of Ref. [43]. Further, the expression also reduces to the expression for bulk viscosity in Ref [75] when medium dependence of the single particle energy is taken into account . Eq.(4.2.36), Eq.(4.2.52) and Eq.(4.2.53) for the dissipation coefficients shall be the focus of our the discussion in what follows. Let us note that in these equations so far, the unknown quantity is the estimation of the relaxation time  $\tau^a$ . As mentioned earlier,  $\tau^a$ , in general, will be energy dependent but we shall be taking energy averaged estimation of the relaxation time by taking thermal averaging of the scattering cross section.

### 4.2.1 Transition rates and thermal averaging

The key quantity in estimating the transport coefficient within the relaxation time approximation is the thermal averaged transition rate  $\bar{W}$ . The same e.g. for a general fermion fermion scattering process  $a, b \rightarrow c, d$  is given as

$$\bar{W}_{ab} = \frac{1}{n_a n_b} \int d\pi_a d\pi_b f^a(p_a) f^b(p_b) W_{ab}(s) \quad (4.2.54)$$

In the above,  $f_i$  are the distribution functions for the fermions and  $d\pi_i = (1/(2\pi)^3) d\mathbf{p}^i / 2E_i$ ,  $n_i = (g_i/(2\pi)^3) \int d\mathbf{p}_i f(\mathbf{p}_i)$  is the number density of i-th species with degeneracy  $g_i$ . Further, the quantity  $W_{ab}(s)$  is dimensionless, Lorentz invariant and is dependent only on the mandelstam variable  $s$  and is given as

$$W_{ab}(s) = \frac{1}{1 + \delta_{ab}} \int d\pi_c d\pi_d (2\pi)^4 \delta^4(p_a + p_b - p_c - p_d) |\bar{M}|^2 (1 - f_c(\mathbf{p}_c))(1 - f_d(\mathbf{p}_d)). \quad (4.2.55)$$

Here, we have included the Pauli blocking factors. The quantity  $W_{ab}(s)$  can be related to the cross section by noting that

$$\frac{d\sigma}{dt} = \frac{1}{64\pi s} \frac{1}{p_{ab}} |\bar{M}|^2 \quad (4.2.56)$$

where  $p_{ab} = \sqrt{(s - 4m^2)}/2$  is the magnitude of the three momentum of the incoming particles in the center of mass (CM) frame if the masses of the particles are the same. Thus in the CM frame, we have, using the delta function and integrating over the final momenta

$$W_{ab}(s) = \frac{2\sqrt{s(s - 4m^2)}}{1 + \delta_{ab}} \int_{t_{min}}^0 dt \left( \frac{d\sigma}{dt} \right) (1 - f_c(\frac{\sqrt{s}}{2}, \mu))(1 - f_d(\frac{\sqrt{s}}{2}, \mu)) \quad (4.2.57)$$

where, we have  $t_{min} = -(s - 4m^2)$  for non identical particle case and  $t_{min} = -1/2(s - 4m^2)$  for identical particles in the final state.

Once  $W_{ab}$  is calculated as a function of  $s$ , one has to do the thermal averaging of the transition rate using Eq.(4.2.54) . To perform the integration over  $d\pi_a d\pi_b$

in Eq.(4.2.54), we note that the volume element  $d\mathbf{p}_a d\mathbf{p}_b$  is given by

$$d\mathbf{p}_a d\mathbf{p}_b = 4\pi|\mathbf{p}_a|E_a dE_a 4\pi|\mathbf{p}_b|E_b dE_b \frac{1}{2}d(\cos\theta) \quad (4.2.58)$$

where,  $\theta$  is the angle between the three momenta  $\mathbf{p}_a$  and  $\mathbf{p}_b$ . It is somewhat convenient to change the integration variables from  $E_a, E_b, \theta$  to  $E_+, E_-, s$  given by

$$\begin{aligned} E_+ &= E_a + E_b, & E_- &= E_a - E_b \\ s &= 2m^2 + 2E_a E_b - 2|\mathbf{p}_a||\mathbf{p}_b| \cos\theta \end{aligned}$$

so that the volume element becomes

$$d\mathbf{p}_a d\mathbf{p}_b = 2\pi^2 E_a E_b dE_+ dE_- ds \quad (4.2.59)$$

The integration region ( $E_1 > m, E_2 > m, |\cos\theta| \leq 1$ ) transforms into

$$|E_-| < X, \quad E_+ \geq \sqrt{s}, \quad s \geq 4m^2$$

. where,  $X = \sqrt{1 - \frac{4m^2}{s}} \sqrt{E_+^2 - s}$ . It is then possible to perform the integration over the variable  $E_-$  analytically when the distribution functions in Eq.(4.2.54) are fermionic distribution functions  $f(x) = (1 + \exp(\beta x - \mu))^{-1}$ . Thus the thermal averaged transition rate is given by

$$\bar{W}_{ab} = \frac{1}{n_a n_b} \frac{g_a g_b}{(2\pi)^4} \frac{1}{8} \int_{4m^2}^{\infty} ds \int_{\sqrt{s}}^{\infty} dE_+ \int_{-X}^x dE_- f^a\left(\frac{E_a + E_b}{2}, \mu, \beta\right) f^b((E_a - E_b), \mu, \beta) W_{ab}(s) \quad (4.2.60)$$

The thermal relaxation time for each species is then given as

$$\tau_a^{-1} = \sum_b n_b \bar{W}_{ab} \quad (4.2.61)$$

where, the summation runs over all species of quarks and  $\bar{W}_{ab}$  is the sum of the transition rates of all processes with  $a, b$  as the initial states. In the present case

of two flavors we consider the following possible scattering.

$$u\bar{u} \rightarrow u\bar{u}, \quad u\bar{d} \rightarrow u\bar{d}, \quad u\bar{u} \rightarrow d\bar{d},$$

$$uu \rightarrow uu, \quad ud \rightarrow ud, \quad \bar{u}\bar{u} \rightarrow \bar{u}\bar{u},$$

$$\bar{u}\bar{d} \rightarrow \bar{u}\bar{d}, \quad d\bar{d} \rightarrow d\bar{d}, \quad d\bar{d} \rightarrow u\bar{u},$$

$$d\bar{u} \rightarrow d\bar{u}, \quad dd \rightarrow dd, \quad \bar{d}\bar{d} \rightarrow \bar{d}\bar{d},$$

One can use i-spin symmetry, charge conjugation symmetry as well as the crossing symmetry to relate the matrix element square for the above 12 processes to get related to each other and one has to evaluate only two independent matrix elements to evaluate all these 12 processes. We can choose as in Ref. [90]) these to be the processes  $u\bar{u} \rightarrow u\bar{u}$  and  $u\bar{d} \rightarrow u\bar{d}$  and use the symmetry conditions to calculate the rest. We note however that while the matrix elements are related the thermal averaged rates are not as they involve also the thermal distribution functions for the initial states as well as the Pauli blocking factors for the final states. The corresponding matrix element square are written down in Ref. [91] which we do not repeat here.

### 4.3 Results and discussion

The 2 flavor NJL model as given in Eq.(4.1.1), within which we shall be discussing the results, has three parameters— namely, the four point coupling  $G$ , the three momentum cutoff  $\Lambda$  to regularize the integrals appearing in the mass gap equation, and, the integrals involving meson masses and the current quark mass  $m$  which we take to be the same for u and d quarks. Within the mean field approximation for the thermodynamic potential, and the RPA approximation for the meson masses, these three parameters are fixed by fitting the pion mass, the pion decay constant and the quark condensate. While the pion mass  $m_\pi = 135$  MeV [92] and pion decay constant  $f_\pi = 92.4$  MeV [93] are known somewhat accurately, the uncertainties in the quark condensates are

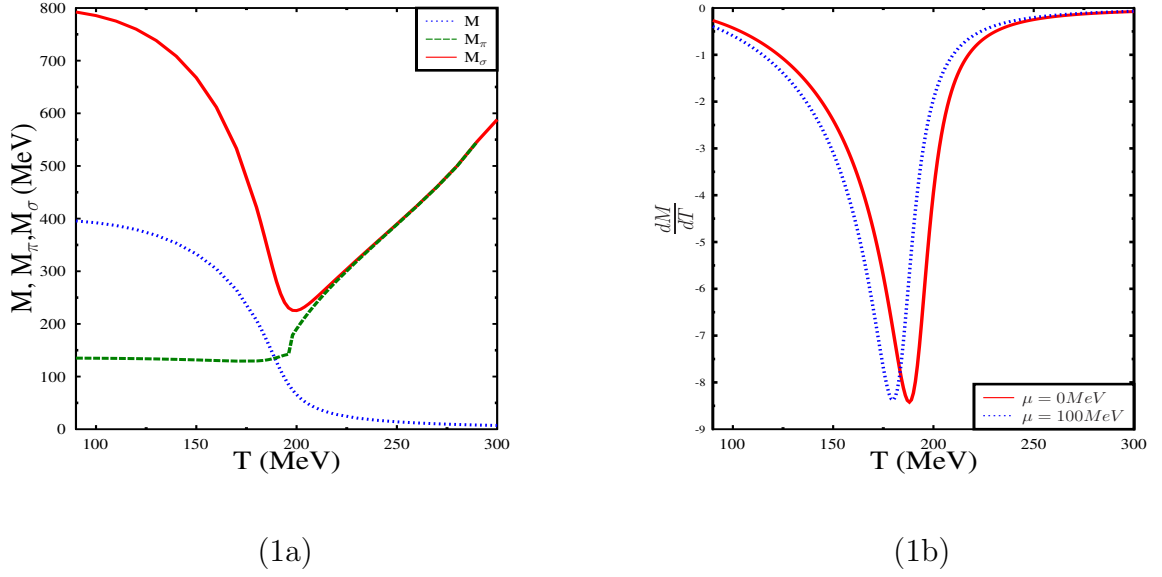


Figure 4.1: Temperature dependence of the constituent quark mass  $M$ , and pion and sigma meson masses at  $\mu = 0$  [Fig. (1a)] and temperature derivative of the constituent quark mass for  $\mu = 0$  MeV and  $\mu = 100$  MeV [Fig. (1b)].

rather large. Whereas, extraction from QCD sum rules turn out to be in the range  $190 \text{ MeV} < -\langle \bar{u}u \rangle^{1/3} < 260 \text{ MeV}$  ( at renormalization scale of  $1 \text{ GeV}$ ) [94], extraction from lattice simulation turns out to be  $-\langle \bar{u}u \rangle^{1/3} \sim 231 \text{ MeV}$ . We have used the parameter set here  $m = 5.6 \text{ MeV}$ ,  $\Lambda = 587.9 \text{ MeV}$  and  $G\Lambda^2 = 2.44$ . This leads to the vacuum value of the constituent quark mass to be  $M \simeq 400 \text{ MeV}$ , while the condensate value as  $-\langle \bar{u}u \rangle^{1/3} = 241 \text{ MeV}$ .

Let us first discuss the thermodynamics of the two flavor NJL model as relevant for the calculation of the transport coefficients.

With the parameters as above, the gap equation is first solved using Eq.(4.1.3) for a given temperature and chemical potential. This is then used to solve for the masses of the pion and sigma masses using Eq.(4.1.12) and Eq.(4.1.13) within the random phase approximation. In Fig.(1a), we have plotted the constituent quark mass, and the meson masses so derived as a function of temperature for  $\mu = 0$ . There is a crossover from low temperature region where there is a large difference between the pion and sigma meson masses while at high temperature, they become degenerate. and increase linearly with temperature. The constituent

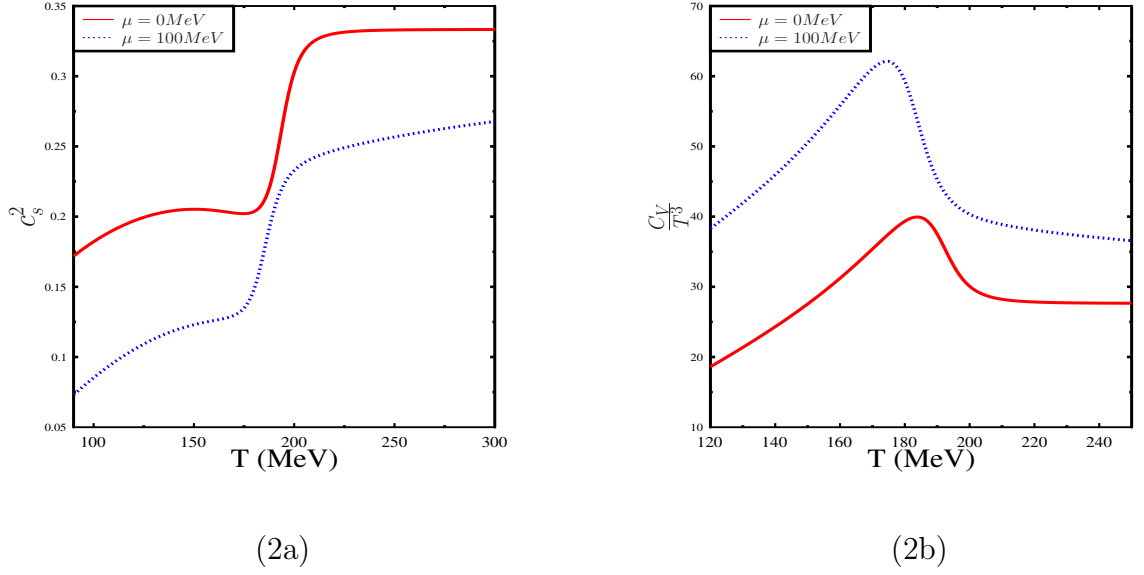
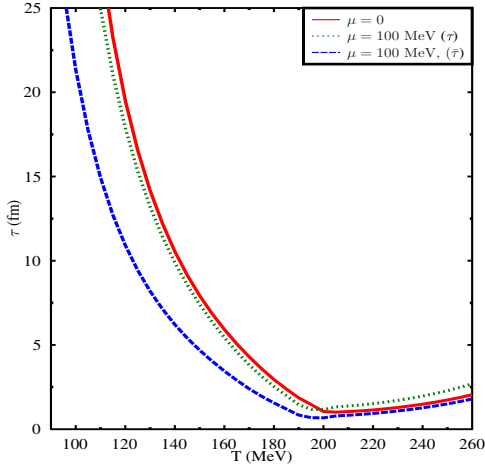


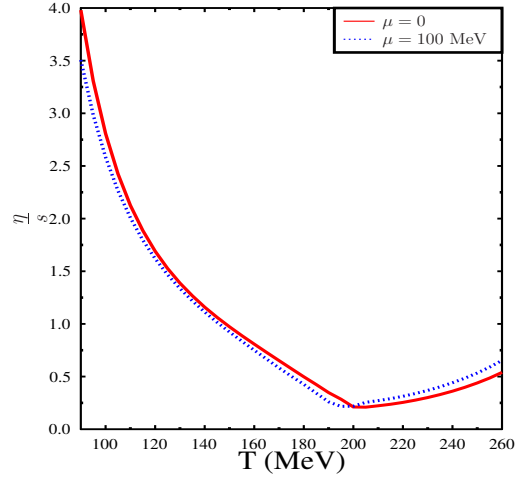
Figure 4.2: Temperature dependence of square of the velocity of sound [Fig. (2a)] and  $C_v/T^2$  [Fig. (2b)] for  $\mu = 0$  MeV and  $\mu = 100$  MeV and temperature derivative of the constituent quark mass for  $\mu = 0$  MeV and  $\mu = 100$  MeV.

quark mass decrease to a small values but never vanishes. The chiral crossover transition  $T_\chi$  turns out to be about 188 MeV for  $\mu = 0$  and about 180 MeV for  $\mu = 100$  MeV. These are defined by the peak in the derivative of the constituent mass ( $dM/dT$ ) which we have shown in Fig.(1b). Let us note here that the constituent mass at  $T_\chi$  turns out to be about 145 MeV. On the other hand, one can have the other characteristic temperature namely, the Mott temperature  $T_M$  defined through the  $m_\pi(T_M) = 2M(T_M)$  i.e. the temperature when the twice the constituent quark mass become equal to that of the pion mass. As may be observed in Fig.1-a the Mott temperature for pions is about 197 MeV. This temperature is relevant in the present case where we estimate the relaxation time using quark scattering involving meson exchange.

Next, we show, in Fig 2-a, the temperature dependence of the square of the velocity of sound  $v_n^2 = (dp/de)_n$  at constant quark number density as defined in Eq.(4.2.28). The velocity of sound do not show any dip around the critical temperature  $T_\chi$ , but rises around the critical temperature and approaches the value of  $\frac{1}{3}$  at high temperatures. In Fig. 2-b , we show the dependence of specific



(3a)



(3b)

Figure 4.3: Fig. (3a) shows relaxation time as a function of temperature for  $\mu = 0$  MeV and for  $\mu = 100$  MeV. In Fig. (3b), shear viscosity to entropy density ratio is shown for  $\mu = 0$  MeV and  $\mu = 100$  MeV.

heat  $c_V \equiv (d\epsilon/dT)_\mu$  scaled by  $T^3$ . This quantity shows a peak at  $T_C$  and which occurs at lower temperature as the density is increased. At high temperature however,  $C_V/T^3$  approaches a constant at small chemical potential. We would like to mention that the behavior of velocity of sound shows different behavior as compared to lattice simulations [15] where it shows a minimum and then rises to a value little less than the ideal gas limit of  $1/3$ . The present results for the sound velocity is similar in nature to linear sigma model calculations of Ref. [43] with a lighter sigma meson of mass about 600 MeV. The behavior of specific heat is also similar to as observed in Ref [43]. This behavior, as we shall observe later, gets reflected in the results for the bulk viscosity.

Next, we discuss the estimation of averaged relaxation time as a function of temperature. Let us recall that this quantity is inversely related to the transition rate  $\bar{W}_{ab}n_b$  as in Eq.(4.2.61) with  $W_{ab}$  is the transition rate of all processes with species  $a, b$  in the the initial states and is related to the corresponding scattering cross section as in Eq.(4.2.57). In general, the dominant contribution here comes from quark anti-quark scattering from s channel through propagation of

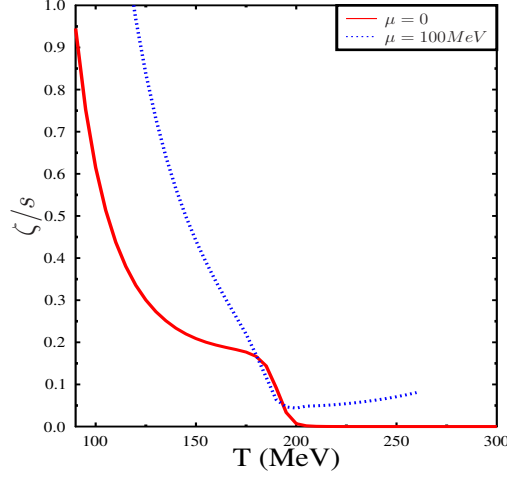
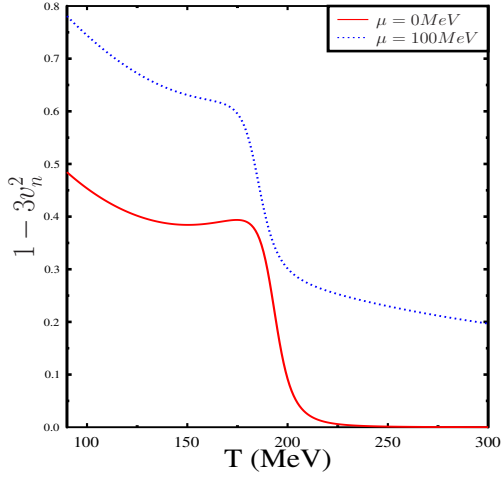


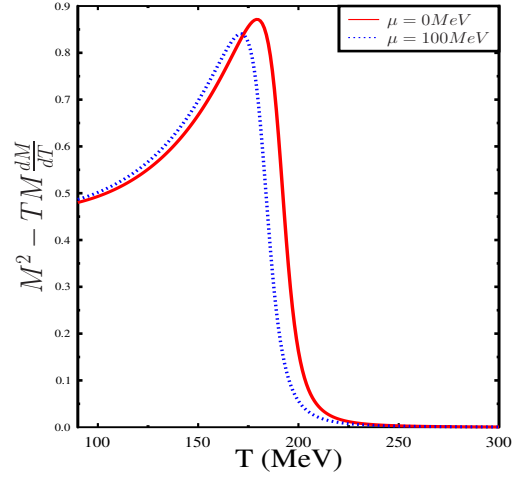
Figure 4.4: Ratio of bulk viscosity to entropy density for  $\mu = 0$  MeV and for  $\mu = 100$  MeV.

the resonance states, the pions and the sigma. The mass of sigma meson decrease with increase in temperature becoming a minimum at the Mott transition temperature  $T_M$  leading to an enhancement of the cross section. This, in turn, leads to a minimum in the relaxation time. Beyond the transition temperature the resonance masses increase with temperature linearly leading to a smaller cross section and hence an increase in the relaxation time beyond the critical temperature. This generic feature is observed in Fig.3-a.

Let us note the  $\tau$  depends both on the transition rate and the density of the particles of the initial state other than the species ‘ $a$ ’. It turns out that the transition rate is dominant for the process  $u\bar{d} \rightarrow u\bar{d}$ . At finite chemical potential, for temperatures greater than the transition temperature, quark density is larger compared to the anti quarks. As there are fewer anti quarks to scatter off, the cross section for quark-anti quark scattering decreases leading to  $\tau(\mu) > \tau(\mu = 0)$ . On the other hand, for anti-quarks, there are more quarks to scatter off at nonzero  $\mu$  as compared to at  $\mu = 0$ . This leads to a lower value for relaxation time for the anti quark at finite  $\mu$  as compared to  $\mu = 0$  case. On the other hand, for temperatures below the critical temperature, while the quark-anti quark transition rate is dominant, the density of anti quark is sup-



(5a)



(5b)

Figure 4.5: the violation of conformality measure  $C_1 1 - 3V_n^2$  [Fig. (5a)] and  $C_2 = M^2 - TM \frac{dM}{dT}$  [Fig. (5b)] as a function of temperature for  $\mu = 0$  MeV and for  $\mu = 100$  MeV.

pressed very much by the constituent quark mass for  $\mu \neq 0$ . The quark number density however is enhanced contribution from quark quark scattering becomes more important resulting in a smaller value for the relaxation time at finite  $\mu$  compared to  $\mu = 0$  case. In Fig(3-b) we have plotted the shear viscosity to entropy ratio ( $\frac{\eta}{s}$ ) as a function of temperature for  $\mu = 0$  MeV and  $\mu = 100$  MeV. As expected from the  $\tau$  behavior with temperature,  $\eta/s$  has a minimum at the critical temperature beyond which it increase slowly. At finite  $\mu$   $\eta/s$  is larger as compared to vanishing  $\mu$ . This is due to two reasons. Firstly,  $\tau$  at finite  $\mu$  is larger and, further, the quark density is also larger as compared to the anti quarks at finite density.

In Fig. (4) we show the ratio of bulk viscosity to entropy density ( $\frac{\zeta}{s}$ ) as a function of temperature. The bulk viscosity increases rapidly near the critical temperature as temperature decrease from high temperature beyond the critical temperature to temperatures below it. However, it is not a maximum at the critical temperature. After the rapid rise near critical temperature it increases

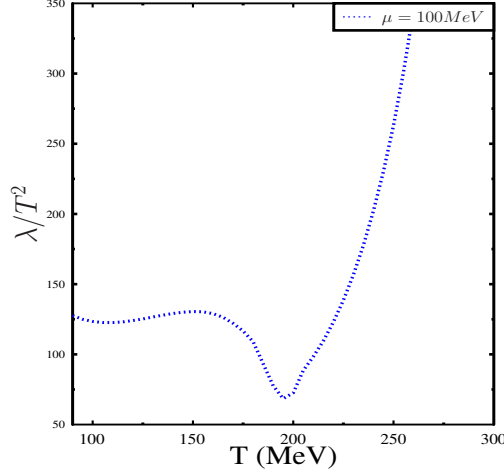


Figure 4.6: Thermal conductivity in units of  $T^2$  for  $\mu = 100$  MeV.

slowly. Let us note that one can rewrite the expression for the bulk viscosity as

$$\begin{aligned} \zeta &= \frac{1}{9T} \sum_a \int d\Gamma^a \frac{\tau^a}{E_a^2} \left[ \mathbf{p}^2 (1 - 3v_n^2) + 3v_n^2 \left( M^2 - TM \frac{dM}{dT} - \mu M \frac{dM}{dT} \right) \right. \\ &\quad \left. + 3 \left( \frac{\partial P}{\partial n} \right)_\epsilon \left( M \frac{dM}{d\mu} - E_a t^a \right) \right]^2 f_a^0 (1 - f_a^0) \end{aligned} \quad (4.3.1)$$

At zero baryon density, bulk viscosity depends quadratically upon the violation of conformality measures  $C_1 = 1 - 3V_0^2$  and  $C_2 = M^2 - TM \frac{dM}{dT}$  [43]. The behavior of these two parameters are plotted as a function of temperature in Fig (5). For comparison, we have also plotted the corresponding quantities at non zero  $\mu$ . As may be observed,  $\zeta/s$  is largest when the violation of conformality is large. At finite baryon density,  $(1 - v_n^2)$  does not vanish nor the factor  $(\partial P/\partial n)_\epsilon$  as a result of which the ratio  $\zeta/s$  does not vanish unlike  $\mu = 0$  case. The behavior of bulk viscosity is similar qualitatively to that of linear sigma model of Ref. [43]. Our results regarding the ration  $\eta/s$  qualitatively look similar as compared to that of Ref. [37]. However, the bulk viscosity to entropy ratio look different as we have implemented the Landau Lifshitz matching conditions explicitly leading to different expression for  $\zeta$ . This apart, while estimating the average relaxation time we have used the transition rate calculated in a covariant manner similar

to Ref. [91] where as Ref. [37] uses a probability distribution to calculate the thermal averaged cross section similar to [90].

Finally, in Fig. (6) we have plotted thermal conductivity of quark matter at  $\mu = 100\text{MeV}$  in units of  $T^2$ . As may be noted, the ratio  $\lambda/T^2$  shows a non monotonic behavior with a minimum at the critical temperature. The origin of this again is related to the minimum of the relaxation time at the critical temperature. The present behavior is in contrast to the same obtained in Ref. [95] where the same ratio shows a monotonically decreasing function of temperature. The behavior of  $\lambda/T^2$  was also studied in Ref. [96] where, the ratio showed a increasing behavior with temperature with however a slower rise with temperature as compared to the results shown in Fig. 6. Thermal conductivity was also estimated for within chiral perturbation theory for hot pion gas in Ref. [80]. The variation of thermal conductivity here is also non monotonic with temperature. Within the Green Kubo approach, thermal conductivity was estimated for two flavors in Ref. [97] within the instanton liquid model where however the thermal conductivity saturates beyond  $T=150\text{ MeV}$  in contrast to the present calculation.

## 4.4 Conclusion

In this chapter we estimated the transport properties of hot and dense quark matter by solving the Boltzmann kinetic equation within relaxation time approximation. The thermodynamical quantities as well as medium dependent quark and meson masses are estimated within two flavor NJL model. To estimate the relaxation time we have considered the quark-antiquark two body scatterings through exchange of pion and sigma resonances. Since the meson masses are minimum at the transition temperatures beyond which they are degenerate and increase linear with temperature, the meson propagator occurring in the transition amplitude lead to a large contribution to the cross section for the quark, anti quark scattering. This eventually leads to a smaller relaxation time which, in turn, lead to a minimum in the temperature dependence of the relaxation time. While computing the averaged relaxation time we have performed the procedure

---

in a manifestly covariant manner, rather than multiplying an ad hoc probability function to estimate the thermal averaged cross section. We have used the expressions for the transport coefficients that are manifestly positive definite as they should be. The expression for shear viscosity only depends on the relaxation time and the distribution functions. However, both the expressions for the coefficients of bulk viscosity and thermal conductivity involve equation of state. The expressions for the transport coefficients are direct generalization of their counterparts at zero chemical potential. All the three transport coefficients are minimum at the Mott temperature.



# Chapter 5

## Summary and outlook

In this thesis we studied the phenomenological aspects of strongly interacting matter under extreme conditions of temperature and density. We were especially interested in the phenomenology of matter created in heavy-ion collision experiments regarding its thermodynamics and transport properties. In Chapter 1 we briefly discussed the phase diagram of quantum chromodynamics with special emphasis on the hadronic and the quark-gluon-plasma phase which were phases of interest in this thesis. We discussed the evolution of matter created in HICs from thermalized quark-gluon matter to freely streaming hadrons which are finally detected in detectors. We discussed the relativistic hydrodynamics as an effective theory valid for long wavelength and small frequencies. We saw that apart from ideal hydrodynamics viscous effects are also very important to describe the evolution of matter created in HICs. Computing these viscosity coefficients, namely, shear viscosity ( $\eta$ ), bulk viscosity ( $\zeta$ ) and thermal conductivity ( $\lambda$ ), was the central theme of our thesis.

To carry out the study of hadronic phase it is necessary to determine the correct equation of state of hadronic matter consisting pions, kaons,  $\eta$  mesons, baryons and other heavy resonances. At vanishing chemical potential the LQCD simulations give the equation of state of hadronic matter with reasonably good accuracy. However, it fails to do so at finite  $\mu$ . In Chapter 2 we discussed the hadron resonance gas model as an effective model successfully describing the hadronic phase of QCD at  $\mu = 0$  as well as  $\mu \neq 0$ . The success of ideal

HRG is attributed to the fact that it reproduces LQCD results quite well at low temperature. We further discussed the possible improvements in ideal HRG model in order to account for the short range repulsive interactions and the chiral symmetry of QCD. Former aspect of QCD can be accounted by excluded volume corrections in the ideal HRG model where we attribute finite hardcore radius to each hadron whereas the later aspect can be accounted by including medium dependent hadron masses in the partition function of ideal HRG model. We found that with these improvements the HRG model agrees with the LQCD even at higher temperature ( $T \sim 170$  MeV).

In Chapter 1 we discussed the importance of studying the transport coefficients of strongly interacting matter. In Chapter 3 we discussed the estimation of transport coefficients of hadronic matter. The thermodynamics of hadronic matter was estimated using HRG model and its various improvements. We used two different formalisms, *viz.*, Kubo's formalism and relativistic kinetic theory. We derived bulk viscosity coefficient in terms of thermodynamical quantities using Kubo's formula together with the QCD low energy theorems at finite temperature and density. We found that the bulk viscosity to entropy density ratio ( $\zeta/s$ ) increases with the temperature while at finite chemical potential,  $\zeta/s$  become higher as compared to  $\mu = 0$  and is related to the fact that the velocity of sound becomes smaller due to finite chemical potential with the excitation of heavier baryons contributing more to the energy density as compared to the pressure. Unlike the Kubo formalism, ratio  $\zeta/s$  estimated using relativistic kinetic theory decreases with the temperature and almost vanishes near the transition temperature ( $T_c$ ).

The shear viscosity to entropy density ratio estimated using the relativistic kinetic theory shows decreasing behavior with temperature. Further, at finite chemical potential  $\eta/s$  shows same behavior as a function of temperature but ratio is smaller as compared to  $\mu = 0$ . This decrease is solely due to rapid increase in entropy density at finite  $\mu$ . At finite baryon density  $\eta T/(\epsilon + P)$  is correct measure of fluidity. We found that the effect of finite  $\mu$  is more pronounced for  $\eta T/(\epsilon + P)$  and this is again attributed to the rapid rise in enthalpy.

To complete this analysis we made the connection of viscosity coefficients with the heavy ion collision experiments by computing both  $\eta/s$  and  $\zeta/s$  along chemical freeze-out line where we found that along chemical freeze-out curve both the ratios,  $\eta/s$  and  $\eta T/(\epsilon + P)$ , remains constant apart from initial rise. This suggest that the fluid behavior of the hadron gas does not change along chemical freeze-out curve. Further we found that the ratio  $\zeta/s$  decreases monotonically and then becomes independent of center-of-mass energy along freeze-out.

Finally in Chapter 4 we estimated the transport coefficients, shear ( $\eta$ ) and bulk viscosity ( $\zeta$ ) as well as thermal conductivity ( $\lambda$ ) of hot and dense quark matter again using relativistic Boltzmann equation in relaxation time approximation within ambit of two flavor NJL model. To estimate the relaxation time we have considered the quark-antiquark two body scatterings through exchange of pion and sigma resonances. We found that since the meson masses are minimum at the transition temperatures beyond which they are degenerate and increase linear with temperature, the meson propagator occurring in the transition amplitude lead to a large contribution to the cross section for the quark-antiquark scattering. This leads to a smaller relaxation time which, in turn, lead to a minimum in the temperature dependence of the relaxation time. This behavior of the relaxation time is reflected in all the transport coefficients,  $\eta/s$ ,  $\zeta/s$  and  $\lambda/T^2$ , which showed the minimum at the Mott temperature.

In this thesis we pursued our goal to understand the strongly interacting matter where we tried to address many questions starting from finding the correct equation of state for hadronic matter using HRG model and for quark matter using NJL model and finally estimated the transport coefficients of both hadronic as well as quark matter realizing their importance in the evolution of matter created in heavy ion collision. In this endeavor we further raised many question which needs to be explored. In the early stages of off central heavy-ion collisions very strong, although transient, magnetic field is generated. Such magnetic field breaks the rotational symmetry in the system and stress tensor becomes anisotropic. Thus all the transport coefficients become anisotropic in presence of magnetic field. Thus detailed study of the transport properties of

strongly interacting matter in presence of magnetic field would be very interesting. Also in the phase diagram of QCD, it is still not well settled issue how the transport coefficients might behave at or very close to the critical point. These might be the interesting avenues that needs further examination.

# Bibliography

- [1] R. S. Bhalerao, *Relativistic heavy-ion collisions*, in “Proceedings, 1st Asia-Europe-Pacific School of High-Energy Physics (AEPSHEP),” (2014), pp. 219–239.
- [2] G. S. Denicol, C. Gale, S. Jeon, and J. Noronha, *Fluid behavior of a baryon-rich hadron resonance gas*, *Phys. Rev.* **C88**, 064901 (2013).
- [3] A. S. Khvorostukhin, V. D. Toneev, and D. N. Voskresensky, *Viscosity Coefficients for Hadron and Quark-Gluon Phases*, *Nucl. Phys.* **A845**, 106–146 (2010).
- [4] T. Muta, *Foundations of Quantum Chromodynamics: An Introduction to Perturbative Methods in Gauge Theories, (3rd ed.)*, vol. 78 of *World scientific Lecture Notes in Physics* (World Scientific, Hackensack, N.J., 2010).
- [5] W. Greiner, S. Schramm, and E. Stein, *Quantum chromodynamics* (2007).
- [6] T. Banks, S. Raby, L. Susskind, J. Kogut, D. R. T. Jones, P. N. Scharbach, and D. K. Sinclair, *Strong-coupling calculations of the hadron spectrum of quantum chromodynamics*, *Phys. Rev. D* **15**, 1111–1127 (1977).
- [7] E. D. Bloom *et al.*, *High-Energy Inelastic  $e p$  Scattering at 6-Degrees and 10-Degrees*, *Phys. Rev. Lett.* **23**, 930–934 (1969).
- [8] M. Breidenbach, J. I. Friedman, H. W. Kendall, E. D. Bloom, D. H. Coward, H. C. DeStaebler, J. Drees, L. W. Mo, and R. E. Taylor, *Observed Behavior of Highly Inelastic electron-Proton Scattering*, *Phys. Rev. Lett.* **23**, 935–939 (1969).

- 
- [9] H. D. Politzer, *Reliable Perturbative Results for Strong Interactions?* Phys. Rev. Lett. **30**, 1346–1349 (1973).
- [10] D. J. Gross and F. Wilczek, *Ultraviolet Behavior of Nonabelian Gauge Theories*, Phys. Rev. Lett. **30**, 1343–1346 (1973).
- [11] P. Petreczky, *Lattice QCD at non-zero temperature*, J. Phys. **G39**, 093002 (2012).
- [12] J. Goldstone, *Field Theories with Superconductor Solutions*, Nuovo Cim. **19**, 154–164 (1961).
- [13] A. Chodos, R. L. Jaffe, K. Johnson, C. B. Thorn, and V. F. Weisskopf, *A New Extended Model of Hadrons*, Phys. Rev. **D9**, 3471–3495 (1974).
- [14] A. Chodos, R. L. Jaffe, K. Johnson, and C. B. Thorn, *Baryon Structure in the Bag Theory*, Phys. Rev. **D10**, 2599 (1974).
- [15] A. Bazavov *et al.*, *Equation of state in (2+1)-flavor QCD*, Phys. Rev. **D90**, 094503 (2014).
- [16] A. M. Polyakov, *Thermal Properties of Gauge Fields and Quark Liberation*, Phys. Lett. **B72**, 477–480 (1978).
- [17] T. Banks and A. Casher, *Chiral Symmetry Breaking in Confining Theories*, Nucl. Phys. **B169**, 103 (1980).
- [18] F. Gelis, E. Iancu, J. Jalilian-Marian, and R. Venugopalan, *The Color Glass Condensate*, Ann. Rev. Nucl. Part. Sci. **60**, 463–489 (2010).
- [19] P. Romatschke, *New Developments in Relativistic Viscous Hydrodynamics*, Int. J. Mod. Phys. **E19**, 1–53 (2010).
- [20] J.-Y. Ollitrault, *Relativistic hydrodynamics for heavy-ion collisions*, Eur. J. Phys. **29**, 275–302 (2008).
- [21] A. Dobado, F. J. Llanes-Estrada, and J. M. Torres-Rincon, *Brief introduction to viscosity in hadron physics*, AIP Conf. Proc. **1322**, 11–18 (2010).

- 
- [22] S. Voloshin and Y. Zhang, *Flow study in relativistic nuclear collisions by Fourier expansion of Azimuthal particle distributions*, *Z. Phys.* **C70**, 665–672 (1996).
- [23] T. Hirano and M. Gyulassy, *Perfect fluidity of the quark gluon plasma core as seen through its dissipative hadronic corona*, *Nucl. Phys.* **A769**, 71–94 (2006).
- [24] P. Kovtun, D. T. Son, and A. O. Starinets, *Viscosity in strongly interacting quantum field theories from black hole physics*, *Phys. Rev. Lett.* **94**, 111601 (2005).
- [25] S. Borsanyi, Z. Fodor, C. Hoelbling, S. D. Katz, S. Krieg, and K. K. Szabo, *Full result for the QCD equation of state with 2+1 flavors*, *Phys. Lett.* **B730**, 99–104 (2014).
- [26] J. R. Bhatt, H. Mishra, and V. Sreekanth, *Cavitation and thermal dilepton production in QGP*, *Nucl. Phys.* **A875**, 181–196 (2012).
- [27] A. Monnai and T. Hirano, *Effects of Bulk Viscosity at Freezeout*, *Phys. Rev.* **C80**, 054906 (2009).
- [28] G. S. Denicol, T. Kodama, T. Koide, and P. Mota, *Effect of bulk viscosity on Elliptic Flow near QCD phase transition*, *Phys. Rev.* **C80**, 064901 (2009).
- [29] K. Dusling and T. Schfer, *Bulk viscosity, particle spectra and flow in heavy-ion collisions*, *Phys. Rev.* **C85**, 044909 (2012).
- [30] U. Heinz and R. Snellings, *Collective flow and viscosity in relativistic heavy-ion collisions*, *Ann. Rev. Nucl. Part. Sci.* **63**, 123–151 (2013).
- [31] J. Noronha-Hostler, G. S. Denicol, J. Noronha, R. P. G. Andrade, and F. Grassi, *Bulk Viscosity Effects in Event-by-Event Relativistic Hydrodynamics*, *Phys. Rev.* **C88**, 044916 (2013).

- [32] J. Noronha-Hostler, J. Noronha, and F. Grassi, *Bulk viscosity-driven suppression of shear viscosity effects on the flow harmonics at energies available at the BNL Relativistic Heavy Ion Collider*, Phys. Rev. **C90**, 034907 (2014).
- [33] P. Bozek and I. Wyskiel, *Directed flow in ultrarelativistic heavy-ion collisions*, Phys. Rev. **C81**, 054902 (2010).
- [34] J.-B. Rose, J.-F. Paquet, G. S. Denicol, M. Luzum, B. Schenke, S. Jeon, and C. Gale, *Extracting the bulk viscosity of the quarkgluon plasma*, Nucl. Phys. **A931**, 926–930 (2014).
- [35] A. Dobado, F. J. Llanes-Estrada, and J. M. Torres-Rincon,  *$\eta/s$  and phase transitions*, Phys. Rev. **D79**, 014002 (2009).
- [36] C. Sasaki and K. Redlich, *Bulk viscosity in quasi particle models*, Phys. Rev. **C79**, 055207 (2009).
- [37] C. Sasaki and K. Redlich, *Transport coefficients near chiral phase transition*, Nucl. Phys. **A832**, 62–75 (2010).
- [38] F. Karsch, D. Kharzeev, and K. Tuchin, *Universal properties of bulk viscosity near the QCD phase transition*, Phys. Lett. **B663**, 217–221 (2008).
- [39] I. A. Shushpanov, J. I. Kapusta, and P. J. Ellis, *Low-energy theorems for QCD at finite temperature and chemical potential*, Phys. Rev. **C59**, 2931–2933 (1999).
- [40] A. Dobado, F. J. Llanes-Estrada, and J. M. Torres-Rincon, *Minimum of  $\eta/s$  and the phase transition of the Linear Sigma Model in the large- $N$  limit*, Phys. Rev. **D80**, 114015 (2009).
- [41] A. Wiranata and M. Prakash, *Shear Viscosities from the Chapman-Enskog and the Relaxation Time Approaches*, Phys. Rev. **C85**, 054908 (2012).
- [42] A. Wiranata, V. Koch, M. Prakash, and X. N. Wang, *Shear viscosity of hadrons with  $K$ -matrix cross sections*, Phys. Rev. **C88**, 044917 (2013).

- [43] P. Chakraborty and J. I. Kapusta, *Quasi-Particle Theory of Shear and Bulk Viscosities of Hadronic Matter*, Phys. Rev. **C83**, 014906 (2011).
- [44] N. Demir and S. A. Bass, *Shear-Viscosity to Entropy-Density Ratio of a Relativistic Hadron Gas*, Phys. Rev. Lett. **102**, 172302 (2009).
- [45] V. Ozvenchuk, O. Linnyk, M. I. Gorenstein, E. L. Bratkovskaya, and W. Cassing, *Shear and bulk viscosities of strongly interacting infinite parton-hadron matter within the parton-hadron-string dynamics transport approach*, Phys. Rev. **C87**, 064903 (2013).
- [46] M. I. Gorenstein, M. Hauer, and O. N. Moroz, *Viscosity in the excluded volume hadron gas model*, Phys. Rev. **C77**, 024911 (2008). [,214(2007)].
- [47] J. Noronha-Hostler, J. Noronha, and C. Greiner, *Transport Coefficients of Hadronic Matter near  $T(c)$* , Phys. Rev. Lett. **103**, 172302 (2009).
- [48] J. Noronha-Hostler, J. Noronha, and C. Greiner, *Hadron Mass Spectrum and the Shear Viscosity to Entropy Density Ratio of Hot Hadronic Matter*, Phys. Rev. **C86**, 024913 (2012).
- [49] P. Senger, *Particle production in heavy-ion collisions*, Progress in Particle and Nuclear Physics **53**, 1–23 (2004).
- [50] K. Itakura, O. Morimatsu, and H. Otomo, *Shear viscosity of a hadronic gas mixture*, Phys. Rev. **D77**, 014014 (2008).
- [51] S. Ghosh, *Nucleon thermal width owing to pion-baryon loops and its contributions to shear viscosity*, Phys. Rev. **C90**, 025202 (2014).
- [52] M. M. Wang, Y. Jiang, B. Wang, W. M. Sun, and H.-S. Zong, *Calculation of bulk viscosity of QCD at zero temperature and finite chemical potential*, Mod. Phys. Lett. **A26**, 1797–1806 (2011).
- [53] P. Huovinen and P. Petreczky, *QCD Equation of State and Hadron Resonance Gas*, Nucl. Phys. **A837**, 26–53 (2010).

- [54] A. Majumder and B. Muller, *Hadron Mass Spectrum from Lattice QCD*, Phys. Rev. Lett. **105**, 252002 (2010).
- [55] R. Hagedorn, *Statistical thermodynamics of strong interactions at high-energies*, Nuovo Cim. Suppl. **3**, 147–186 (1965).
- [56] C. Amsler *et al.*, *Review of Particle Physics*, Phys. Lett. **B667**, 1–1340 (2008).
- [57] S. Borsanyi, G. Endrodi, Z. Fodor, S. D. Katz, S. Krieg, C. Ratti, and K. K. Szabo, *QCD equation of state at nonzero chemical potential: continuum results with physical quark masses at order  $\mu^2$* , JHEP **08**, 053 (2012).
- [58] S. Borsanyi, G. Endrodi, Z. Fodor, A. Jakovac, S. D. Katz, S. Krieg, C. Ratti, and K. K. Szabo, *The QCD equation of state with dynamical quarks*, JHEP **11**, 077 (2010).
- [59] D. H. Rischke, M. I. Gorenstein, H. Stoecker, and W. Greiner, *Excluded volume effect for the nuclear matter equation of state*, Z. Phys. **C51**, 485–490 (1991).
- [60] I. S. Gradshteyn and I. M. Ryzhik, *Table of integrals, series, and products* (Elsevier/Academic Press, Amsterdam, 2007), seventh ed. Translated from the Russian, Translation edited and with a preface by Alan Jeffrey and Daniel Zwillinger, With one CD-ROM (Windows, Macintosh and UNIX).
- [61] S. Leupold, *Four-quark condensates and chiral symmetry restoration in a resonance gas model*, J. Phys. **G32**, 2199–2218 (2006).
- [62] J. Jankowski, D. Blaschke, and M. Spalinski, *Chiral condensate in hadronic matter*, Phys. Rev. **D87**, 105018 (2013).
- [63] T. Hatsuda and T. Kunihiro, *QCD phenomenology based on a chiral effective Lagrangian*, Phys. Rept. **247**, 221–367 (1994).
- [64] S. P. Klevansky, *The Nambu-Jona-Lasinio model of quantum chromodynamics*, Rev. Mod. Phys. **64**, 649–708 (1992).

- [65] A. Andronic, P. Braun-Munzinger, J. Stachel, and M. Winn, *Interacting hadron resonance gas meets lattice QCD*, Phys. Lett. **B718**, 80–85 (2012).
- [66] G. P. Kadam and H. Mishra, *Dissipative properties of hot and dense hadronic matter in an excluded-volume hadron resonance gas model*, Phys. Rev. **C92**, 035203 (2015).
- [67] P. Braun-Munzinger, I. Heppe, and J. Stachel, *Chemical equilibration in Pb + Pb collisions at the SPS*, Phys. Lett. **B465**, 15–20 (1999).
- [68] M. Albright, J. Kapusta, and C. Young, *Matching Excluded Volume Hadron Resonance Gas Models and Perturbative QCD to Lattice Calculations*, Phys. Rev. **C90**, 024915 (2014).
- [69] G. D. Yen, M. I. Gorenstein, W. Greiner, and S.-N. Yang, *Excluded volume hadron gas model for particle number ratios in A+A collisions*, Phys. Rev. **C56**, 2210–2218 (1997).
- [70] V. Vovchenko, D. V. Anchishkin, and M. I. Gorenstein, *Hadron Resonance Gas Equation of State from Lattice QCD*, Phys. Rev. **C91**, 024905 (2015).
- [71] G. P. Kadam and H. Mishra, *Bulk and shear viscosities of hot and dense hadron gas*, Nucl. Phys. **A934**, 133–147 (2014).
- [72] R. Venugopalan and M. Prakash, *Thermal properties of interacting hadrons*, Nucl. Phys. **A546**, 718–760 (1992).
- [73] G. Endrudi, *QCD equation of state at nonzero magnetic fields in the Hadron Resonance Gas model*, JHEP **04**, 023 (2013).
- [74] G. S. Bali, F. Bruckmann, G. Endrudi, Z. Fodor, S. D. Katz, S. Krieg, A. Schafer, and K. K. Szabo, *The QCD phase diagram for external magnetic fields*, JHEP **02**, 044 (2012).
- [75] S. Gavin, *TRANSPORT COEFFICIENTS IN ULTRARELATIVISTIC HEAVY ION COLLISIONS*, Nucl. Phys. **A435**, 826–843 (1985).

- [76] O. Moroz, *Shear and bulk viscosities of the hadron gas within relaxation time approximation and its test*, Ukr. J. Phys. **58**, 1127–1131 (2013).
- [77] P. Gondolo and G. Gelmini, *Cosmic abundances of stable particles: Improved analysis*, Nucl. Phys. **B360**, 145–179 (1991).
- [78] M. Cannoni, *Relativistic  $\langle \sigma v_{rel} \rangle$  in the calculation of relics abundances: a closer look*, Phys. Rev. **D89**, 103533 (2014).
- [79] N. O. Agasian, *Low-energy theorems of hot and dense QCD in a magnetic field*, Phys. Atom. Nucl. **74**, 1230–1234 (2011). [Yad. Fiz.74,1259(2011)].
- [80] D. Fernandez-Fraile and A. Gomez Nicola, *Transport coefficients and resonances for a meson gas in Chiral Perturbation Theory*, Eur. Phys. J. **C62**, 37–54 (2009).
- [81] J. Liao and V. Koch, *On the Fluidity and Super-Criticality of the QCD matter at RHIC*, Phys. Rev. **C81**, 014902 (2010).
- [82] P. Danielewicz and M. Gyulassy, *Dissipative Phenomena in Quark Gluon Plasmas*, Phys. Rev. **D31**, 53–62 (1985).
- [83] T. D. Cohen, *Is there a 'most perfect fluid' consistent with quantum field theory?* Phys. Rev. Lett. **99**, 021602 (2007).
- [84] E. Lu and G. D. Moore, *The Bulk Viscosity of a Pion Gas*, Phys. Rev. **C83**, 044901 (2011).
- [85] A. Dobado, F. J. Llanes-Estrada, and J. M. Torres-Rincon, *Bulk viscosity of low-temperature strongly interacting matter*, Phys. Lett. **B702**, 43–48 (2011).
- [86] J. Cleymans, H. Oeschler, K. Redlich, and S. Wheaton, *Comparison of chemical freeze-out criteria in heavy-ion collisions*, Phys. Rev. **C73**, 034905 (2006).
- [87] P. Bozek, *Bulk and shear viscosities of matter created in relativistic heavy-ion collisions*, Phys. Rev. **C81**, 034909 (2010).

- [88] M. Buballa, *NJL model analysis of quark matter at large density*, Phys. Rept. **407**, 205–376 (2005).
- [89] M. Albright and J. I. Kapusta, *Quasiparticle Theory of Transport Coefficients for Hadronic Matter at Finite Temperature and Baryon Density*, Phys. Rev. **C93**, 014903 (2016).
- [90] P. Zhuang, J. Hufner, S. P. Klevansky, and L. Neise, *Transport properties of a quark plasma and critical scattering at the chiral phase transition*, Phys. Rev. **D51**, 3728–3738 (1995).
- [91] P. Rehberg, S. P. Klevansky, and J. Hufner, *Elastic scattering and transport coefficients for a quark plasma in  $SU(3)$  at finite temperatures*, Nucl. Phys. **A608**, 356–388 (1996).
- [92] A. G. Akeroyd, S. Baek, G.-C. Cho, and K. Hagiwara, *On the possibility of a very light  $A0$  at low  $\tan\beta$  in the MSSM*, Phys. Rev. **D66**, 037702 (2002).
- [93] B. R. Holstein, *How large is  $f(\pi)$ ?* Phys. Lett. **B244**, 83–87 (1990).
- [94] H. G. Dosch and S. Narison, *Direct extraction of the chiral quark condensate and bounds on the light quark masses*, Phys. Lett. **B417**, 173–176 (1998).
- [95] R. Marty, E. Bratkovskaya, W. Cassing, J. Aichelin, and H. Berrehrh, *Transport coefficients from the Nambu-Jona-Lasinio model for  $SU(3)_f$* , Phys. Rev. **C88**, 045204 (2013).
- [96] S. Mattiello, *Transport coefficients of the quark-gluon plasma in ultrarelativistic limit*, (2012).
- [97] S.-i. Nam, *Thermal conductivity of the quark matter for the  $SU(2)$  light-flavor sector*, Mod. Phys. Lett. **A30**, 1550054 (2015).



## Publications attached with the thesis

1. *Bulk and shear viscosities of hot and dense hadron gas,*  
**Guru Prakash Kadam** and H. Mishra, Nucl. Phys. A **934**, 133 (2014).
2. *Transport properties of hadronic matter in magnetic field,*  
**Guru Prakash Kadam**, Mod. Phys. Lett. A **30**, no. 10, 1550031 (2015).
3. *Dissipative properties of hot and dense hadronic matter in an excluded-volume hadron resonance gas model,*  
**Guru Prakash Kadam** and H. Mishra, Phys. Rev. C **92**, no. 3, 035203 (2015).
4. *Medium modification of hadron masses and the thermodynamics of hadron resonance gas model,*  
**Guru Prakash Kadam** and H. Mishra, Phys. Rev. C **93**, no. 2, 025205 (2016).

